THE UNIVERSITY OF
SYDNEY

Application of Numerical Simulation in Cardiovascular Medicine

Michael Hwai Ren Chang

A thesis submitted in fulfilment of the requirements for the degree of

Master of Philosophy

Concord Repatriation General Hospital

Department of Cardiology

Faculty of Medicine

The University of Sydney

February 2015

Declaration

This thesis is submitted to the University of Sydney in fulfilment of the requirement for the Degree of Master of Philosophy (MD).

I, Michael Chang, hereby declare that the work presented in this thesis is, to the best of my knowledge and belief, original except as acknowledged in the text. I hereby declare that I have not submitted this material, either in full or in part, for a degree at this or any other institution.

Acknowledgements

I will always be deeply grateful to my supervisor, Leonard Kritharides, for his guidance and support during this extra-long journey. He has truly been the ideal supervisor: a counsel in time of difficulty, and an appropriate critic in time of exuberance. I am most appreciative for the time and patience he has generously set aside to mentor me through this process. I look forward to the many collaborative efforts we will have together in the future.

I would like to thank my associate supervisors, Ben Freedman for his advice and help in the studies included in this thesis.

Many other colleagues have been instrumental throughout the project (in no particular order): Andy Yong, Afiqah Hamzah, Ashkan Javadzadegan, George Lau, Jack Ling, Masud Behnia, John Yiannikas, Lloyd Ridley, Neville Sammel, Jane McCrohon, James Otton and Michael Feneley. I would like to specially mention Andy Yong who has been my guide and friend throughout this long journey.

I would like to thank the staffs at the Radiology department from both Concord and St Vincent Hospitals for their help. The thesis would also not be possible without all the patients and volunteers who have selflessly agreed to be part of the studies.

Lastly, I would like to thank my parents, Chien Lung Chang and Lee Duang Chang who have helped and supported me in too many ways to mention here.

Table of Contents

Abstract

Introduction:

The purpose of this thesis is to study atherosclerotic risk and thrombotic risk through application of numerical simulation to cardiovascular geometry and morphology. This has been applied to two specific situations, the angle of take-off of the left main coronary artery and the morphology of the left atrial appendage.

A. The distribution of atherosclerotic plaque and the plaque rupture rate in isolated left main coronary disease is different to that seen in left main disease with multi-vessel disease, suggesting local biomechanical forces play an important part in governing plaque formation and rupture. The varying vertical left main coronary artery take-off angulation may impact on the wall shear stress.

B. Different left atrial appendage morphologies seem to have different risk of thromboembolism, in patients with atrial fibrillation and low $CHADS_2$ VASC score. From this observation, it can be hypothesized that left atrial morphology subtype with a more complex structure can lead to higher volume of blood stagnation.

Aim:

A. To investigate the effects of vertical take-off angulation of the left main coronary artery from aorta and varying stenosis severities on wall shear stress in the left main coronary artery.

B. To investigate the impact of different left atrial appendage morphologies on slow vortical flow estimated by flow dynamics.

Methods:

A. Artificially created and patient-specific computed tomography-derived 3-dimensional digital models of the left main coronary artery with varying vertical take-off angulation and artery stenoses were generated. These were exported for numerical simulation to calculate the wall shear stress values and mapping in each model set.

B. Patient-specific computed tomography-derived 3-dimensional digital model sets of different left atrial appendage morphologies were exported for numerical simulation to calculate the volume and distribution of slow vortical flow. Left atrial appendage emptying was assessed.

Results:

A. The study of left main take off demonstrated that the preferred development site of atherosclerotic plaques in pathological studies corresponds to regions of low wall shear stress. Both peak wall shear stress and mean wall shear stress increased with more vertical take-off, and this relationship was accentuated by increasing stenosis severity. The more vertically angled LMCA take-off from aorta in the presence of significant stenosis severity was also associated with a larger area of low wall shear stress. These findings may explain the higher atherosclerotic plaque rupture rate and higher percentage of proximally located plaque seen in isolated left main coronary artery disease

B. For complex geometry, the Cauliflower left atrial appendage subtype contained the greatest volume of slow vortical flow at low shear rate across a range of different left atrial appendage emptying velocities. This rheological mechanistic observation correlates well with the clinical observation that the highest rate of clinical thromboembolism is seen with the Cauliflower subtype in patients with low $CHADS_2$ VASC score atrial fibrillation. However, in the presence of severely depressed left atrial appendage function differences between left atrial appendage morphology subtypes diminish.

Conclusion:

A. LMCA angulation may be an additional important factor to be considered in the clinical evaluation of the pathogenesis and progression of LMCA atheromatous disease.

B. Stasis of blood, assessed in this study by the volume of slow vortical flow, is shown to depend on left atrial appendage morphology, and also depends on left atrial appendage function/emptying velocity. Under conditions when function is mildly to moderately reduced, then it is likely that morphology is an important variable.

List of Abbreviations

3

3D: 3-Dimension

3D-QCA: 3-Dimension Quantitative Coronary Analysis

A

AF: Atrial fibrillation

C

CA: Coronary Angiography

CFD: Computational Flow Dynamic

CT: Computed Tomography

CTCA: Computed Tomography Coronary Angiography

CT_{FFR}: Fraction Flow Reserve calculated from Computed Tomography

D

DICOM: Digital Imaging and Communications in Medicine

E

EF: Ejection Fraction

F

FFR: Fraction Flow Reserve

H

HR: Hazard Ratio

I

IGES: Initial Graphics Exchange Specification

IVUS: Intravascular Ultrasound

L

LA: Left Atrium

LAA: Left Atrial Appendage

LAA PEV: Left Atrial Appendage Peak Emptying Velocity

LAA EF: Left Atrial Appendage Ejection Fraction

LAD: Left Anterior Descending

LCX: Left Circumflex

LMCA: Left Main Coronary Artery

LMCAD: Left Main Coronary Artery Disease

M

MDCT: Multi-Detector Computed Tomography

MLD: Minimal Luminal Diameter

MLA: Minimal Luminal Area

MSCT-CA: Multi-Slice Computed Tomography-Coronary Angiography

MRI: Magnetic Resonance Image

mWSS: Mean Wall Shear Stress

O

OR: Odd Ratio

P

PEV: Peak Emptying Velocity

pWSS: Peak Wall Shear Stress

Q

QCA: Quantitative Coronary Analysis

R

RCA: Right Coronary Artery

ROC: Receiver Operating Characteristic

RR: Relative Risk

S

SEC: Spontaneous Echo Contrast

SV: Stroke Volume

W

WSS: Wall Shear Stress

Chapter 1: Introduction: Numerical Simulation In Cardiovascular Medicine

1.1 Introduction

While numerical simulation has facilitated the design of aeroplanes [1], automobiles [2] and sportswear [3] since 1990s, the application of numerical simulation in medicine is limited. With advances in computation technology, numerical simulation has recently been applied increasingly in cardiovascular simulation. Examples include the mapping and measurement of wall shear stress and its correlation with atherosclerotic plaque formation in coronary arteries [4-7], surgical planning and the prediction of rupture risk of abdominal aortic aneurysms[8] and the non-invasive estimation of fractional flow reserve (CT_{FFR}) across a coronary arterial stenosis using computed tomography (CT) derived images [9, 10]. In the future this technology may guide patient-specific management and surgical planning.

1.2 Computational Fluid Dynamics (CFD)

A common method of numerical simulation used in the cardiovascular system is computational fluid dynamics (CFD) which allows simulation of the rheological properties of fluids within complex biological geometries and allows biomechanical forces to be calculated. The main principle of the numerical simulation of CFD is the analysis of the fluid domain as afinite number of small calculating units with the whole domain termed a “meshed file”. The mesh files with numerous calculating units incorporate the physical laws of conservation of mass, energy and momentum, and are then used to calculate the biomechanical vectors and rheological behaviour of the fluid flow in a given biological geometry in a set condition.

CFD simulation allows non-invasive calculation of biomechanical vectors and rheological behaviour within complex 3-dimensional geometries derived from true biological models. The sophisticated mapping and measurement of wall shear stress (WSS) and its correlation with the later development of atherosclerotic plaque and rupture in the coronary artery is a classic example of the potential power of CFD simulation [11-19]. In contrast to non-invasive CFD simulation, direct measurement of wall shear stress in the coronary artery *in vivo* provides relatively limited simple mapping of WSS which may be confounded by equipment interference and complicated by peri-procedural risk [20]. The recent development of CT_{FFR} shows the future potential of CFD simulation to favorably change clinical practice. This allows the non-invasive calculation of the FFR across a stenotic lesion in the coronary artery using the coronary artery luminal structure obtained from computed tomography without passing a pressure wire in to the coronary artery [21, 22].

The second advantage of the CFD simulation is that it allows the calculation of forces relevant to complicated geometries derived from biological structures which are not possible by direct measurement. For example, the risk of rupture of a saccular abdominal aortic aneurysm with a complex geometry cannot predicted accurately by the simple pressure derived from the simple Laplace formula. In contrast, accurate tensile stress can be calculated using CFD in such complex structure and provides a better rupture risk prediction [8].

In this thesis, the aim is to apply CFD numerical simulation in the cardiovascular system to elucidate the potential fluid dynamic mechanisms in two specific situations - the left main coronary artery and the left atrial appendage.

1.3 Left Main Coronary Artery Disease (LMCAD)

In the first project, the aim is to look at the biomechanical forces such as wall shear stress in the proximal segment of the left main coronary artery (LMCA) and how they relate to LMCA anatomy and angulation of take-off from the aortic root. Wall shear

stress has been extensively studied in coronary arteries, including the LMCA but with little clinical validation of the models used.

To achieve the goal, we first performed a detailed literature review, which identified that the isolated LMCA disease had a different distribution of plaque [23, 24] and higher incidence of plaque rupture [24] compared to LMCA disease with multi-vessel involvement [23, 25, 26]. These differences raise the possibility that local haemodynamic factors play an important role. Among haemodynamic factors, high take-off angulation LMCA from the aorta with highly (vertically) placed anomalous LMCA ostium may be considered to be malignant [27], adversely affecting local fluid dynamics.

Firstly, a LMCA morphological and anatomical survey using CT coronary angiography in order to choose physiologically relevant models was performed. Two patient-specific CT-derived models with two extreme LMCA vertical take-off angulations were chosen for further modelling. CFD simulation on LMCA was performed both with aorta attached to LMCA and detached for comparison of the results, as simulation in aortic detached LMCA results in signification reduction of simulation time. CFD simulation was then introduced to LMCA models with varying vertical take-off angle from aorta, in both artificial models and authentic patient-derived models and evaluated its impact on WSS along the LMCA.

1.4 Left Atrial Appendage Morphology (LAA Morphology)

In the second project, the aim is to investigate the rheological properties of different left atrial appendage (LAA) morphologies. Recent studies had shown four different LAA morphology subtypes are associated with different risk of stroke in patients with atrial fibrillation and with low clinical risk scores (low CHADS VASC score)[28-31]. These LAA morphology subtypes have been named as the “Chickenwing”, “Windsock”, “Cactus” and the complex “Cauliflower” morphology. To date, there is no mechanism explaining the clinical association between stroke risk and LAA

morphology. There is however older literature describing increased risk of stroke in patients with severe spontaneous echo contrast (SEC) in the left atrium [32-34].

A literature review on left atrial appendage morphology and current clinical, haemodynamic and echocardiographic parameters that predict the risk of stroke in patient in atrial fibrillation was performed. From the literature review, it appeared that both the LAA geometry and contractile function play important roles in determining the degree of shear rate and the amount of the spontaneous echo contrast (SEC, a marker of slow blood flow) in the LAA. It is speculated that the LAA morphologies with complex geometry increased the amount of slow vortical flow at low shear rate (which represents SEC seen in echocardiogram studies). Therefore, in the second study, CFD simulation will be applied to different LAA morphology subtypes while fixing the LAA function. The amount of slow vortical flow at low shear rate was then calculated for different LAA morphologies and comparison made regarding the propensity to slow vortical flow across the four different LAA morphology subtypes.

1.5 Reference

1. Tinoco, E.N., *The challenging role of computation fluid dynamics in airplane development.* American Institute of Aeronautics and Astronautics Inc, 1998: p. 161-174.
2. Kobayashi, T. and M. Tsubokura, *CFD Application in Automotive Industry*, in *100 Volumes of 'Notes on Numerical Fluid Mechanics'*, E. Hirschel and E. Krause, Editors. 2009, Springer Berlin Heidelberg. p. 285-295.
3. Marinho, D.A., et al., *Effect of wearing a swimsuit on hydrodynamic drag of swimmer.* Brazilian Archives of Biology and Technology, 2012. **55**: p. 851-856.
4. Malek, A.M., S.L. Alper, and S. Izumo, *Hemodynamic shear stress and its role in atherosclerosis.* JAMA, 1999. **282**(21): p. 2035-42.
5. Caro, C.G., J.M. Fitz-Gerald, and R.C. Schroter, *Atheroma and arterial wall shear. Observation, correlation and proposal of a shear dependent mass transfer mechanism for atherogenesis.* Proc R Soc Lond B Biol Sci, 1971. **177**(46): p. 109-59.
6. Wootton, D.M. and D.N. Ku, *Fluid mechanics of vascular systems, diseases, and thrombosis.* Annu Rev Biomed Eng, 1999. **1**: p. 299-329.
7. Zarins, C.K., et al., *Carotid bifurcation atherosclerosis. Quantitative correlation of plaque localization with flow velocity profiles and wall shear stress.* Circ Res, 1983. **53**(4): p. 502-14.
8. Vorp, D.A., *Biomechanics of abdominal aortic aneurysm.* J Biomech, 2007. **40**(9): p. 1887-902.
9. Min, J.K., et al., *Diagnostic accuracy of fractional flow reserve from anatomic CT angiography.* JAMA, 2012. **308**(12): p. 1237-45.
10. Koo, B.K., et al., *Diagnosis of ischemia-causing coronary stenoses by noninvasive fractional flow reserve computed from coronary computed tomographic angiograms. Results from the prospective multicenter DISCOVER-FLOW (Diagnosis of Ischemia-Causing Stenoses Obtained Via Noninvasive Fractional Flow Reserve) study.* J Am Coll Cardiol, 2011. **58**(19): p. 1989-97.
11. Soulis, J.V., et al., *Wall shear stress in normal left coronary artery tree.* J Biomech, 2006. **39**(4): p. 742-9.
12. Suo Jin1, Y.Y., John Oshinski1,2 , Allen Tannenbaum1, James Gruden2 and Don Giddens1, *Flow Patterns and Wall Shear Stress Distributions at Atherosclerotic-Prone Sites in a Human Left Coronary Artery - An Exploration*

Using Combined Methods of CT and Computational Fluid Dynamics. Proceedings of the 26th Annual International Conference of the IEEE EMBS 2004.

13. Verhey, J.F. and C. Bara, *Influence on fluid dynamics of coronary artery outlet angle variation in artificial aortic root prosthesis.* Biomed Eng Online, 2008. **7**: p. 9.
14. Asakura, T. and T. Karino, *Flow patterns and spatial distribution of atherosclerotic lesions in human coronary arteries.* Circ Res, 1990. **66**(4): p. 1045-66.
15. Goubergrits, L., et al., *CFD analysis in an anatomically realistic coronary artery model based on non-invasive 3D imaging: comparison of magnetic resonance imaging with computed tomography.* Int J Cardiovasc Imaging, 2008. **24**(4): p. 411-21.
16. Frauenfelder, T., et al., *In-vivo flow simulation in coronary arteries based on computed tomography datasets: feasibility and initial results.* Eur Radiol., 2007. **17**(5): p. 1291-300.
17. Wellnhofer, E., et al., *Novel non-dimensional approach to comparison of wall shear stress distributions in coronary arteries of different groups of patients.* Atherosclerosis, 2009. **202**(2): p. 483-90.
18. Yong, A.S., et al., *Intracoronary shear-related up-regulation of platelet P-selectin and platelet-monocyte aggregation despite the use of aspirin and clopidogrel.* Blood, 2011. **117**(1): p. 11-20.
19. Fry, D.L., *Certain histological and chemical responses of the vascular interface to acutely induced mechanical stress in the aorta of the dog.* Circ Res, 1969. **24**(1): p. 93-108.
20. Doriot, P.A., et al., *In-vivo measurements of wall shear stress in human coronary arteries.* Coronary Artery Dis., 2000. **11**(6): p. 495-502.
21. Ko, B.S., et al., *Combined CT coronary angiography and stress myocardial perfusion imaging for hemodynamically significant stenoses in patients with suspected coronary artery disease: a comparison with fractional flow reserve.* JACC Cardiovasc Imaging, 2012. **5**(11): p. 1097-111.
22. Tashakkor, A.Y., et al., *The Emerging Role of Cardiac Computed Tomography for the Assessment of Coronary Perfusion: A Systematic Review and Meta-analysis.* Canadian Journal of Cardiology, 2012. **28**(4): p. 413-422.
23. Fajadet, J. and A. Chieffo, *Current management of left main coronary artery disease.* European Heart Journal, 2012. **33**(1): p. 36-50.

24. Kang, S.J., et al., *Intravascular ultrasound-derived predictors for fractional flow reserve in intermediate left main disease.* JACC Cardiovasc Interv, 2011. **4**(11): p. 1168-74.
25. Thompson, C.A., et al., *Classification and atherosclerosis distribution in patients with left main coronary disease.* J Interv Cardiol, 2009. **22**(5): p. 431-6.
26. Tyczynski, P., et al., *Intravascular ultrasound assessment of ruptured atherosclerotic plaques in left main coronary arteries.* Am J Cardiol, 2005. **96**(6): p. 794-8.
27. Nishida, N., Y. Hata, and K. Kinoshita, *High takeoff of the left main coronary artery at autopsy after sudden unexpected death in a male.* Pathology, 2014. **46**(4): p. 361-4.
28. Di Biase, L., et al., *Does the left atrial appendage morphology correlate with the risk of stroke in patients with atrial fibrillation? Results from a multicenter study.* J Am Coll Cardiol, 2012. **60**(6): p. 531-8.
29. Anselmino, M., et al., *Left atrial appendage morphology and silent cerebral ischemia in atrial fibrillation patients.* Heart Rhythm, 2013.
30. Khurram, I.M., et al., *Relationship between left atrial appendage morphology and stroke in patients with atrial fibrillation.* Heart Rhythm, 2013. **10**(12): p. 1843-9.
31. Kimura, T., et al., *Anatomical characteristics of the left atrial appendage in cardiogenic stroke with low CHADS2 scores.* Heart Rhythm, 2013. **10**(6): p. 921-5.
32. Black, I.W., et al., *Left atrial spontaneous echo contrast: a clinical and echocardiographic analysis.* J Am Coll Cardiol, 1991. **18**(2): p. 398-404.
33. Black, I.W., et al., *Hematologic correlates of left atrial spontaneous echo contrast and thromboembolism in nonvalvular atrial fibrillation.* J Am Coll Cardiol, 1993. **21**(2): p. 451-7.
34. Fatkin, D., R.P. Kelly, and M.P. Feneley, *Relations between left atrial appendage blood flow velocity, spontaneous echocardiographic contrast and thromboembolic risk in vivo.* J Am Coll Cardiol, 1994. **23**(4): p. 961-9.

Chapter 2: Literature Review Left Main Coronary Artery Anatomy and Atherosclerosis

2.1 LMCA Anatomy

The left main coronary artery (LMCA) stems from the left aortic sinus, below the sinotubular junction. It branches into the left anterior descending (LAD) and left circumflex arteries (LCX) and supplies at least 75% of coronary blood flow to the left ventricle [1]. The clinical significance of LMCA disease (LMCAD) and its poor clinical prognosis have attracted extensive anatomical and angiographic analysis since the 1960s. Assessment of left main stenosis severity by fractional flow reserve (FFR) is an area of contemporary interest and is not straight forward because of the complex effects of downstream stenoses [2, 3]. Understanding the LMCA and its normal variation will be vital for successful deployment of these technologies.

2.1.1 The Normal LMCA and Its Morphological and Dimensional Parameters

2.1.1.1 Length of LMCA

The length of LMCA is determined by measuring the centreline distance originating from the ostium to the bifurcation of the LMCA. Early studies of the length of the LMCA were dominated by post-mortem autopsy and angiographic assessments. The average length in most cohorts ranges from 8 to 13.5 mm [4] with a wide range (from 1 to 26 mm). The LMCA was documented to reach 44mm in length in one angiographic case report [5]. A large retrospective analysis of the LMCA by 64 multi-slice computed tomography coronary angiography (MSCT-CA) showed that 4.7% of LMCAs were shorter than 5 mm [6], while the average length in other 64 slice MSCT-CA studies ranged from 9.9 to 11.2 mm [7-9].

Three interesting associations have been made in association with shorter LMCA arteries. Firstly, a high incidence (up to 85%) of short LMCA (<10mm) was seen in patients with bicuspid aortic valves [10]. Shorter length LMCA was associated with left dominance of the coronary vasculature in one study [11], although other investigations did not come to the same conclusion [4, 9, 12, 13]. Thirdly, a shorter LMCA stem was associated with left bundle branch block [14], and was explained as being due to increasing atherosclerosis in these subjects [15]. However, a more recent MSCT-CT cohort was not supportive of this conclusion [16]. An intravascular ultrasound (IVUS) study demonstrated significant difference in spatial location of atherosclerotic plaque in shorter LMCAs (<10mm) in comparison to longer LMCAs [17]. In this study, shorter LMCA segments (<10mm) tended to have ostial atherosclerotic plaque more than distal plaque, but did not comment on any difference in the degree of atherosclerosis according to LMCA length. Longer LMCAs have been associated with trifurcation of the distal segment rather than the usual bifurcation [18].

2.1.1.2 Shape and Size of LMCA Luminal Cross-sectional Area

MSCT-CA and IVUS, being 3-dimensional modalities, allow accurate assessment of both luminal diameter and luminal area, while angiography, being a series of 2-dimensional images, only allows measurement of LMCA diameter in each field of view with a derived luminal area. Majority of earlier studies using angiography, anatomical dissection and IVUS methods to analyse the cross-sectional area of the normal LMCA considered it be circular in shape [19-22], while only a small number described elliptic shapes [23]. Recent MSCT-CA studies reveal more typically elliptical than circular contour for the LMCA cross-section [4, 7], and highlight the importance of accurate rendering of three-dimensional configurations of the coronary artery *in vivo*, without 2-D (angiography) or fixation (post-mortem) artefact

The minimal luminal area (MLA) is an important parameter referred to IVUS literature as guiding the decision to revascularise patients with stenosis of the LMCA. A large IVUS cohort of normal LMCAs measured the mean MLA to be 16.25 mm^2 [24]. Cross-sectional areas of LMCA had been measured at proximal, mid and distal segments to provide detailed analysis, though some studies only assessed the ostium and bifurcation. The luminal area of proximal, mid and distal segments of the LMCA in one MSCT-CA study were 20.1mm^2, 14.2 $mm^2$and 15 mm^2 in men and 15.7 mm^2, 10.7 $mm^2$and 11 mm^2 in women respectively [7]. The luminal area of LMCA is also affected by LMCA length, with smaller MLA in longer LMCAs. These differences in normal LMCA are under-appreciated in clinical literature, which commonly refers to single measurements of the LMCA in deciding clinical management, regardless of the LMCA segment, the length of the LMCA or the gender of the patient.

2.1.1.3 Luminal Diameter of LMCA

Earlier studies commonly considered the LMCA as having a uniform luminal diameter and cross-sectional area along its entire length. As result, only one diameter was measured per LMCA segment in those cohorts. Representative results yielded mean LMCA diameters of 4.8-5.2mm [21] and 4.9mm [4].

As indicated earlier, more precise analysis of LMCA diameter should divide the LMCA into proximal, mid and distal segments and separately analyse results according to gender as these both affect the diameter of LMCA. One angiographic study of normal LMCA found a mean diameter of 4.5mm in all three segments in males and 4.0mm, 3.9mm and 3.8mm respectively in proximal, mid and distal segments in females [22]. Another MSCT-CA study reported mean diameters in long/short axes across proximal, mid and distal LMCA segments in males of 5.3mm/3.4mm, 4.3mm/3.9mm, 4.5mm/4mm and in females of4.8mm/4mm, 3.6mm/3.4mm, 4mm/3.3mm respectively [7]. The smaller diameters in women may be explained

by the difference in body surface area. Three-dimensional quantitative coronary artery (3D-QCA) analysis using stereoscopic reconstruction of angiographically normal LMCAs from two views of biplane coronary angiograms measured 3.96mm±0.8mm (range 2mm–6.9mm), 4.04mm ± 0.8mm (range 1.83mm–6.74mm), and 3.75mm ±0.74mm (range1.97mm–6.45mm) for the proximal, mid and distal MLD of the angiographically normal LMCA [25].

Interestingly, the normal LMCA diameter can be predicted by the diameter of its branching arteries [26]. For example, in bifurcating LMCA, the mean ratio of the diameter of the left main to the sum of the diameters of its two immediate branches was 0.65 +/- 0.04. An increase in the LMCA diameter had been observed in presence of atherosclerosis [9]. This likely due to outward remodelling of LMCA in response to plaque deposition, the so-called Glagov effect, rather than being the pre-morbid calibre of the artery [27].

2.1.1.4 The LMCA Ostium

The aortic sinus, which is also known as the sinus of Valsalva, is the initial dilated section of aortic root that houses the aortic valve cusps. Circumferentially, most coronary ostia arise from the point of maximum curvature of the aortic sinuses. Most LMCA ostia arise from the mid-third of the left posterior aortic sinus with some either positioned more anteriorly or posteriorly [7, 28]. Vertically, the LMCA ostium has been described as being located above the level of free edge of aortic cusp, on or immediate below the supra-valvular ridge [28]. The transition of the LMCA ostium to the LMCA coronary artery adopts a funnel shape in the three-dimensional configuration [7, 29].

2.1.1.5 Incidence of Bifurcation andthe Degree of Bifurcation

Most frequently, the LMCA terminates as a bifurcation, with less frequent termination as a trifurcation [4, 9, 25]. Ethnicity and gender may play a role as there are more trifurcations reported (60%) in non-Caucasian female cohorts [30]. The LMCA gives rise to the LAD and LCX arteries and the bifurcation angle between these arteries scan vary significantly. The LMCA bifurcation angle is defined as the angle measurement between the LAD and LCX arteries.

Anatomical studies have shown that the bifurcation angle is approximately 86.7±28.8° (range=40-165°) [4]. Most MSCT-CA studies have measured the bifurcation angle at the end-diastolic phase of the cardiac cycle, but also allow assessment of the angle in the end-systolic phase. Earlier16-slice MSCT-CA studies demonstrated a mean angle of 80°±27° (range 34° to 180°) [31]. Recent 64-slice MSCT-CA studies reported end-diastolic mean bifurcation angles of 69.3°± 33.3° (range=14°-200°) [9], 72° ±22°[32],84°±27° (range= 23°-173°) [18] and 87.8°±22.3°(range= 68.8°-101.4°) [33]. 3D-QCA of the LMCA bifurcation of normal LMCAs derived using two views from a biplane coronary angiogram correlated well with both histological and MSCT-CA data, with average end-diastolic angles of 95.6°±23.6°[34]and 75°±25°[25].

There appear to be a number of clinical associations and ramifications of varying LMCA bifurcation angles. Firstly, a wider LMCA bifurcation angle is correlated with higher incidence of atherosclerotic lesions in LMCA [25, 33, 35]. There is no clear cut-off value at which this occurs, but one reference refers to bifurcation angles greater than 88.5° being associated with a higher incidence of atherosclerotic lesions. Secondly, increasing age seems to be associated with increased bifurcation angle [25]. On the other hand, there is a reduction of bifurcation angle after percutaneous intervention to the LMCA, but the change in angle does not appear to translate into any clinical outcome at long term follow up [34]. Lastly, and importantly, bifurcation angles change throughout the cardiac cycle, reducing in systole [18, 34], though the significance of cyclical variations is unclear.

2.1.1.6 Spatial Relationship of the LMCA to its Ostium, the Aortic Wall andthe Central Axis of the Aorta

Few studies have assessed the spatial relationship of the LMCA to its ostium and to the aortic wall. In one anatomical study 56.8% of LMCAs were anterior to the ostium and 74.7% were caudal to the ostium on the vertical plane [4].

One angiographic study used a semi-geographical coordinate system in Euclidean space to describe the vector length of LMCA (the shortest distance from centre of ostium to centre point of proximal, mid and bifurcation regions of the LMCA), the vertical (positive if downward) and the horizontal angle (positive if toward left hand side) relative to the LMCA ostium [19]. The mean results for (vector length(r)/vertical angle(Φ)/horizontal angle(θ) as illustrated in Figure 2.1) for proximal, mid and distal segment of LMCA were 3mm/83°/7°, 7mm/80°/4° and 11mm/79°/0°respectively [22]. A recent CT study defined the take-off angles of the LMCA to the adjacent aortic wall in both axial and sagittal planes [7]. In the axial plane the LMCA comes off at 44.4±10° for posteriorly situated ostia, and 106±15° for mid or anteriorly situated ostia respectively. In the vertical plane, the mean take-off LMCA angle to aortic wall caudally is 54.9±20° (angle between caudal perspective of LMCA wall to aortic wall) and cranially 98.1±16° (angle between cranial perspective of LMCA wall to aortic wall). Both vector description and take-off angulation of LMCA provide additional anatomical and possible biomechanical parameters in proximal and mid segments of LMCA.

Figure 2.1

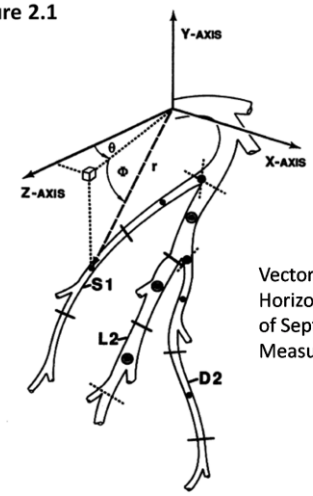

Vector Length (r), Vertical Angulation (Φ) and Horizontal Angulation (θ) from LMCA Ostium of Septal Vessel (S1). LMCA Can be Measured Using the Same Method

Figure 2.1: *Vector Length (r), Vertical Angulation (Φ) and Horizontal Angulation (ϑ) from LMCA Ostium of Septal Vessel (S1). LMCA Can be Measured Using the Same Method*

2.1.2 Embryological Development of Proximal Coronary Artery Segments

The embryological development of the coronary artery circulation involves three distinctive processes, including vasculogenesis, angiogenesis and arteriogenesis [36, 37]. In the early embryonic stages, the coronary circulation does not exist and blood flows through the cardiac lumen to supply cardiac tissue through simple diffusion. As the wall of cardiac tissues thickens, hypoxia drives the formation of a dedicated coronary vasculature [38]. The initial step is the formation of a vascular plexus from blood islands over the epicardial surface via a process known asvasculogenesis [39, 40]. These blood islands contain aggregates of mesenchymal precursor cells and haematopoietic stem cells which proliferate to form a vascular plexus. Angiogenesis follows via the generation of capillaries sprouting from the newly formed vascular network and their maturing into stable vessels [38, 41]. Both vasculogenesis and angiogenesis are driven by the hypoxic gradient, triggered by lack of oxygenation as result of simple diffusion. Connections of the proximal parts of the coronary arteries to the aorta occur at a later stage in embryonic development. Before the 1980s, it always had been controversial as to whether

coronary arteries bud and branch from the aortic sinus of Valsalva to connect the epicardial coronary artery [42] or resulted as an in-growth of coronary vessels into aorta. The observation that coronary vessels were always evident in the wall of the aortic sinus before coronary orifice formation favoured the model of in-growth of coronary vessels into the aorta [43]. It is currently accepted that the proximal artery develops from the complex capillary network formed by vasculogenesis and angiogenesis and then invades into the aorta in a controlled fashion. Multiple endothelial strands from the peri-truncal ring of vascular structures penetrate the aorta at the left and right aortic sinuses of Valsalva. These strands then fuse together with only one channel remaining patent to become the definitive coronary artery in each aortic sinus [44]. Apoptosis is then triggered, leading to formation of the coronary arterial orifice at the site of the emerging coronary arteries [44, 45]. Arteriogenesis is then activated by exposure to high aortic pressure once patent connections are established between the aorta and the coronary vessels, leading to arterialisation of these vessels via extensive tissue re-organization and remodelling. This in-growth theory of primitive vessels to form the LMCA provides a plausible explanation of anatomical variations and congenital anomalies of LMCA [46]. Anatomical variations such as the LMCA length and course, its varying attachment angle to the aorta and the position of attachment at different sites within the sinus of Valsalva can be explained by this process. It is thought that other geometrical features such as the diameter and bifurcation angle of LMCA may well be determined by the vascular plexuses formed as a result of angiogenesis.

2.1.3 LMCA Anomaly

The commonest anomaly is the absence of the LMCA, with the left anterior descending and left circumflex arteries arising separately from the coronary sinus. A single coronary artery origin is observed when both left and right coronary arteries arise from one origin or when one single coronary artery supplies the whole heart. These variations are considered clinically benign. In addition, rare congenital LMCA

atresia can occur when the LMCA ends blindly with no LMCA ostium. Congenital LMCA atresia results in blood flow which is centripetal (retrograde flow from smaller to larger calibre vessels which may resemble both LAD and LCX) rather than centrifugal (anterograde flow from larger proximal vessels to the smaller distal vessels) [47]. Myocardial ischaemia can occur under these conditions.

Other anomalies of the LMCA origin range from minor degrees of displacement of the LMCA origin on the aortic sinus to highly anomalous origin from the pulmonary artery. Minor variations in aortic origin include vertical and/or horizontal displacement of the LMCA origin. More highly positioned LMCA origins vertically above the aortic coronary sinus result in so-called "high take-off" LMCA with sharp angulation and are uncommon. There is conflicting opinion as to whether this type of minor variation carries malignant [48, 49] or benign clinical outcome [50]. A horizontally displaced LMCA origin can include origin from the right aortic coronary sinus. This anomaly can be associated with a slit-like hypoplastic ostium of the LMCA and/or a course of the left coronary artery between the aorta and pulmonary artery – both of which may be linked with sudden cardiac death [51]. Anomalous origin of the LMCA from the pulmonary artery is associated with myocardial ischaemia, infarction or ventricular arrhythmia. It was first described as Bland-Garland-White syndrome [52] in 1933. Its incidence is approximately 0.26% and most infants with the syndrome do not survive into adulthood if not surgically corrected. Corrective surgery in adulthood can prevent ventricular tachyarrhythmia and sudden cardiac death [53].

2.2 Definition of LMCA Disease and Prognosis

With the advent of coronary angiography, the poor long term prognosis of LMCA disease was recognised [54] and different revascularization strategies have since been developed to improve its clinical outcome. LMCA disease should be considered if there is more than 50% diameter stenosis. Overall, the incidence of LMCA disease in a recent CT series was 2.8% [55]. The risk of progression and

clinical outcome are strongly associated with the initial severity of stenosis at time of diagnosis. Early literature demonstrated that if the LMCA stenosis was between 50-70% the survival rate was 91% at 1year and 66% at 3years, whereas if >70%, then survival was 72% at 1 year and 41% at 3 years [54].

Intermediate severity stenosis of the LMCA refers to approximately 50% stenosis on coronary angiography and this can present a management dilemma. Functionally significant (based on ischemia or reduced fractional flow reserve) intermediate severity LMCA disease has higher mortality over the short and intermediate term, and therefore requires constant monitoring and possible early intervention [56].

2.2.1 Atherosclerosis

Atherosclerosis is the commonest aetiology for LMCA disease. It develops and accelerates as results of multiple clinical risk factors including hypertension, diabetes mellitus, genetic pre-disposition, cigarette smoking and dyslipidemia. The contribution of specific local haemodynamic factors has been suggested but is relatively poorly studied.

LMCA disease is commonly associated with diffuse coronary artery and other vascular disease, as systemic effects from cardiovascular risk factors likely play a dominant role in leading to the diffuse deposition of atherosclerotic plaque. One study showed that 40% of patients with LMCA disease had carotid stenosis whereas only 5.3% of those with single vessel disease had carotid stenosis [57]. Similarly, the LMCA is almost always involved when there is multi-vessel disease [58, 59]. Isolated LMCA disease is uncommon and accounts for around 1% of all LMCA disease [60]. The specific pattern of distribution and location of LMCA plaque suggests local haemodynamic factors also play a role.

2.2.2 Spatial Distribution and Location of LMCA Atherosclerotic Plaque

The spatial distribution of atheromatous plaque was studied in the 1970's using histopathological studies of necropsy subjects which allowed detailed mapping on the spatial distribution of atherosclerosis in the LMCA. These studies suggested early plaque development tends to locate in the ostial and distal segments involving the bifurcation [61] (Figure 2.2). In addition, atherosclerotic lesions in the proximal segment of the LMCA tend to arise from 10 to 12 o'clock section of left main ostium, if viewed as a clock face and from inside of the aorta. Atheroma is usually located between 10-2o'clock in the RCA [62] (Figure2.3). Approximately 65% of LMCA atherosclerotic plaque resides in the distal segment of LMCA, involving the bifurcation, while the ostial segment accounts for 23%, and the trunk of the LMCA is least involved [63, 64]. This is particularly the case with longer LMCA (>10mm), the presence of multi-vessel disease and diabetes mellitus [60]. On the other hand, isolated ostial or trunk disease of the LMCA is well recognised [64, 65]. Shorter LMCA segments (<10 mm) tend to have ostial atherosclerotic plaque more than distal [17]. Female gender carries a greater risk of ostial LMCA lesions than male gender [66].

Figure 2.2

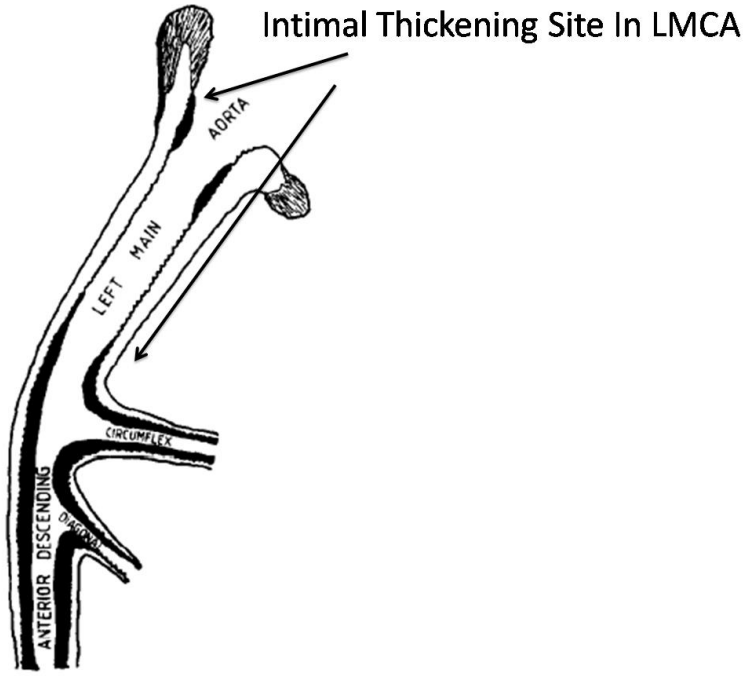

Figure 2.2: *Distribution and Location of Early Intimal Thickening (Precursor to Atherosclerosis) in LMCA [61]. Intimal Thickening Tends to Occur in the Ostial/Proximal and Distal LMCA Segments.*

Figure 2.3

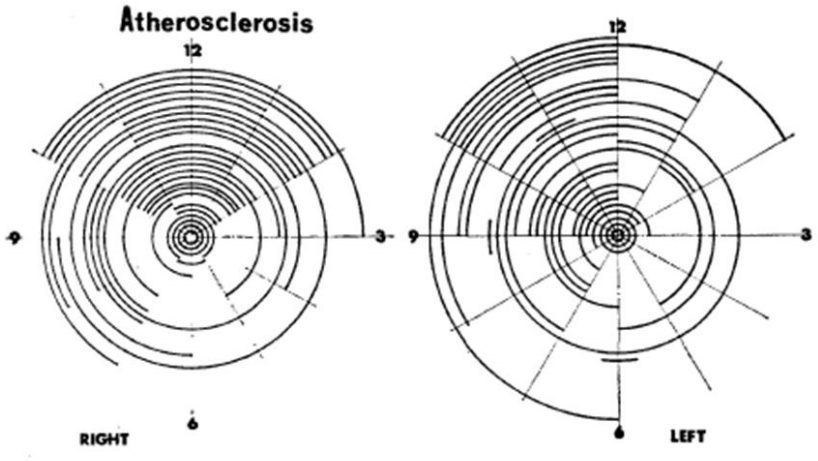

Figure 2.3: *Location of the Atherosclerotic Plaque Around the Left and Right Coronary Ostia [62].*

2.2.3 Sites of LMCA Plaque Rupture

Plaque rupture in the LMCA plaque occurs less frequently when compared to the proximal segment of the three main coronary arteries. It has been suggested that "thin-cap atheroma" with necrotic-rich core plaques which are at high risk for rupture are commonly seen in the proximal segment of the main coronary arteries but are uncommon in the LMCA [67, 68]. LMCA plaques have less necrotic core and resemble the plaque composition found in the more distal segments of left coronary artery. Interestingly, lesions in the distal LMCA plaque have higher necrotic core content compared to proximal LMCA plaque [69]. This is supported by the one retrospective IVUS study that showed that all LMCA plaque ruptures occurred in the distal half of the LMCA [70]. However, a recent IVUS study with 55 consecutive cases involving only isolated intermediate LMCA stenosis showed 77% of LMCA plaque ruptures occurred in either proximal segments or the shaft of the LMCA [65].

2.2.4 Potential Influence by Local Haemodynamics - Wall Shear Stress

The pivotal biomechanical force that contributes to atherosclerotic plaque formation or rupture is wall shear stress (WSS). In the presence of pulsatile blood flow in the coronary artery, blood flow exerts a biomechanical stress to the luminal side of arterial wall. The tangential stress exerted by flowing blood, termed the wall shear stress, is perpendicular to the tensile pressure resulting from the difference of systolic and diastolic pressure difference.

Perturbation of coronary arterial WSS has been implicated in the development and progression of atheromatous plaques, as well as the pathogenesis of plaque rupture and thrombosis. Previous studies have shown that regions of relatively low shear stress within the arterial tree have higher propensity towards atheroma formation [71] due to endothelial remodelling [72] and intimal hyperplasia [73, 74]. High WSS on the other hand, has been shown *in vitro* to contribute to platelet activation and endothelial erosion [75, 76], and may lead to plaque rupture.

In LMCA, most WSS studies emphasize the distal segment, involving the bifurcation and the flow divider. Fewer studies have specifically analysed the WSS location and distribution in the proximal segment of LMCA, while no-specific attention has been given to address the how WSS and its distribution been affected by the geometrical factors such as variation in take-off angle of the LMCA from aorta [77-79].

2.3 Comment: Isolated LMCA Disease as a Distinct Entity

The LMCA is interesting in its anatomical and morphological features with varying congenital anomalies, perplexing embryological development and adverse prognostic clinical manifestation when significantly diseased. Through LMCA literature review, there are two apparently unrelated observations which may share

certain common associations. Firstly, isolated LMCA disease tends to have plaque deposition in the proximal LMCA segment [64, 65] and these plaques have a higher rate of plaque rupture [65] when compare to more usual LMCA disease with multi-vessel involvement [63, 64, 70]. The particular location of the more proximally located plaque at between 10-12 o'clock and higher plaque rupture rate suggests local haemodynamic factors likely play an important role in isolated LMCA disease. Secondly the sharp take-off angulation of LMCA from aorta is expected to alter local fluid dynamics and may be a potential source of variation in clinical outcome. The LMCA with high vertically placed anomalous LMCA ostium (vertically sharp take-off LMCA from aorta) may therefore not be a harmless anomaly [49] as previously thought. Since the LMCA take-off angulation can affect the local fluid dynamics this raises the question as to whether take-off angulation determines preferential proximal plaque location and higher plaque rupture. The aim of the studies on LMCA fluid dynamics in this thesis were to investigate the effects of LMCA angulation on wall shear stress under basal conditions and under conditions of coronary stenosis. The hypothesis is that LMCA with higher take off will have lower shear stress in the area of preferential plaque formation- the area of 10-12 o'clock- and that in the presence of coronary stenosis, LMCA with higher take off will increase wall shear stress and increase the risk of plaque rupture.

2.4 Reference

1. Kalbfleisch, H. and W. Hort, *Quantitative study on the size of coronary artery supplying areas postmortem.* American Heart Journal, 1977. **94**(2): p. 183-8.
2. Yong, A.S., et al., *Fractional flow reserve assessment of left main stenosis in the presence of downstream coronary stenoses.* Circ Cardiovasc Interv, 2013. **6**(2): p. 161-5.
3. Daniels, D.V., et al., *The impact of downstream coronary stenoses on fractional flow reserve assessment of intermediate left main disease.* JACC Cardiovasc Interv, 2012. **5**(10): p. 1021-5.
4. Reig, J. and M. Petit, *Main trunk of the left coronary artery: anatomic study of the parameters of clinical interest.* Clinical Anatomy, 2004. **17**(1): p. 6-13.
5. Surucu, H. and M. Meric, *Review of the literature: The longest documented left main coronary artery.* Int J Cardiol, 2012.
6. Erol, C. and M. Seker, *The prevalence of coronary artery variations on coronary computed tomography angiography.* Acta Radiol, 2012. **53**(3): p. 278-84.
7. Zeina, A.R., U. Rosenschein, and E. Barmeir, *Dimensions and anatomic variations of left main coronary artery in normal population: multidetector computed tomography assessment.* Coronary Artery Dis., 2007. **18**(6): p. 477-82.
8. Cademartiri, F., et al., *Prevalence of anatomical variants and coronary anomalies in 543 consecutive patients studied with 64-slice CT coronary angiography.* European Radiology, 2008. **18**(4): p. 781-91.
9. Christensen, K.N., et al., *Anatomic assessment of the bifurcation of the left main coronary artery using multidetector computed tomography.* Surg Radiol Anat, 2010. **32**(10): p. 903-9.
10. Johnson, A.D., J.H. Detwiler, and C.B. Higgins, *Left coronary artery anatomy in patients with bicuspid aortic valves.* Br Heart J, 1978. **40**(5): p. 489-93.
11. Kronzon, I., P. Deutsch, and E. Glassman, *Length of the left main coronary artery: its relation to the pattern of coronary arterial distribution.* Am J Cardiol, 1974. **34**(7): p. 787-9.
12. Penther, P., et al., *The length of the left main coronary artery: pathological features.* American Heart Journal, 1977. **94**(6): p. 705-9.
13. Nowak, D., et al., *No relationship between the length of the left coronary artery main stem and the type of coronary vasculature in human fetuses from*

a morphological perspective. Medical Science Monitor, 2009. **15**(1): p. CR20-5.

14. Lewis, C.M., et al., *Coronary arteriographic appearances in patients with left bundle-branch block.* Circulation, 1970. **41**(2): p. 299-307.
15. Gazetopoulos, N., et al., *Length of main left coronary artery in relation to atherosclerosis of its branches. A coronary arteriographic study.* Br Heart J, 1976. **38**(2): p. 180-5.
16. Cademartiri, F., et al., *Assessment of left main coronary artery atherosclerotic burden using 64-slice CT coronary angiography: correlation between dimensions and presence of plaques.* Radiol Med, 2009. **114**(3): p. 358-69.
17. Maehara, A., et al., *Intravascular ultrasound assessment of the stenoses location and morphology in the left main coronary artery in relation to anatomic left main length.* Am J Cardiol, 2001. **88**(1): p. 1-4.
18. Gauss, S., et al., *Analysis of left main coronary artery and branching geometry by coronary CT angiography.* Int J Cardiol, 2011. **146**(3): p. 469-70.
19. Leung, W.H., M.L. Stadius, and E.L. Alderman, *Determinants of normal coronary artery dimensions in humans.* Circulation, 1991. **84**(6): p. 2294-306.
20. St Goar, F.G., et al., *Intravascular ultrasound imaging of angiographically normal coronary arteries: an in vivo comparison with quantitative angiography.* Journal of the American College of Cardiology, 1991. **18**(4): p. 952-8.
21. Vieweg, W.V., J.S. Alpert, and A.D. Hagan, *Caliber and distribution of normal coronary arterial anatomy.* Cathet Cardiovasc Diagn, 1976. **2**(3): p. 269-80.
22. Dodge, J.T., Jr., et al., *Lumen diameter of normal human coronary arteries. Influence of age, sex, anatomic variation, and left ventricular hypertrophy or dilation.* Circulation, 1992. **86**(1): p. 232-46.
23. Ge, J., et al., *Intravascular ultrasound imaging of angiographically normal coronary arteries: a prospective study in vivo.* Br Heart J, 1994. **71**(6): p. 572-8.
24. Fassa, A.A., et al., *Intravascular ultrasound-guided treatment for angiographically indeterminate left main coronary artery disease: a long-term follow-up study.* Journal of the American College of Cardiology, 2005. **45**(2): p. 204-11.
25. Rubinshtein, R., et al., *Anatomic features of the left main coronary artery and factors associated with its bifurcation angle: A 3-dimensional quantitative coronary angiographic study.* Catheterization & Cardiovascular Interventions, 2011.

26. Laslett, L., *Normal left main coronary artery diameter can be predicted from diameters of its branch vessels.* Clin Cardiol, 1995. **18**(10): p. 580-2.
27. Berry, C., et al., *Remodeling is a more important determinant of lumen size than atheroma burden in left main coronary artery disease.* American Heart Journal, 2010. **160**(1): p. 188-194 e1.
28. Turner, K. and V. Navaratnam, *The positions of coronary arterial ostia.* Clinical Anatomy, 1996. **9**(6): p. 376-80.
29. Aviram, G., et al., *Coronary ostium-straight tube or funnel-shaped? A computerized tomographic coronary angiography study.* Acute Card Care, 2006. **8**(4): p. 224-8.
30. Baptista, C.A., L.J. DiDio, and J.C. Prates, *Types of division of the left coronary artery and the ramus diagonalis of the human heart.* Jpn Heart J, 1991. **32**(3): p. 323-35.
31. Pflederer, T., et al., *Measurement of coronary artery bifurcation angles by multidetector computed tomography.* Investigative Radiology, 2006. **41**(11): p. 793-8.
32. Kawasaki, T., et al., *The bifurcation study using 64 multislice computed tomography.* Catheterization & Cardiovascular Interventions, 2009. **73**(5): p. 653-8.
33. Rodriguez-Granillo, G.A., et al., *Multislice CT coronary angiography for the detection of burden, morphology and distribution of atherosclerotic plaques in the left main bifurcation.* The International Journal of Cardiovascular Imaging, 2007. **23**(3): p. 389-92.
34. Girasis, C., et al., *3-Dimensional bifurcation angle analysis in patients with left main disease: a substudy of the SYNTAX trial (SYNergy Between Percutaneous Coronary Intervention with TAXus and Cardiac Surgery).* JACC Cardiovasc Interv, 2010. **3**(1): p. 41-8.
35. Sun, Z. and Y. Cao, *Multislice CT angiography assessment of left coronary artery: correlation between bifurcation angle and dimensions and development of coronary artery disease.* Eur J Radiol, 2011. **79**(2): p. e90-5.
36. Loukas, M., et al., *The normal and abnormal anatomy of the coronary arteries.* Clinical Anatomy, 2009. **22**(1): p. 114-28.
37. Smart, N., K.N. Dube, and P.R. Riley, *Coronary vessel development and insight towards neovascular therapy.* Int J Exp Pathol, 2009. **90**(3): p. 262-83.
38. Carmeliet, P., *Angiogenesis in health and disease.* Nat Med, 2003. **9**(6): p. 653-60.

39. Risau, W. and I. Flamme, *Vasculogenesis.* Annu Rev Cell Dev Biol, 1995. **11**: p. 73-91.
40. Bernanke, D.H. and J.M. Velkey, *Development of the coronary blood supply: changing concepts and current ideas.* Anat Rec, 2002. **269**(4): p. 198-208.
41. Risau, W., *Mechanisms of angiogenesis.* Nature, 1997. **386**(6626): p. 671-4.
42. Hutchins, G.M., A. Kessler-Hanna, and G.W. Moore, *Development of the coronary arteries in the embryonic human heart.* Circulation, 1988. **77**(6): p. 1250-7.
43. Bogers, A.J., et al., *Development of the origin of the coronary arteries, a matter of ingrowth or outgrowth?* Anat Embryol (Berl), 1989. **180**(5): p. 437-41.
44. Ando, K., et al., *Development of proximal coronary arteries in quail embryonic heart: multiple capillaries penetrating the aortic sinus fuse to form main coronary trunk.* Circ Res, 2004. **94**(3): p. 346-52.
45. Velkey, J.M. and D.H. Bernanke, *Apoptosis during coronary artery orifice development in the chick embryo.* Anat Rec, 2001. **262**(3): p. 310-7.
46. Silva-Junior, G.d.O., S.W.d.S. Miranda, and C.A. Mandarim-de-Lacerda, *Origin and Development of the Coronary Arteries.* International Journal of Morphology, 2009. **27**: p. 891-898.
47. MURESIAN, H., *Coronary arterial anomalies and variations.* Mædica - a Journal of Clinical Medicine, 2006. **1(4)**(1): p. 11.
48. Menke, D.M., B.F. Waller, and J.E. Pless, *Hypoplastic coronary arteries and high takeoff position of the right coronary ostium. A fatal combination of congenital coronary artery anomalies in an amateur athlete.* Chest, 1985. **88**(2): p. 299-301.
49. Nishida, N., Y. Hata, and K. Kinoshita, *High takeoff of the left main coronary artery at autopsy after sudden unexpected death in a male.* Pathology, 2014. **46**(4): p. 361-4.
50. Rosenthal, R.L., I.A. Carrothers, and J.M. Schussler, *Benign or malignant anomaly? Very high takeoff of the left main coronary artery above the left coronary sinus.* Tex Heart Inst J, 2012. **39**(4): p. 538-41.
51. Liberthson, R.R., *Sudden Death from Cardiac Causes in Children and Young Adults.* New England Journal of Medicine, 1996. **334**(16): p. 1039-1044.
52. Bland, E.F., P.D. White, and J. Garland, *Congenital anomalies of the coronary arteries: Report of an unusual case associated with cardiac hypertrophy.* American Heart Journal, 1933. **8**(6): p. 787-801.

53. Karunadasa, R., et al., *Anomalous Origin of Left Coronary Artery from the Pulmonary Artery: Does the Management in the Adult differ from that of the Infant? Four Cases of the Bland–White–Garland syndrome.* Heart, Lung and Circulation, 2007. **16, Supplement 3**(0): p. S29-S33.
54. Conley, M.J., et al., *The prognostic spectrum of left main stenosis.* Circulation, 1978. **57**(5): p. 947-52.
55. Gemici, G., et al., *Prevalence of left main coronary artery disease among patients referred to multislice computed tomography coronary examinations.* The International Journal of Cardiovascular Imaging, 2009. **25**(4): p. 433-438.
56. Gyenes, G., et al., *The prognostic importance of nonsignificant left main coronary artery disease in patients undergoing percutaneous coronary intervention.* Journal of the American College of Cardiology, 2006. **48**(2): p. 276-80.
57. Kallikazaros, I., et al., *Carotid artery disease as a marker for the presence of severe coronary artery disease in patients evaluated for chest pain.* Stroke, 1999. **30**(5): p. 1002-7.
58. Serruys, P.W., et al., *Percutaneous coronary intervention versus coronary-artery bypass grafting for severe coronary artery disease.* N Engl J Med, 2009. **360**(10): p. 961-72.
59. Taggart, D.P., et al., *Revascularization for unprotected left main stem coronary artery stenosis stenting or surgery.* J Am Coll Cardiol, 2008. **51**(9): p. 885-92.
60. Mahajan, N., et al., *Isolated and significant left main coronary artery disease: demographics, hemodynamics and angiographic features.* Angiology, 2006. **57**(4): p. 464-77.
61. Velican, C. and D. Velican, *Natural resistance to atherosclerosis exhibited by the first centimeter of left and right coronary arteries.* Atherosclerosis, 1984. **50**(2): p. 173-81.
62. Kanoh, T., R. Okada, and K. Kitamura, *A Morphological Study on the Coronary Ostia In Human Autopsy Hearts*

With Special References on the Funnel-Shaped Structure, Overhang Phenomenon and Their Clinical Significance. Japanese Journal of Medicine, 1977. **16**(3): p. 205-214.
63. Thompson, C.A., et al., *Classification and atherosclerosis distribution in patients with left main coronary disease.* J Interv Cardiol, 2009. **22**(5): p. 431-6.

64. Fajadet, J. and A. Chieffo, *Current management of left main coronary artery disease.* European Heart Journal, 2012. **33**(1): p. 36-50.
65. Kang, S.J., et al., *Intravascular ultrasound-derived predictors for fractional flow reserve in intermediate left main disease.* JACC Cardiovasc Interv, 2011. **4**(11): p. 1168-74.
66. Darabian, S., et al., *Ostial lesions of left main and right coronary arteries: demographic and angiographic features.* Angiology, 2008. **59**(6): p. 682-7.
67. von Birgelen, C., et al., *Plaque distribution and vascular remodeling of ruptured and nonruptured coronary plaques in the same vessel: an intravascular ultrasound study in vivo.* Journal of the American College of Cardiology, 2001. **37**(7): p. 1864-1870.
68. Hong, M.-K., et al., *The Site of Plaque Rupture in Native Coronary Arteries: A Three-Vessel Intravascular Ultrasound Analysis.* Journal of the American College of Cardiology, 2005. **46**(2): p. 261-265.
69. Valgimigli, M., et al., *Plaque composition in the left main stem mimics the distal but not the proximal tract of the left coronary artery: influence of clinical presentation, length of the left main trunk, lipid profile, and systemic levels of C-reactive protein.* Journal of the American College of Cardiology, 2007. **49**(1): p. 23-31.
70. Tyczynski, P., et al., *Intravascular ultrasound assessment of ruptured atherosclerotic plaques in left main coronary arteries.* Am J Cardiol, 2005. **96**(6): p. 794-8.
71. Caro, C.G., J.M. Fitz-Gerald, and R.C. Schroter, *Atheroma and arterial wall shear. Observation, correlation and proposal of a shear dependent mass transfer mechanism for atherogenesis.* Proc R Soc Lond B Biol Sci, 1971. **177**(46): p. 109-59.
72. Malek, A.M., S.L. Alper, and S. Izumo, *Hemodynamic shear stress and its role in atherosclerosis.* JAMA, 1999. **282**(21): p. 2035-42.
73. Wootton, D.M. and D.N. Ku, *Fluid mechanics of vascular systems, diseases, and thrombosis.* Annu Rev Biomed Eng, 1999. **1**: p. 299-329.
74. Zarins, C.K., et al., *Carotid bifurcation atherosclerosis. Quantitative correlation of plaque localization with flow velocity profiles and wall shear stress.* Circ Res, 1983. **53**(4): p. 502-14.
75. Yong, A.S., et al., *Intracoronary shear-related up-regulation of platelet P-selectin and platelet-monocyte aggregation despite the use of aspirin and clopidogrel.* Blood, 2011. **117**(1): p. 11-20.

76. Fry, D.L., *Certain histological and chemical responses of the vascular interface to acutely induced mechanical stress in the aorta of the dog.* Circ Res, 1969. **24**(1): p. 93-108.
77. Verhey, J.F. and C. Bara, *Influence on fluid dynamics of coronary artery outlet angle variation in artificial aortic root prosthesis.* Biomed Eng Online, 2008. **7**: p. 9.
78. Suo Jin1, Y.Y., John Oshinski1,2 , Allen Tannenbaum1, James Gruden2 and Don Giddens1, *Flow Patterns and Wall Shear Stress Distributions at Atherosclerotic-Prone Sites in a Human Left Coronary Artery - An Exploration Using Combined Methods of CT and Computational Fluid Dynamics.* Proceedings of the 26th Annual International Conference of the IEEE EMBS 2004.
79. Suo, J., J.N. Oshinski, and D.P. Giddens, *Blood flow patterns in the proximal human coronary arteries: relationship to atherosclerotic plaque occurrence.* Molecular & Cellular Biomechanics: MCB, 2008. **5**(1): p. 9-18.

Chapter 3: Anatomical and Morphological Survey of the Left Main Coronary Artery by Computed Tomography Coronary Angiography

3.1 Introduction

Recent years, there have been substantial improvements in the spatial and temporal resolution of the multi-detector computed tomography (MDCT) coronary angiography and the viewing software. Multiple studies have used this modality to research the LMCA but almost all the MDCT studies have performed measurements only during the diastolic phase as image acquisition during diastolic phase provides better imaging quality of coronary artery [3]. Analysis of the LMCA morphological and anatomical change in both systolic and diastolic phases of the cardiac cycle is required to evaluate if LMCA parameters change with the cycle and assist in determining the need for complex numerical simulation in both systolic and diastolic phases.

A descriptive survey of the LMCA in consecutive adults was conducted using computed tomography (CT) coronary angiography; with the aim to describe the anatomical and morphological features of LMCA in systolic and diastolic phases of cardiac cycle. This provides important parameters that inform modelling studies undertaken in subsequent chapter 4.

3.2 Method

100 consecutive dual-source MDCT coronary angiography studies from 2008 to 2009 performed in the Radiology department of Concord Repatriation General Hospital were analysed retrospectively. Images were acquired using a dual source 64-slice

Siemens Definition MDCT scanner (Siemens Medical Solutions, Forchheim, Germany). Retrospective ECG-gated scanning was used with patients routinely pre-medicated with 600µg of nitroglycerin. Beta-blockers were only given when pre-scan heart rates exceeded 90 beats per minute. Axial images were reconstructed at 0.75mm slice thickness and 0.3mm increment to deliver a final spatial resolution of 0.33mm x 0.33mm x 0.75mm for reconstruction of 3D models. Measurements of the LMCA were obtained using a Siemens workstation (Siemens Medical Solutions, Forchheim, Germany). The morphological and anatomical measurement were performed at (70% phase) and systolic (20% phase) phases of the cardiac cycle.

3.2.1 LMCA Morphology, Anatomical Features And Their Definition

3.2.1.1 LMCA Centreline

Both LMCA “centreline length” and “vector length” were both measured. The LMCA centreline length was defined as the LMCA centreline distance between the midpoint of the LMCA ostium and the LMCA bifurcation point. The vector length was defined as the shortest distance between the midpoint of the ostium and bifurcation point. Tortuosity index of the LMCA has also derived from centreline length and vector length ratio, adapting the simple arc to chord length ratio of the blood vessel [4].

Figure 3.1

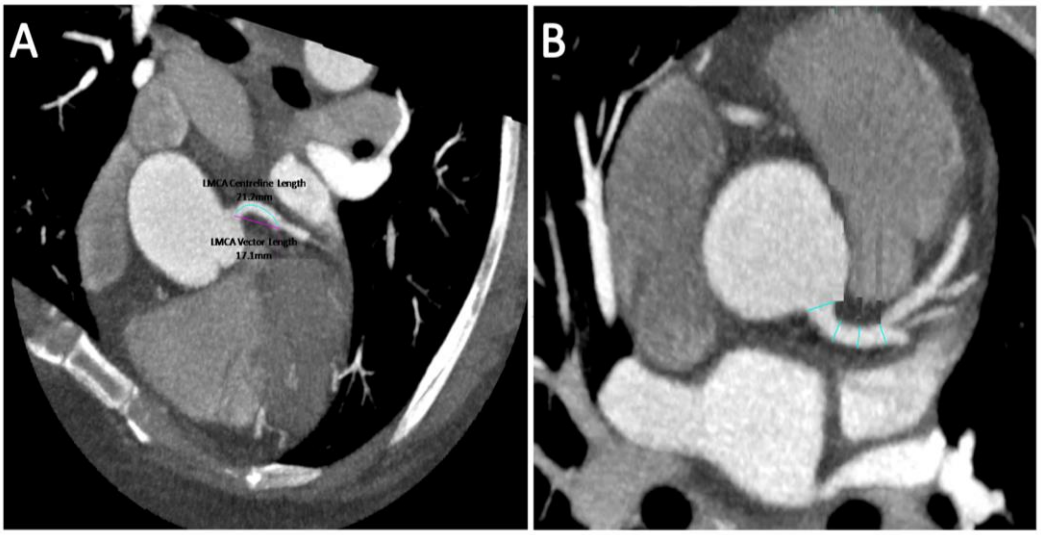

Figure 3.1 A. *LMCA Centreline Length and LMCA Vector Length****. B.*** *Division of LMCA Segments into Proximal, Mid and Distal Segment.*

3.2.1.2 LMCA Luminal Diameter and Cross-sectional Area

The LMCA was subdivided into proximal, mid and distal segments with each segment approximating one-third of the entire LMCA centreline length. The luminal diameters in both short and long axes (same diameter if circular cross-section) and cross-sectional areas in individual segments were measured using the in-built tool set of the imaging viewer. The LMCA at each individual segment was planed carefully to ensure true cross-sectional values were measured for all parameters.

3.2.1.3 LMCA Angulation

The LMCA angulations were measured with reference to LMCA ostium. The LMCA vector take-off angulation is defined as the vertical (sagittal plane) and horizontal

(axial plane) angles between the vector and the ostial axis (an axis perpendicular to the tangential plane of LMCA ostium and passing through LMCA center, Fig 3.2). The LMCA bifurcation angulation was also measured.

Figure 3.2

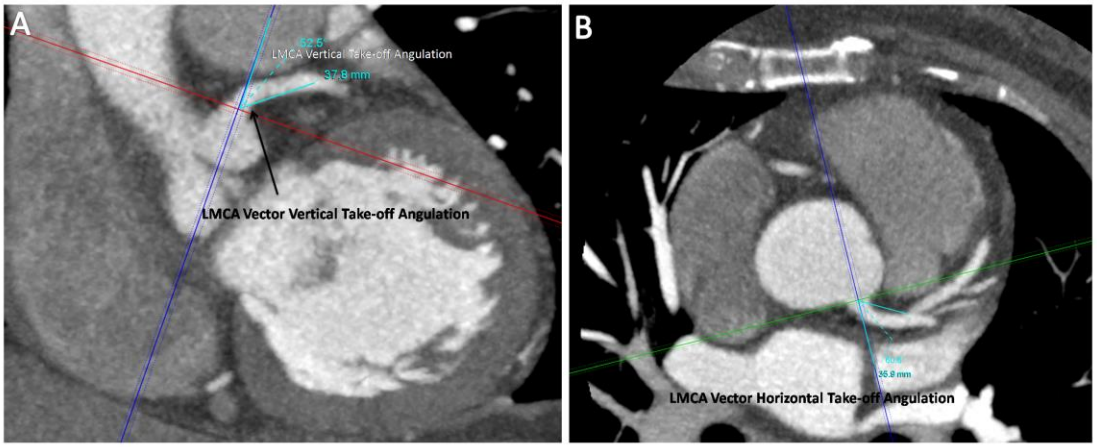

Figure 3.2 A. *LMCA Vector Vertical Take-off Angulation****. B.*** *LMCA Vector Horizontal Take-off Angulation*

3.2.1.4 LMCA Atherosclerotic Plaque Location

The presence and location either calcified, soft plaque or mixed atherosclerotic plaque along the proximal, mid and distal segment of LMCA was also surveyed.

3.3 Statistical analysis

Data are expressed as mean ± range. Paired and unpaired t-tests were used to determine the difference in LMCA parameters in both systolic and diastolic phase of the cardiac cycle and other analysis after confirming that data were parametric in

their distribution. Statistical analyses were performed using GraphPad Prism 5.0 (GraphPad Software Inc. La Jolla, California).

3.4 Result

100 consecutive dual-source MDCT coronary angiography studies from 2008 to 2009 were analysed retrospectively in the local radiology department. 4 studies were excluded due to inadequate imaging quality in systolic phase for analysis. The mean age for the cohort is 59 years (range from 19years to 88 years) with 54% been male gender. The result is summarized in Table 3.1.

Table3.1	LMCA survey cohort M=Male, F=Female, NS=Non Significant.						Previous studies
	Subgroups		Systolic	Diastolic	Difference (Value and confidence interval)	P value	Diastolic
LMCA length (mean± range, cm)	Vector	All	1.33 (0.5-0.29)	1.37 (0.51-2.3)	0.03(0.01-0.06)	P<0.01	1.1[5]
	Centreline	All	1.5 (0.50-2.8)	1.61 (0.51-3.5)	0.07 (-0.07-0.22)	NS (p=0.35)	0.8 to 1.35 (1-4.4)[6-10]
		Male Female	NA	M 1.66 (0.58-3.5) F 1.55 (0.51-3.3)	0.11 (-0.1-0.33) (Between gender)	NS (P=0.31)	NA
LMCA tortuosity index(define in Methods)		NA	NA	1.16 (1-1.76)	NA	NA	
LMCA take-off angulation (mean ± range, degrees)	Vector angle to ostial axis	Vertical (Sagittal plane)	$60^{\circ}(12^{\circ}$-$102^{\circ})$	59° (8°-114°)	1° (-4°-1°)	P=0.22	54.9±20°[8]
		Horizontal (Axial plane)	$38^{\circ}(0^{\circ}$-$111^{\circ})$	$37^{\circ}(0^{\circ}$-$122^{\circ})$	-1° (-4°-2°)	P=0.54	NA.
LMCA luminal diameter (mean±range, mm)	Proximal	Long axis	5.5 (3-7.9)	5.5 (3-8.6)	0.1 (0.1-0.2)	NS (P=0.27)	M 5.3, F 4.8[8]
		Short axis	4.3 (1-6.7)	4.6 (2.9-7.0)	0.3 (0.1-0.4)	P<0.01	M 3.4, F 4
	Mid	Long axis	4.7(1.6-7)	4.9 (3-8.6)	0.1 (0-0.2)	NS (P=0.09)	M 4.3, F 3.6
		Short axis	4.0 (1.2-5.6)	4.3 (2.9-6.6)	0.3 (0.1-0.4)	P<0.01	M 3.9, F 3.4
	Distal	Long axis	5 (3-8)	5.1 (3.3-8.3)	0.1 (0-0.2)	P=0.04	M 4.3, F 4
		Short axis	4.2 (1.2-6.8)	4.4 (2.5-6.7)	0.2 (0-0.3)	P=0.01	M 3.9, F 3.3
LMCA Cross-sectional area (mean ± range, mm^2)	Proximal	All	20 (5-53)	21.8 (6-54)	1.7 (-0.5-4)	NS (P=0.13)	16.25 [11]
		Male Female	NA	M 24 (11-54) F 18.9 (6-31)	5.4 (2--8.5)	P<0.01	M 20.1, F 15.7 [8]
	Mid	All	17.5 (3-38)	18.8 (9-44)	1.4 (-0.3-3.1)	NS (P=0.11)	16.25
		Male Female	NA	M 20 (9-44) F 16.6 (9-25)	4 (2-6.5)	P<0.01	M 14.2, F 10.7
	Distal	All	18.8 (5-45)	20.3 (8-54)	1.4 (-0.7-3.5)	NS (P=0.19)	16.25
		Male Female	NA	M 22 (8-44) F 17 (8-28)	5.2 (2.4-8.1)	P<0.01	M 15, F 11

3.4.1 LMCA Centreline

In the whole cohort, LMCA centreline length was marginally longer in diastole than in systole {1.61cm in diastolic phase, 1.5cm in systolic, p=0.35}. The LMCA vector length also demonstrated a variation with the cardiac cycle, but this represented only 0.3mm difference. In women, the mean LMCA centreline length is 1.55cm (range 0.58cm-3.5cm) which is slightly but not significantly (p=0.31) shorter than in men who measured 1.66cm (range 0.51cm-3.3cm).

3.4.2 LMCA Angulation

In the diastolic phase, the mean vertical LMCA vector take-off angulations were 59° (range from 8°-114°) in the sagittal plane and 37°(range from 0°-122°) in the axial or horizontal plane. There was no significance difference in take-off angulations between the systolic and diastolic phases.

3.4.3 LMCA Luminal Diameter and Cross-sectional Area

In the diastolic phase, the mean luminal long axis diameter in the proximal, mid and segments of the LMCA were 5.5mm (range from 3mm-8.6mm), 4.9mm (range from 3.3mm-8.6mm) and 5.1mm (range from 3.3mm-8.3mm) respectively. The short axis luminal diameters were 4.6mm (range from 2.9mm-7mm), 4.3mm (range from 2.9mm-6.6mm) and 4.4mm (range from 2.5mm-6.7mm). Overall, the LMCA tends to adopt more of elliptical cross-sectional area. In the systolic phase, there were significant reductions in the luminal diameter in the short axis but not in long axis diameter.

The mean proximal, mid and distal LMCA cross-sectional areas in diastole were 22mm^2 (range from 6 mm^2-54 mm^2), 19 mm^2 (range from 9 mm^2-36 mm^2), and 20 mm^2 (range from 8 mm^2-44 mm^2). There is a statistically significant reduction in the cross-sectional area in the mid and distal LMCA segment in the systolic phase relative to the diastolic phase. Women had a significantly smaller cross-sectional area in the proximal (female 18.9 mm^2 (6-31 mm^2) vs male 24 mm^2 (11-54 mm^2) $p<0.01$) and distal (female 17 mm^2 (8-28 mm^2) vs male 22 mm^2 (8-44 mm^2) $p<0.01$) segment of the LMCA in comparison to men.

3.4.4 LMCA atherosclerotic Plaque Location

In this cohort, 45% of all LMCA segments had either obstructive or non-obstructive atherosclerotic plaque. Approximately 28% of proximal LMCA segments, 29% of mid segments and 41% of the distal segments had disease. There were no ulcerated plaques or plaque ruptures identified.

3.5 Discussion

This study has identified several important features of LMCA anatomy. These include that the LMCA angulation of take-off from the aorta is highly variable, the LMCA is more typically an ellipse than a circle in its cross-sectional diameter, and that there is a significant difference in LMCA diameter comparing proximal to distal segments and comparing men and women.

There was a wide range of the LMCA vector take-off angulation, dependent partially on the vertical and horizontal variation in location of LMCA origin. The diverse LMCA angulation can be expected to affect WSS in the most proximal LMCA segments, and

therefore also affect the risk of developing atherosclerotic plaque in the LMCA. The absence of the angle variation during the cardiac cycle suggests a relative fixed anatomical position of the LMCA, despite dragging forces arising from the contracting myocardium and the effects of pulsatile blood flow. This survey did not encounter anomalously high-positioned LMCA origin with extreme sharp vertical angulation as described in previous literature [12, 13].

Furthermore, there was a statistically significant difference ($P<0.02$) in the long and short axis diameter across all LMCA segments suggesting elliptical cross-sectional morphology as opposed to circular configuration. This elliptical shaped cross-section has been described in MDCT literature [6, 8, 14]. In addition, comparison of diastolic and systolic phases identifies a more pronounced reduction in short axis luminal diameter than in long axis diameter implying systole renders the LMCA more elliptical in cross section. However, such reduction is only in the order to 0.2-0.3mm in value, and may not have clinical significance. Interestingly, despite subtle differences in short axis luminal diameter, there is no significant overall reduction in cross-sectional area between the two phases of the cardiac cycle. The significant difference in cross-sectional area between genders has been previously observed [8].

This survey results had also shown that the LMCA centreline is slightly longer in length than was reported in previous studies while no gender difference in length is found. Overall, the LMCA was not very tortuous with the averaged tortuosity index of the LMCA around 1.15 in the diastolic phase.

Finally, while there was not plaque rupture detected, the atherosclerotic plaque distribution in this cohort is more consistent with pattern seen in LMCD with multi-vessel disease with more plaque in the distal LMCA.

3.6 Limitation

There are several limitations to the retrospective descriptive LMCA survey. Firstly there are no detailed clinical demographic factors to be included in analysis. The severity of the LMCA atherosclerosis was not accurately quantified and therefore cannot comment on whether stenotic LMCA atherosclerotic plaque affects LMCA angulation and cross-sectional morphological conformation.

3.7 Conclusion

There are small variations in the both anatomical and morphological features of the LMCA in the diastolic and systolic phases of the cardiac cycle with some LMCA parameter changes reaching statistical significance. The values reported in this analysis for angulation will allow accurate modelling of the effect of LMCA angulation on WSS in later studies in this thesis.

3.8 Reference

1. Verhey, J.F. and C. Bara, *Influence on fluid dynamics of coronary artery outlet angle variation in artificial aortic root prosthesis.* Biomed Eng Online, 2008. **7**: p. 9.
2. Chwan Ng, A.C., et al., *Coronary ostial morphology after modified Bentall operation assessed with dual-source multidetector computed tomography.* J Cardiovasc Comput Tomogr, 2010. **4**(3): p. 206-12.
3. Nagatani, Y., et al., *Multidetector-row computed tomography coronary angiography: optimization of image reconstruction phase according to the heart rate.* Circ J, 2007. **71**(1): p. 112-21.
4. Lotmar, W., A. Freiburghaus, and D. Bracher, *Measurement of vessel tortuosity on fundus photographs.* Albrecht Von Graefes Arch Klin Exp Ophthalmol, 1979. **211**(1): p. 49-57.
5. Dodge, J.T., Jr., et al., *Lumen diameter of normal human coronary arteries. Influence of age, sex, anatomic variation, and left ventricular hypertrophy or dilation.* Circulation, 1992. **86**(1): p. 232-46.
6. Reig, J. and M. Petit, *Main trunk of the left coronary artery: anatomic study of the parameters of clinical interest.* Clinical Anatomy, 2004. **17**(1): p. 6-13.
7. Surucu, H. and M. Meric, *Review of the literature: The longest documented left main coronary artery.* Int J Cardiol, 2012.
8. Zeina, A.R., U. Rosenschein, and E. Barmeir, *Dimensions and anatomic variations of left main coronary artery in normal population: multidetector computed tomography assessment.* Coronary Artery Dis., 2007. **18**(6): p. 477-82.
9. Cademartiri, F., et al., *Prevalence of anatomical variants and coronary anomalies in 543 consecutive patients studied with 64-slice CT coronary angiography.* European Radiology, 2008. **18**(4): p. 781-91.
10. Christensen, K.N., et al., *Anatomic assessment of the bifurcation of the left main coronary artery using multidetector computed tomography.* Surg Radiol Anat, 2010. **32**(10): p. 903-9.

11. Fassa, A.A., et al., *Intravascular ultrasound-guided treatment for angiographically indeterminate left main coronary artery disease: a long-term follow-up study.* Journal of the American College of Cardiology, 2005. **45**(2): p. 204-11.
12. Menke, D.M., B.F. Waller, and J.E. Pless, *Hypoplastic coronary arteries and high takeoff position of the right coronary ostium. A fatal combination of congenital coronary artery anomalies in an amateur athlete.* Chest, 1985. **88**(2): p. 299-301.
13. Rosenthal, R.L., I.A. Carrothers, and J.M. Schussler, *Benign or malignant anomaly? Very high takeoff of the left main coronary artery above the left coronary sinus.* Tex Heart Inst J, 2012. **39**(4): p. 538-41.
14. Ge, J., et al., *Intravascular ultrasound imaging of angiographically normal coronary arteries: a prospective study in vivo.* Br Heart J, 1994. **71**(6): p. 572-8.

Chapter 4: Computational Fluid Analysis of the Left Main Coronary Artery: The Effects of Angulation and Stenosis Severity on Wall Shear Stress

4.1 Introduction

Disease of the left main coronary artery (LMCA) is associated with poor prognosis and significant morbidity [1-4]. Isolated LMCA atherosclerotic plaque tends to deposit in the proximal LMCA segment [5, 6] and these plaques also have a greater risk of rupture [6] compared to the atherosclerosis seen in more distal LMCA disease with multi-vessel involvement [5, 7, 8]. This raises the possibility that local biomechanical forces such as wall shear stress play a role in determining the site of this plaque deposition and its risk of rupture. The LMCA originates from the aorta at varying take-off angles [9], and a vertically displaced LMCA ostium may have adverse clinical sequelae [10]. It is very likely that the angle of origin of the LMCA alters local biomechanical forces. The aim is to investigate the effects of LMCA angulation and stenosis severity on wall shear stress using computational fluid dynamics.

Perturbation of coronary arterial wall shear stress (WSS) has been implicated in the development and progression of atheromatous plaques, as well as the pathogenesis of plaque rupture and thrombosis. Previous studies have shown that regions of relatively low shear stress within the arterial tree have higher propensity towards atheroma formation [11] due to endothelial remodelling [12] and intimal hyperplasia [13, 14]. High WSS on the other hand, has been shown in vitro to contribute to platelet activation and endothelial erosion [15].

Several studies have used computational fluid dynamics to estimate physiological parameters within the LMCA [16-19]. However, most recent studies have not

incorporated the aorta and left main artery origin into models used for simulation [16, 20-22], most likely because of the increased calculation time that would be required to incorporate the more complex simulation. It is unknown whether incorporation of the aorta into models for computational fluid dynamic (CFD) simulations affects shear stress calculations significantly, and how this interacts with WSS in the presence of varying LMCA stenosis. While CFD coronary artery studies omitting the aorta do provide detailed mapping and values of wall shear stress [23], they are unable to integrate the effect of LMCA vertical take-off angulations' impact on the WSS. One study which used computer generated models showed no difference in calculated physiological parameters (velocity and pressure profile) resulting from varying take-off angles of left main re-implantation onto aortic grafts [18]. However, it is unknown whether a varying take-off angulation of native LMCA affects WSS and the potential compounding effects of angulation and left main coronary stenosis on local fluid dynamics has not been investigated.

The aim of this study is to investigate the effect of incorporation of the aorta into CFD models and the effect of varying left main take-off angulation in the presence of varying stenosis severity on WSS. To achieve this, computer-generated models was developed; that allowed inclusion or exclusion of the aorta, and allowed variable LMCA angulation and stenosis severity. The results were then verified using patient-specific models obtained from computed tomography (CT) scans of patients.

4.2 Methods

4.2.1 Computer Generated Three Dimensional (3D) Models of the Aorta and LMCA

Model sets were created using computer-aided design software (SolidWorks 2008 SP0, SolidWorks Inc. Concord, M.A.). Aortic and left main artery dimensions were

chosen to replicate physiological measurement from previous CT coronary angiogram literatures [9, 24]. Smooth filleting of the sharp edges was performed using previous described methods [17, 25, 26] to better represent real anatomy and minimize artifactual elevation of WSS. The body of the aortic model was widened in the mid-portion to resemble the sinus of Valsalva [18]. To investigate the effect of incorporating the aorta into the models, models without and with aorta were created. Varying degrees of proximal stenosis (50 %, 70 %, 75 %, 80 %, 85 % and 90 % area stenosis) were then introduced into these models. To investigate the effect of left main vertical take-off angulation, artificial models generated included the aorta with attached left main at varying vertical take-off angles: 0, 30, 45, 60 degrees. Varying degrees of stenosis were then introduced to the LMCA ostium.

4.2.2 CT Coronary Angiography

CT images of 2 patients (patient A and B) with widely differing LMCA angulation were chosen from a pool of CT coronary angiography scans performed at our institution to generate "CT-derived models" of the aorta and LMCA. Images were obtained using a dual source 64-slice Siemens Definition multi-detector CT (MDCT) scanner (Siemens Medical Solutions, Forchheim, Germany). Retrospective ECG-gated scanning was used. Patients were routinely pre-medicated with 600µg of sublingual nitroglycerin. Beta-blockers were only given when pre-scan heart rates exceeded 90 beats per minute. Axial images were reconstructed at 0.75mm slice thickness and 0.3mm increment to deliver a final spatial resolution of 0.33mm x 0.33mm x 0.75mm for reconstruction of 3D models. Measurements of the LMCA were obtained using a Siemens workstation (Siemens Medical Solutions, Forchheim, Germany). The vertical take-off angle was measured as the sagittal angle between the LMCA (line between the midpoint of the ostium and centreline of the LMCA proximal segment) and the plane perpendicular to aortic axis.

4.2.3 3D Model of the Aorta and LMCA Reconstructed From CT images (CT-derived Models)

3D geometrical models of the coronary tree (CT-derived models) were extracted from CT image sets, using DICOM-viewing software Osirix (LaTour Hospital, Geneva, Switzerland) in the diastolic phase. 3D models were generated, refined and exported in IGES format using Geomagic 9.0 (Geomagic U.S., Research Triangle Park, N.C.). Varying degrees of stenosis severity were then introduced into these models and their effect on WSS estimated.

4.2.4 Computational Fluid Dynamic Analysis

For CFD analysis, all the above finalised geometrical models were converted into standard neutral format recognized by ANSYS 11.0 (ANSYS Inc, Canonsburg, P.A.). All model sets had minimum mesh elements (combined tetrahedron and prisms counts) of at least one million and the wall boundaries were inflated at 0.1mm for finer mesh to achieve good level of simulation accuracy as previously described [27].

As the aim of the study was to investigate the effect of differing geometry on shear stress calculations, the physiological parameters input as boundary conditions were kept constant for all models. Mass flow was set at 88.33g/s in the aortic inlet, 85.68g/s in aortic outlet, and 2.65g/s in left main outlet to achieve a mass flow of 2.65g/s within the LMCA, a value which is consistent with previous studies [18, 20, 28]. For studies without the aorta, the same mass flow of 2.65g/s was used in the LMCA.

Constant laminar flow and Newtonian fluid properties were adopted as in previous studies [29, 30]. The wall was assumed to be rigid with no deformation, non-slip and with zero velocity. These assumptions have been widely used in previous studies [31]. Blood density was assumed to be 1060kg/m3, blood viscosity was assumed to be 0.0035Pas and reference temperature was set at 37°C. Fluid-solid interaction simulation and unsteady flow throughout different cardiac cycles was not used in simulation as the LMCA anatomical and morphological survey only showed small variations in the both anatomical and morphological features of the LMCA in the diastolic and systolic phases of the cardiac cycle. This drastically reduced the simulation process time.

4.2.5 Statistical Analysis

Two-way ANOVA analyses were used to determine the interactive effect of incorporation of the aorta and stenosis severity on WSS, and varying angulation and stenosis severity on WSS. Statistical analyses were performed using GraphPad Prism 5.0 (GraphPad Software Inc. La Jolla, California).

4.3 Result

4.3.1 Effect on Peak and Mean WSS in LMCA Segment of Aortic Attachment

Figure 1A and **1B** represent artificial models with LMCA and stenosis without inclusion of aorta. The artificial model representing the aorta and LMCA attachment with 0 degree (orthogonal) LMCA take-off angulation is shown in **Figure 1C**. Varying degrees of stenosis were then introduced to the model (representative **Figure 1D** shown).

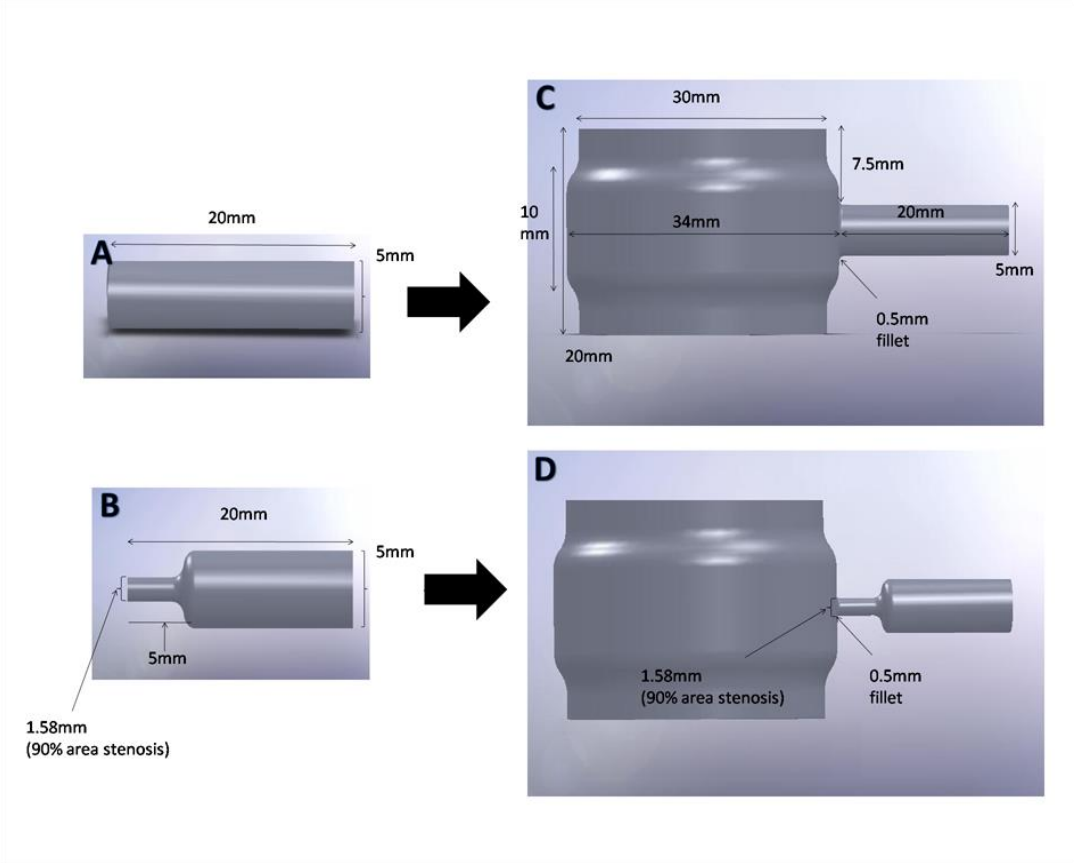

Figure 1: Computer Generated Models Representing the Proximal Ascending Aorta and Left Main Coronary Artery without angulation. (A) *Model without aorta and without stenosis;* ***(B)*** *Model without aorta and with 90% area ostial stenosis of LMCA;* ***(C)*** *Model with aorta but without coronary stenosis, showing dimensions and fillet sized used;* ***(D)*** *Model with aorta and with 90% area ostial stenosis of LMCA.*

Models that incorporated the aorta had lower peak wall shear stress (pWSS) for orthogonal model (p= 0.005) (**Figure 2A**). This difference was further accentuated in the presence of increasing left main proximal stenosis severity. However, mean wall shear stress (mWSS) was not affected by exclusion or inclusion of aorta (**Figure 2B**).

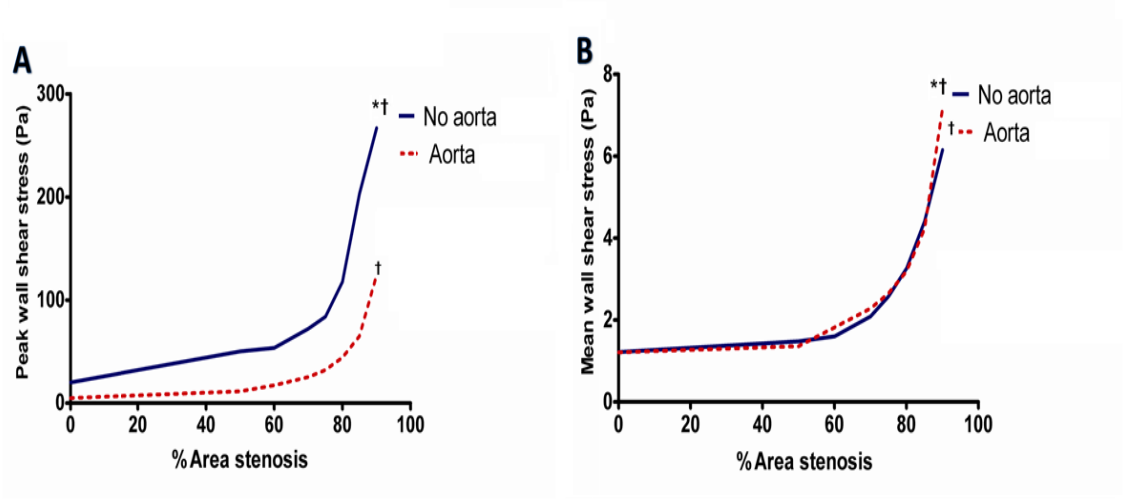

Figure 2: Effect of the Incorporation of Aorta and Coronary Ostial Stenosis on Wall Shear Stress in Computer Generated Models. (A) *Peak wall shear stress (pWSS) versus percentage area stenosis for orthogonal model without and with the aorta. * p=0.005 for difference between the group without aorta and with the group incorporating the aorta. † p<0.0001 for within group effect of increasing stenosis severity.* ***(B)*** *Mean wall shear stress (mWSS) versus percentage area stenosis without and with the aorta. * p=0.34 for difference between the group without aorta and with the group incorporating the aorta. † p<0.0001 for within group effect of increasing stenosis severity.*

There was a clear difference in the distribution of WSS between models that incorporated the aorta and the ones that did not. LMCA segment simulations alone demonstrate a pWSS zone including the whole of the entry site circumferentially (**Figure 3A & B**). Inclusion of the aorta results in a pWSS zone which resides only in superior zone of LMCA ostium in the non-stenosed model (**Figure 3C**). The pattern of pWSS dissipation down the LMCA also changes from a symmetrical pattern to an asymmetrical pattern (**Figure 3A & 3C**). Increasing proximal stenosis severity did not have an additional effect than that already described for change in WSS distribution (**Figure 3B & 3D**). The colour map shows that pWSS is highest on inferior surface of LMCA ostium in model with ostial stenosis (**Figure 3D**).

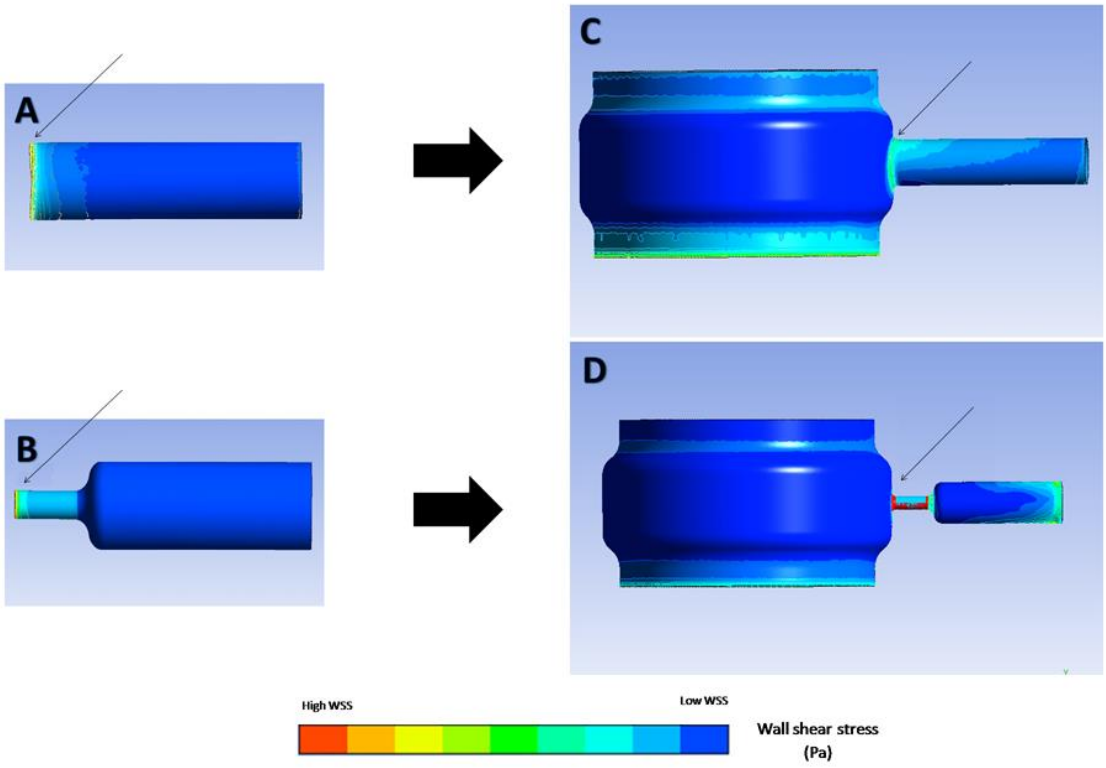

Figure 3: Comparison of Wall Shear Stress (WSS) Distribution between Models without the Aorta and with the Aorta. (A) *LMCA model without the aorta, without LMCA stenosis;* ***(B)*** *Stenosed LMCA model without the aorta;* ***(C)*** *LMCA model incorporating the aorta, without LMCA stenosis;* ***(D)*** *Stenosed LMCA model with the aorta. Arrows indicating region of high wall shear stress.*

4.3.2 The Effect of Varying LMCA Angulation and Stenosis Severity on WSS in Artificial Models

Models with different vertical LMCA take-off angles: 0, 30, 45, 60 degrees (all with aortic attachment) were also created (**Figure 4A-D**) based on the range of angles seen in the survey of the LMCA by CTCA (**Chapter 3**). Varying degrees of proximal stenosis severity (50%, 70%, 75%, 80%, 85% and 90% area stenosis) were then introduced into these models (**Figure 4E-H**).

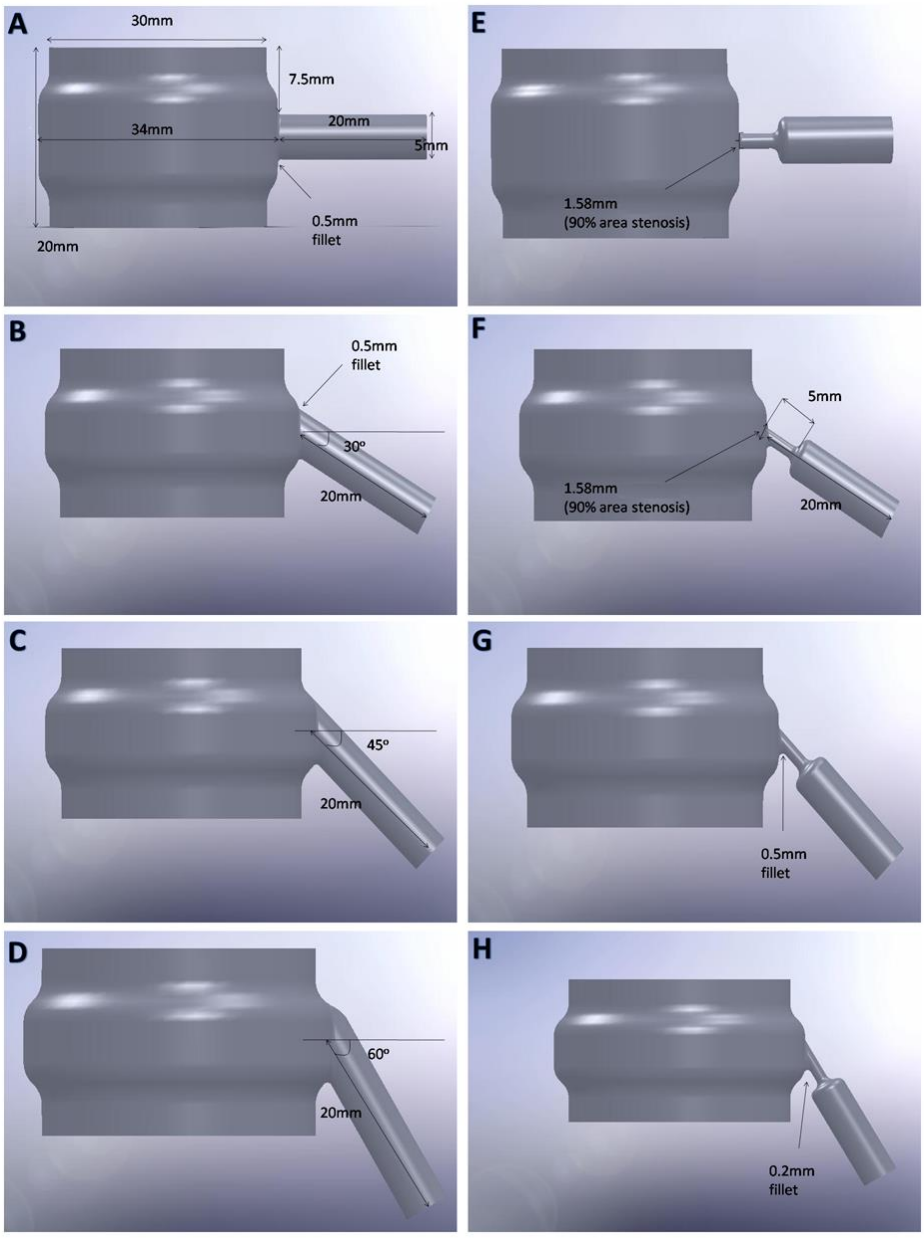

Figure 4: Computer Generated Models Representing the Proximal Ascending Aorta and Left Main Coronary Artery with Varying Degrees of Angulation. ***(A)*** *Baseline model with 0 degree angulation showing dimensions and fillet size used.* ***(B)*** *Model with 30 degree angulation.* ***(C)*** *Model with 45 degree angulation.* ***(D)*** *Model with 60 degree angulation.* ***(E-H)*** *Corresponding figures with 90% area stenosis introduced.*

Increasing LMCA angulation resulted in higher pWSS ($p=0.005$) and mWSS ($p<0.001$), and this difference was accentuated by increasing stenosis severity (**Figure 5 A-B**).

By two-way ANOVA, increasing stenosis severity also significantly increased pWSS ($p<0.0001$) and mWSS ($p<0.0001$).

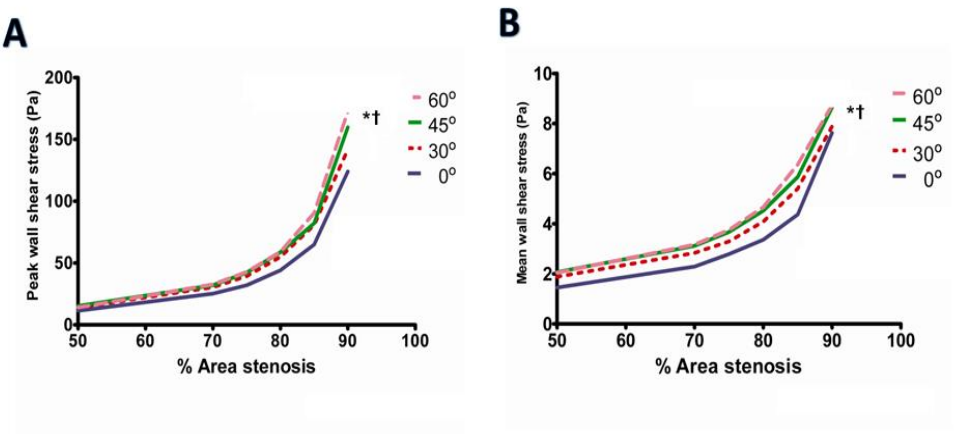

Figure 5: Effect of Varying Left Main Coronary Artery (LMCA) Angulation and Stenosis Severity on Wall Shear Stress in Computer Generated Models. ***(A)*** *Peak wall shear stress (pWSS) versus % area stenosis in the presence of varying LMCA angulation showing significant increase in pWSS with increasing angulation and stenosis. * $p=0.005$ for difference between the groups of different angulation. † $p<0.0001$ for within group effect of increasing stenosis severity on pWSS.* ***(B)*** *Mean wall shear stress (mWSS) versus % area stenosis in the presence of varying LMCA angulation showing increased mWSS with increasing angulation and stenosis. * $p<0.0001$ for difference between the groups of different angulation. † $p<0.0001$ for within group effect of increasing stenosis severity on mWSS*

WSS distribution was altered by angulation, a zone of low WSS developed in the superior aspect of the LMCA ostium, and became larger as the degree of LMCA angulation increases in the models without stenosis (**Figure 6A-D**). This change was also evident in the models with stenosis (**Figure 6E-H**). The zone of low WSS however, became smaller with increasing stenosis severity. Peak WSS was also lower in the angulated models incorporating the aorta compared to models without the aorta.

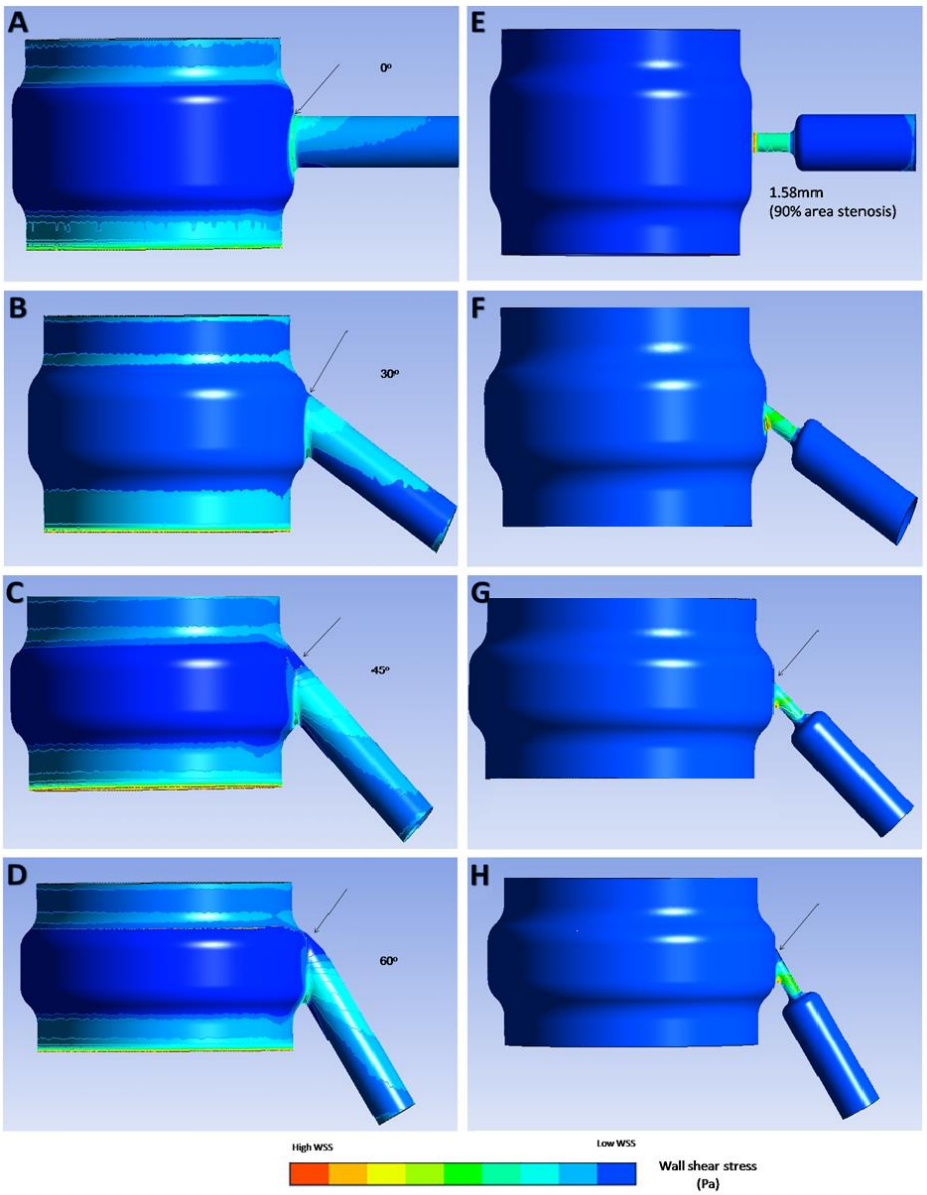

Figure 6: Wall Shear Stress (WSS) Distribution in the Presence of Varying Degrees of Left Main Coronary Artery (LMCA) Angulation. (A-D) *Models with increasing degrees of LMCA angulation without stenosis.* ***(E-H)*** *Corresponding models with 90% area stenosis. Arrows point to regions of low WSS.*

4.3.3 The Effect of Varying LMCA Angulation and Stenosis Severity on WSS in Patient-Specific CT-Derived Models

To investigate the effect of varying angulation in patient-specific models, the MDCT coronary angiogram images of patient A and B are shown in **Figures 7A-7B**. Resultant 3D model sets of the patient A and B are shown (**Figure 7C-D**). The changes in WSS distribution in the CT-derived models between patient A and patient B were similar to that of the computer generated models (**Figure 7E-F**). Patient B who had the more acute angulation (both vertical, coronal and therefore resultant vector take-off angulation) had a more prominent region of low WSS on the superior surface of the LMCA. Quantitatively, pWSS stress was higher in subject B ($p=0.009$) (Fig. 8) at all levels of stenosis.

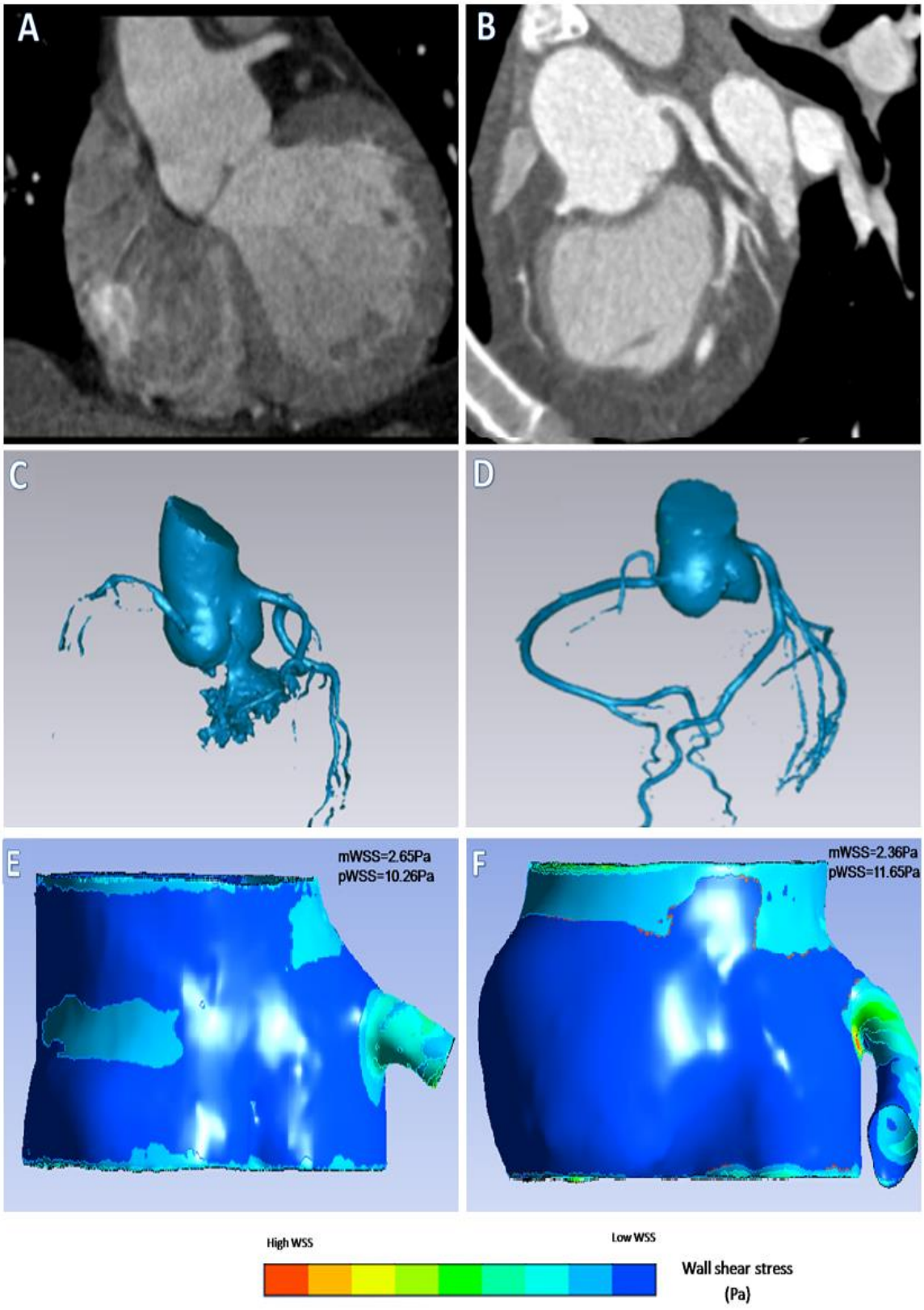
A
B
C
D
E
mWSS=2.65Pa
pWSS=10.26Pa
F
mWSS=2.36Pa
pWSS=11.65Pa
High WSS
Low WSS
Wall shear stress
(Pa)

Figure 7: Representative CT Coronary Angiogram Images with Corresponding 3D Reconstruction of the Proximal Aorta and Coronary Arteries and Wall Shear Stress Mapping (WSS) Map. Sagittal CT Images of patient left main coronary artery (LMCA) for **(A)** Patient A who had 25^{o} LMCA angulation and **(B)** Patient B who had 58^{o} LMCA angulation. **(C-D)** Corresponding 3D reconstructed model images of patients. **(E-F)** Corresponding WSS maps.

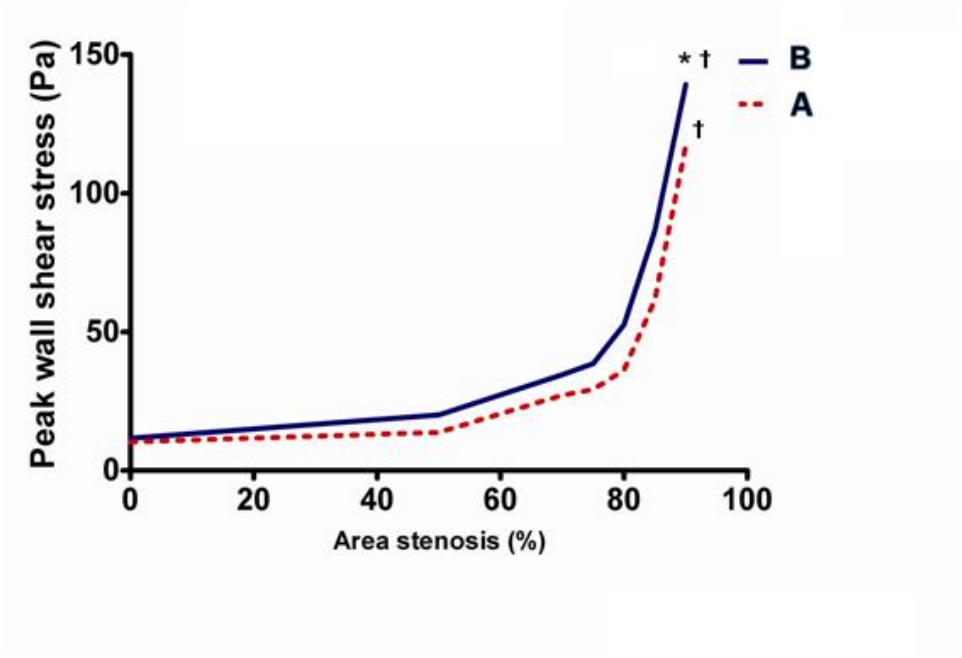

Figure 8: The Effect of Varying Left Main Coronary Artery (LMCA) Angulation and Stenosis Severity on Wall Shear Stress (WSS) in Authentic Patient-Derived Models. Peak wall shear stress (pWSS) versus % area stenosis showing significantly higher pWSS in model of patient B compare to model of patient A in the presence of increasing stenosis severity. * p=0.009 for difference between A and B. † p<0.0001 for effect in the presence of increasing stenosis severity within group A and B.

4.4 Discussion

4.4.1 Importance of Incorporation of the Aorta into CFD Models to Calculate LMCA WSS

Most studies that have used CFD to calculate WSS in the LMCA have not incorporated the aorta in their models [16, 20-22]. These results show that incorporating the aorta yielded lower pWSS levels and a different distribution of WSS. These differences are likely due to the fact that absence of the aorta causes an inaccurate depiction of flow at the LMCA entry site, causing an artificial increase in WSS values [32]. The preferred development site of atherosclerotic plaques in pathological studies [33] [34] corresponds to regions of low WSS in the models that incorporate the aorta (**Figure 6A-D and 7E-F**). The accurate understanding of WSS clearly mandates the incorporation of the aorta.

4.4.2 The Effect of Varying Vertical LMCA Angulation on WSS

Both pWSS and mWSS increased with increasing LMCA vertical take-off angulation, and this relationship was accentuated by increasing stenosis severity. One study that investigated this issue showed no functional difference between angulated and non-angulated LMCAs [18]. However, this comparison was performed in the absence of stenosis, and used velocity profile and pressure as their dependent variables. As these results show, the difference between angulated and non-angulated models was apparent in the extent of area of low WSS, not only the numerical value of the WSS, and was further altered in the presence of increased stenosis severity (**Figure 7**). The more vertically angled LMCA take-off from aorta in the presence of significant stenosis severity is associated with higher pWSS. Since pWSS leads to endothelial erosion, this suggests that the LMCA vertical take-off

angulation can provide a plausible insight of the higher atherosclerotic plaque rupture rate seen in the isolated LMCA disease.

In addition, the relationship is complex with heterogeneous distribution of WSS at the left main ostium and proximal LMCA segment. With increasing angulation, there was also an increase in the area of low WSS on the superior aspect of the LMCA ostium and proximal LMCA segment. This low WSS site is known to be prone to atheroma formation in previous histopathological studies [33] [34]. This suggests that more acutely take-off angled LMCA may have a tendency towards atheroma formation in the superior aspect of left man ostium and proximal segment. This could potentially explain the finding of that the isolated LMCA disease had a higher percentage of proximally located atherosclerotic plaque deposition [5, 6]. Furthermore, these results also show that this low WSS zone decreases with increasing stenosis, suggesting a complex interaction between WSS, atheroma formation and progression. Further anatomical or CT study is required to validate the possibility that LMCA angulation independently portends a worse prognosis.

4.5 Limitation

There are several limitations in this study. Firstly, the simulation have only adopted constant laminar flow. Secondly, Newtonian fluid properties was assumed. As the aim of this study was to investigate the effect of geometry on WSS calculations, these assumptions are used for the simulations. With these assumptions, the shear stress value and mapping obtained from these simulations for normal LMCA are consistent with that previously reported in the literature and correlates well with histopathological studies. Lastly, the horizontal take-off angulation of LMCA was not simulated in the study and may require further investigation in future study.

4.6 Conclusion

The aorta should be incorporated into future models used for WSS calculation by CFD simulation when interrogate the WSS in the LMCA. Both peak and mean WSS increases with increasing amount of LMCA origin angulation, and this is accentuated by increasing stenosis severity. In addition, an area of low wall shear stress develops superiorly in the LMCA with increasing angulation. These results suggest that LMCA angulation may be an additional important factor to be considered in the clinical evaluation of the pathogenesis and progression of LMCA atheromatous disease.

4.7 Reference

1. Anonymous., *Long-term results of prospective randomised study of coronary artery bypass surgery in stable angina pectoris. European Coronary Surgery Study Group.* Lancet, 1982. **2**(8309): p. 1173-80.
2. Anonymous., *National Heart, Lung, and Blood Institute Coronary Artery Surgery Study. A multicenter comparison of the effects of randomized medical and surgical treatment of mildly symptomatic patients with coronary artery disease, and a registry of consecutive patients undergoing coronary angiography.* Circulation, 1981. **63**(6 Pt 2): p. I1-81.
3. Anonymous., *Prospective randomised study of coronary artery bypass surgery in stable angina pectoris. Second interim report by the European Coronary Surgery Study Group.* Lancet, 1980. **2**(8193): p. 491-5.
4. K. Detre, H.H., T. Takaro, *Veterans Administration Cooperative Study of Surgery for Coronary Arterial Occlusive Disease. III. Methods and baseline characteristics, including experience with medical treatment. By the Veterans Administration Cooperative Group for the Study of Surgery for Coronary Arterial Occlusive Disease.* Am J Cardiol, 1977. **40**(2): p. 212-25.
5. Fajadet, J. and A. Chieffo, *Current management of left main coronary artery disease.* European Heart Journal, 2012. **33**(1): p. 36-50.
6. Kang, S.J., et al., *Intravascular ultrasound-derived predictors for fractional flow reserve in intermediate left main disease.* JACC Cardiovasc Interv, 2011. **4**(11): p. 1168-74.
7. Thompson, C.A., et al., *Classification and atherosclerosis distribution in patients with left main coronary disease.* J Interv Cardiol, 2009. **22**(5): p. 431-6.
8. Tyczynski, P., et al., *Intravascular ultrasound assessment of ruptured atherosclerotic plaques in left main coronary arteries.* Am J Cardiol, 2005. **96**(6): p. 794-8.
9. Zeina, A.R., U. Rosenschein, and E. Barmeir, *Dimensions and anatomic variations of left main coronary artery in normal population: multidetector computed tomography assessment.* Coronary Artery Dis., 2007. **18**(6): p. 477-82.

10. Nishida, N., Y. Hata, and K. Kinoshita, *High takeoff of the left main coronary artery at autopsy after sudden unexpected death in a male.* Pathology, 2014. **46**(4): p. 361-4.
11. Caro, C.G., J.M. Fitz-Gerald, and R.C. Schroter, *Atheroma and arterial wall shear. Observation, correlation and proposal of a shear dependent mass transfer mechanism for atherogenesis.* Proc R Soc Lond B Biol Sci, 1971. **177**(46): p. 109-59.
12. Malek, A.M., S.L. Alper, and S. Izumo, *Hemodynamic shear stress and its role in atherosclerosis.* JAMA, 1999. **282**(21): p. 2035-42.
13. Wootton, D.M. and D.N. Ku, *Fluid mechanics of vascular systems, diseases, and thrombosis.* Annu Rev Biomed Eng, 1999. **1**: p. 299-329.
14. Zarins, C.K., et al., *Carotid bifurcation atherosclerosis. Quantitative correlation of plaque localization with flow velocity profiles and wall shear stress.* Circ Res, 1983. **53**(4): p. 502-14.
15. Fry, D.L., *Certain histological and chemical responses of the vascular interface to acutely induced mechanical stress in the aorta of the dog.* Circ Res, 1969. **24**(1): p. 93-108.
16. Soulis, J.V., et al., *Wall shear stress in normal left coronary artery tree.* J Biomech, 2006. **39**(4): p. 742-9.
17. Suo Jin1, Y.Y., John Oshinski1,2 , Allen Tannenbaum1, James Gruden2 and Don Giddens1, *Flow Patterns and Wall Shear Stress Distributions at Atherosclerotic-Prone Sites in a Human Left Coronary Artery - An Exploration Using Combined Methods of CT and Computational Fluid Dynamics.* Proceedings of the 26th Annual International Conference of the IEEE EMBS 2004.
18. Verhey, J.F. and C. Bara, *Influence on fluid dynamics of coronary artery outlet angle variation in artificial aortic root prosthesis.* Biomed Eng Online, 2008. **7**: p. 9.
19. Asakura, T. and T. Karino, *Flow patterns and spatial distribution of atherosclerotic lesions in human coronary arteries.* Circ Res, 1990. **66**(4): p. 1045-66.
20. Goubergrits, L., et al., *CFD analysis in an anatomically realistic coronary artery model based on non-invasive 3D imaging: comparison of magnetic resonance imaging with computed tomography.* Int J Cardiovasc Imaging, 2008. **24**(4): p. 411-21.

21. Frauenfelder, T., et al., *In-vivo flow simulation in coronary arteries based on computed tomography datasets: feasibility and initial results.* Eur Radiol., 2007. **17**(5): p. 1291-300.
22. Wellnhofer, E., et al., *Novel non-dimensional approach to comparison of wall shear stress distributions in coronary arteries of different groups of patients.* Atherosclerosis, 2009. **202**(2): p. 483-90.
23. Kim, H.J., et al., *Patient-specific modeling of blood flow and pressure in human coronary arteries.* Annals of Biomedical Engineering, 2010. **38**(10): p. 3195-209.
24. Hager, A., et al., *Diameters of the thoracic aorta throughout life as measured with helical computed tomography.* J Thorac Cardiovasc Surg, 2002. **123**(6): p. 1060-6.
25. Joy Ku, A.L., Beverly Tang, Charles Taylor, Nathan Wilson, Bill Katz *SIMVASCULAR USERS MANUAL*. 2003. 135.
26. Pivkin, I.V., et al., *Combined effects of pulsatile flow and dynamic curvature on wall shear stress in a coronary artery bifurcation model.* Journal of Biomechanics, 2005. **38**(6): p. 1283-1290.
27. Prakash, S. and C.R. Ethier, *Requirements for mesh resolution in 3D computational hemodynamics.* J Biomech Eng, 2001. **123**(2): p. 134-44.
28. Goubergrits, L., et al., *Coronary artery WSS profiling using a geometry reconstruction based on biplane angiography.* Ann Biomed Eng 2009. **37**(4): p. 682-91.
29. Johnston, B.M., et al., *Non-Newtonian blood flow in human right coronary arteries: Transient simulations.* J Biomech, 2006. **39**(6): p. 1116-1128.
30. Johnston, B.M., et al., *Non-Newtonian blood flow in human right coronary arteries: steady state simulations.* J Biomech, 2004. **37**(5): p. 709-720.
31. Perktold, K., et al., *Validated computation of physiologic flow in a realistic coronary artery branch.* J Biomech, 1998. **31**(3): p. 217-28.
32. Johnson, K., *In vivo coronary wall shear stress determiniation using CT, MRI and computational fluid dynamics.*, in *School of Biomedical Engineering*2007, Georgia Institution of Technology: Atlanta.
33. Velican, C. and D. Velican, *Differences in the pattern of atherosclerotic involvement between non-branched regions and adjacent branching points of human coronary arteries.* Atherosclerosis, 1985. **54**(3): p. 333-42.
34. Kanoh, T., R. Okada, and K. Kitamura, *A Morphological Study on the Coronary Ostia In Human Autopsy Hearts With Special References on the Funnel-*

Shaped Structure, Overhang Phenomenon and Their Clinical Significance. Japanese Journal of Medicine, 1977. **16**(3): p. 205-214.

Chapter 5: Left Atrial Appendage Morphology and Rheological Properties

5.1 Introduction

Cardioembolic cerebral embolism has a high impact on functional status and mortality rate, both in short and long term in patients with atrial fibrillation. Atrial fibrillation accounts for approximately 14-33% of all strokes [1-5] while the left atrial appendage (LAA) is responsible for more than 90% of cardioembolic thromboembolism in atrial fibrillation [6]. Therefore, the LAA has been considered as one of the most lethal and disabling attachments in the human body [7, 8].

The importance of the LAA appendage only gained attention in the early 1980s, with research undertaken in LAA anatomy and function in an attempt to individualize the risk of systemic thromboembolism. In the last decade, simple clinical scoring systems such as the $CHADS_2$ or $CHADS_2VASC$ score have been validated in numerous populations and have largely replaced echocardiographic evaluation in routine clinical practice for predicting the risk of systemic thromboembolism. In this setting, new predictors will need to demonstrate their independent and incremental predictive value beyond that of established clinical scoring systems before being considered as clinically useful [9, 10]. Recent evidence suggests certain LAA morphological subtypes increase the risk of cerebral thromboembolism and are independent of the existing clinical scoring systems [11-14]. This area of research is important as it represents the first development in the role of local left atrial factors in determining stroke risk in many years. How local, anatomical factors relate to alterations in left atrial rheological parameters is not well understood.

This review will re-visit the basic mechanisms for thrombus formation in the LAA with emphasis on LAA echocardiographic and morphological predictors for

thromboembolism. It will attempt to link these two features using rheological/fluid mechanical properties and also discuss their roles in systemic conditions described in clinical predictive scores such as the $CHADS_2$ VASC score.

5.2 Pathogenesis of LAA thrombus Formation in Atrial Fibrillation

The key mediators of thrombosis formation were classically described by alterations in Virchow's triad [15]:1) vascular structure (endothelial injury or dysfunction); 2) blood flow (stasis); 3) haemostasis (hypercoagulability). These are considered in relation to LAA thrombus formation below.

5.2.1 Abnormal structural change (Endothelial injury and dysfunction)

Structural change has been demonstrated in the LAA in atrial fibrillation at both the macroscopic and microscopic levels. At the macroscopic level, chronic exposure to atrial fibrillation is associated with increased LAA volumes and LAA outlet diameter compared to patients in sinus rhythm [13, 55][16-20]. Negative remodeling of the LAA is observed after restoration of normal sinus rhythm [21, 22]. At the microscopic level, there are severe endocardial changes in cohorts with atrial fibrillation, with oedema, fibrinous transformation, small areas of endothelial denudation and thrombus formation [23]. These endothelial changes are thought to increase the tendency to thrombus formation.

5.2.2 Abnormal blood flow(stasis, rheological properties)

That stagnation of blood flow predisposes to thrombus formation was initially described by Virchow. Recently, in vitro studies have demonstrated the importance of two rheological properties in thrombus formation, shear rate and

blood flow velocity. Low shear rate promotes the tendency for blood to initiate thrombus formation while low blood flow velocity promotes thrombus growth [24-26]. Altered rheological properties appear highly likely in the different LAA morphologies and are the focus of this thesis.

5.2.3 Haemostasis (Hypercoagulability)

Early work in atrial fibrillation has demonstrated that slow swirling flow (seen as spontaneous echo contrast in echocardiogram studies) in the left atrium (LA) or LAA is independently associated with higher haematocrit and fibrinogen level [27]. Atrial fibrillation or atrial flutter with depressed LAA function are more prothrombotic than atrial flutter with preserved LAA function. In atrial fibrillation and atrial flutter there is increased fibrinogen turnover (higher D-dimer level) and platelet activation (increased level of beta-thromboglobulin) in patients with impaired LAA function [28-30]. In atrial fibrillation, endothelial activation/dysfunction, altered fibrinolysis and increased platelet activation are all likely to contribute the hypercoagulable state [31, 32]. Plasma biomarkers such as vWF and D-dimer have shown some promise as capable of refining risk stratification [33-35]. In addition, any other systemic condition that leads to a prothrombotic state may provide a lower threshold for initiation of coagulation for any given degree of blood flow stagnation [36].

5.3 Rheological Assessment of the Left Atrial Appendage

5.3.1 Qualitative Assessment of the Left Atrial Appendage

Two important qualitative rheological parameters used in evaluating the LAA are spontaneous echo contrast (SEC) and presence of LAA thrombus, both of which are

known to carry a high risk of systemic thromboembolism (Relative Risk (RR) of 3.7 for LAA SEC and 2.5 for LAA thrombus) [37]. The mechanism of increased risk associated with LAA thrombus is self-evident as LAA thrombus can embolise to cause stroke. Interestingly one study did not show any independent predictive value of LAA thrombus in multivariate analysis [38]. SEC (sometimes referred to as “smoke”) has been described as "a swirling pattern of increased blood echogenicity caused by ultrasonic backscatter from red blood cell aggregates”. These aggregates form due to non-covalent binding between red cells and plasma proteins under conditions of low flow and low shear[39-42] and do not resolve with antiplatelet or anticoagulation treatment [43, 44].

SEC can be defined as "vortical blood flow with slow flow velocity and low shear rate". In one echocardiography study, within the LAA, the highest average velocity for a region with severe LAA SEC was only 3.6cm/s compared to 7.5cm/s in a region with mild LAA SEC [45]. In addition, the overall shear rate was also lower in patients with severe LAA SEC compared to those with mild SEC. The overall descriptive grading of the severity of SEC is arbitrary and has no universal consensus. Mild to severe, mild to dense, or grade 0 to 4 are three different grading systems describing the severity of SEC, with grades 3 to 4 approximately correlating with severe or dense LAA SEC [46]. Severe SEC is known to be associated with a high risk of systemic thromboembolism, up to 22% annual rate in one small prospective study, with a higher predictive risk of cerebral/systemic thromboembolism even in comparison to LAA thrombus [37, 47, 48]. In addition, SEC has been shown to be more severe in the LAA than the left atrium (LA), and this observation can therefore plausibly explain the high incidence of LAA thrombus [49]. Overall, severe SEC has been observed as the most predictive qualitative rheological LAA parameter for thromboembolism.

5.3.2 Quantitative Assessment of the Left Atrial Appendage

5.3.2.1 LAA Functional (Emptying Function) Assessment

Depressed LAA emptying function is observed in all subtypes of atrial fibrillation [50-52] and may be predictive of paroxysmal atrial fibrillation in acute stroke [53]. Multiple studies have shown depressed LAA emptying function is associated with LAA SEC, LAA thrombus and an overall increased risk of thromboembolism in patients with atrial fibrillation[37, 46, 51, 52, 54-56] and in patients with normal sinus rhythm [52, 54, 57-59]. Currently, there are three different echocardiographic parameters that quantify the LAA emptying function: LAA ejection fraction, LAA wall contracting velocity and LAA peak emptying velocity.

5.3.2.2 LAA Ejection Fraction

Earlier methods used simple LAA areas or LAA area biplane methods [50-52] to measure LAA ejection fraction, while recent advances in echocardiography techniques using direct measurement of the LAA emptying function with 3-D echocardiography or speckle tracking allows LAA ejection fraction to be determined more accurately [60-63]. One study found that a LAA ejection fraction<21% increased the risk of LAA thrombus formation and possibly the risk of systemic thromboembolism independent of $CHADS_2$ VASC score. From this study, the ROC area of the curve of LAA ejection fraction was superior to the LAA emptying velocity as risk predictor for LAA thrombus [61].

5.3.2.3 LAA Wall Contracting Velocity

LAA function can be assessed by measuring the LAA wall velocity during the cardiac cycle, using tissue Doppler in both transeosphageal [64, 65] and transthoracic

echocardiography. The LAA wall contracting and relaxing velocity reflect the LAA contractile (emptying) and filling functions respectively [66]. Independent LAA wall velocity studies have shown LAA wall contracting velocity <10cm/s is associated with increased risk of LAA SEC, LAA thrombus and systemic thromboembolism (HR of 3.46 when the LAA wall contracting velocity is <8.7cm/s) [38, 64-69].

5.3.2.4 LAA Peak Emptying Velocity

LAA peak empting velocity is the commonest quantitative measurement that reflects the interaction of the LAA emptying function with the outlet size of the LAA, rather than just the LAA mechanical emptying function. It can be defined as the peak velocity generated by the LAA contraction stroke volumes as it leaves the LAA outlet, measured during transeosphageal echocardiography [52]. Most echocardiography data has emphasized LAA peak emptying velocity since it is the one of the first parameters described to be associated with LA/LAA SEC [46]. LAA peak emptying velocity has also been associated with different LAA SEC severity and risk of future thromboembolic events in patients with atrial fibrillation (relative risk of 1.7 if LAA peak velocity <20cm/s) [37]. LAA peak emptying velocity >40cm/s is rarely associated with SEC, while if below <20cm/s it is almost invariably associated with severe LAA SEC [46].

5.3.2.5 Role of LAA Shear Rate

While shear rate has not been used to predict cerebral thromboembolism, low shear rate had been associated with the presence of LA SEC and LAA SEC [46]. The shear rate is defined as the rate of the change of velocity in the given region [70]. For LAA shear rate, it can be expressed as a simple formula

$$\text{LAA shear rate} = \frac{2 \text{ X LAA peak emptying velocity (LAA PEV)}}{\text{LAA outlet diameter} / 2}$$

. LAA shear rate

therefore is dependent on the both the LAA peak emptying function (LAA PEV) and LAA outlet diameter [71].

5.4 Left Atrial Appendage Morphology

The LAA is the remnant of the left atrium after third weeks of gestation and was subjected to detailed anatomical study in the 1990s [19, 72, 73]. The anatomical study and cast created for the LAA lumen identified a complex morphological nature with multiple "lobes" and "twigs" [19]. This complex structure was not initially thought to link with an increased risk of thromboembolism, but these studies did recommend careful echocardiographic interrogation to exclude LAA thrombus or SEC [72]. Earlier studies did find a positive association between larger LAA volumes and wider LAA outlet neck size and the high risk of systemic thromboembolism [17, 20]. Recently, certain LAA morphologies have been associated with a higher risk of systemic thromboembolism in patients with atrial fibrillation.

5.4.1 LAA Neck Size

The LAA outlet or neck size is on average 1-1.2cm in diameter in patients in normal sinus rhythm [72]. Studies have demonstrated an inconsistent relationship with the risk of stroke. One study did show increased LAA outlet short and long axial diameters in atrial fibrillation [18] were associated with an increased risk of prior stroke (OR 3.59). Another large study reported that the extent of LAA trabeculations and smaller (not larger) LAA orifice diameter were predictive of prior cerebral thromboembolism whereas LAA morphologies (such as cactus and chicken wing) were not independently predictive [13]. It is plausible that LAA neck size does affect the risk of thromboembolism, given that shear rate and the LAA emptying are both dependent on the LAA outlet dimension in an inverse

relationship. However the relationship may be complex and depend on various interacting rheological parameters.

5.4.2 LAA Volume

The normal LAA volume varies according to the method of measurement and the phase of the cardiac cycle in which the LAA volume was measured. Intra-operative observation, anatomical casts, CTCA and cardiac MRI generate different "normal" values, as result of different measurement methods, although the different approaches are generally mutually supportive in their qualitative conclusions. Using anatomical casts, one large study found that the mean LAA luminal volume on average ranged from 0.7 cm3 to 19.2 cm3, with mean LAA volume of 4.3cm3 in patients in sinus rhythm and 7cm3 in patients with AF. CTCA studies have reported shown the mean LAA volume of 6.2±1.9 cm^3 and 7±4 cm^3 in patients in sinus rhythm [16][74], whereas in patients with cryptogenic stroke LAA volume was much larger at 11.1±3.8 cm^3 [16].

MRI studies tend to show large mean LAA volumes, this is likely due to the signal averaging during different phases of the cardiac cycle and inferior spatial resolution when compared to CT. Cardiac MRI supports the earlier studies associating large LAA with stroke risk, one study showing that the mean LAA volume was 28.8+/-13.5cm^3 in stroke subjects and 21.7+/-8.27cm^3 in the non-stroke group [13]. In this cohort, the stroke group also had a higher $CHADS_2$ score. Another cardiac MRI study showed patients with stroke had a mean LAA volume of 22.9+/-9.6cm^3, compared with patients without stroke who had mean LAA volumes of 14.5+/-7.1cm^3, even when both groups had similar $CHADS_2$ scores[18].

5.4.3 LAA Morphology

Despite the variable and complex morphology of LAA, it was not until 2011 that one CT study first suggested an association of the LAA morphological characteristics with risk of systemic thromboembolism [74] and provided a simple LAA morphological classification. A subsequent pilot CT study classifying LAA morphology into chicken-wing and non-chicken-wing subtypes (cactus, windsock and cauliflower) demonstrated a high risk of thromboembolic stroke risk with the non-chicken-wing group, with an annual rate of 4.6%, independent of the $CHADS_2$-VASC score [11]. It also demonstrated that the cauliflower morphology had the highest risk of cerebral thromboembolism. Since then, three CT LAA morphology studies have all demonstrate that cauliflower morphology does confer an increased risk of cerebral embolism [12-14]. The windsock LAA morphology ranks as second highest risk [12]. Although one study dismissed the LAA morphological classification system and indicated that severe trabeculation is responsible for the increased risk of thromboembolism, the cauliflower LAA morphology also has the most severe trabeculation making the distinction difficult. Classifying the LAA morphology into 4 categories carries high inter-observer and intra-observer variability [13]. Interestingly, in these studies it also been noted that the cauliflower subtypes have lower mean LAA volumes in comparison to the other subtypes despite being associated with a higher risk of stroke; a finding not consistent with previous observational studies relating larger LAA volume to risk. This raises uncertainty regarding the robustness of the association between LAA morphology and stroke risk.

5.5 Linking the LAA Morphology to LAA Echocardiographic Rheological Features

Spontaneous echo contrast or SEC can be considered as a precursor for thrombus formation. It is the result of slow swirling blood flow with slow vortical velocity and low shear rate, the two most important precursors for blood clot initiation and growth. Allowing for similar blood haemostatic parameters, the vortex or

stagnation region also has been associated with thrombus formation [75]. Based on fluid dynamics literature, LAA SEC results from the interaction between the LAA morphology and LAA emptying function, with rheological parameters determining the degree of slow swirling velocity and slow shear rate in a given LAA geometry.

5.5.1 LAA Shear Rate and LAA Morphology

LAA shear rate determines the rate of change of vortical or swirling velocity and is calculated by equation (Equation 2) derived from Poiseuilles' law [71]. Lower rate of changing of vortical velocity increased the chance of SEC formation and is pre-set by a given LAA morphological characteristics, the LAA volume and LAA outlet radius; when the LAA emptying function is fixed. This is demonstrated by the following equations.

***Equation 1 [76]*:** In laminar flow with heart rate of 60 beats per minutes,

$$\text{LAA peak emptying velocity}=\frac{2\text{ X Stroke Volume (SV)}}{\text{LAA outlet area}}=\frac{2SV}{\text{LAA outlet area}}$$

This equation is derived from that

$$\text{LAA mean emptying velocity}=\frac{\text{Blood Flow}}{\text{LAA outlet area}}\frac{\text{Stroke Volume (SV)}}{\text{LAA outlet area}}$$

Note if in the setting of laminar flow, r=R=radius and L= length, then analytically the LAA peak emptying velocity can be obtained [76]:

$$\text{LAA mean emptying velocity}=\frac{2}{\text{LAA outlet area}}\int_0^R V_L(r)2\pi r dr=\frac{V_L}{2}=\frac{\text{LAA peak emptying velocity}}{2}$$

Note if in the setting of fully developed turbulent flow, then T=turbulent flow and m is the exponent and dependent on the degree of turbulence [76].

$$\text{LAA mean emptying velocity} = \frac{2}{\text{LAA outlet area}} \int_0^R V_{T\max}(r) 2\pi r dr = \frac{V_{T\max}\,(\text{LAA peak emptying velocity})}{(m+1)\ X\ (m+2)}$$

As m=1/7 in the setting of fully developed turbulence, then

(m+1)X(m+2)=(8/7)X(15/7) = 120/49=2.45, another constant.

Equation 2[71]:

$$\text{LAA shear rate} = \frac{2\ X\ \text{LAA peak emptying velocity(LAAPEV)}}{\text{LAA outlet diameter} / 2} = \frac{2\ \text{LAAPEV}}{\text{LAA outlet radius}}$$

Equation 3[77]:

$$\text{LAA ejection fraction} = \frac{\text{Stroke volume}\ (\text{LAA end-diastolic volume - LAA end-systolic volume})}{\text{LAA volume}\ (\text{LAA end-diastolic volume})}$$

Therefore,

$$\text{Stroke volume (SV)=LAA ejection fraction (LAA EF) X LAA volume, SV=LAA EF X LAA volume}$$

Substituting equation 1 into equation 2, we obtain equation 4.

Equation 4:

$$\text{LAA shear rate} = \frac{2\ X \dfrac{2SV}{\text{LAA outlet area}}}{\text{LAA outlet radius}} = \frac{4SV}{(\text{LAA area X LAA outlet radius})}$$

Substituting equation 3 into 4, then obtains equation 5

Equation 5:

$$\text{LAA shear rate} = \frac{4(\text{LAA EF X LAA volume})}{(\text{LAA area X LAA outlet radius})}$$

Given a fixed LAA emptying function, then LAA EF is fixed.

Then,

$$\text{LAA shear rate} \propto (\text{proportional to}) \frac{\text{LAA volume}}{\text{LAA outlet area X LAA outlet radius}}$$

Since the LAA outlet area is proportional to the square of the LAA outlet radius ($2\pi r^2$) then,

$$\text{LAA shear rate} \propto (\text{proportional to}) \frac{\text{LAA volume}}{2\pi \text{LAA outlet radius}^2 \text{ X LAA outlet radius}} \propto \frac{\text{LAA volume}}{\text{LAA outlet radius}^3}$$

Thus, for a given LAA emptying function, the LAA shear rate is related to LAA volume and LAA outlet radius of a given LAA morphology. It is directly proportional to the LAA volume and inversely proportion to the LAA outlet radius^3. This implies the *larger the LAA outlet* radius/area, or *the smaller the LAA volume*, the lower the LAA shear rate and hence *increased chance of SEC formation.*

However, this does not explain why larger LAA volumes have been associated with a higher incidence of thromboembolism. An increase in LAA volume could be confounded by a coexisting increase in the LAA outlet radius/area. This may partially but inadequately explain this finding [18].

On the other hand, the LAA shear rate for a fixed LAA morphology is directly proportional to the LAA emptying function. The lower the LAA function, the lower the shear rate:

$$\text{LAA shear rate} = \frac{4 \text{ X LAA EF X LAA volume}}{\text{LAA outlet area X LAA outlet radius}} \propto \text{LAA EF, for a given LAA morphology}$$

5.5.2 Slow Vortical Velocity in the Left Atrial Appendage

Using the analogy of abnormal vortex formation observed in severe dilated cardiomyopathy in echocardiography and CMRI, the abnormal vortex is dependent on the interaction between the geometrical structure of the left ventricle and left ventricular function [78-80]. Therefore similar factors are likely to govern the development of slow vortical velocity in the LAA: the LAA emptying function and the geometry of the LAA structure.

Detailed analysis of the slow vortical flow pattern within the LAA is limited by the spatial and temporal resolution of current imaging techniques in comparison to the analyses available for the mapping of vortical flow in the much larger left ventricles. However, the maximum slow vortical velocity in severe LAA SEC has been measured as 3.6cm/s within the LAA [45]. In fluid mechanics, a complex structure should give rise to flow turbulence, therefore generating more abnormal or slow vortical flow, when compared to a structure with simpler geometry [78]. To date this has not been shown to be the case in different LAA morphologies.

5.5.3 Summary

In summary, for a fixed LAA morphology (fixed LAA volume, LAA outlet and complexity of the LAA geometry), the LAA emptying function plays a predominant role in determining both the LAA shear rate and velocity of LAA vortical flow. On the other hand, at a fixed LAA emptying function, the LAA volume and LAA outlet are associated with shear rate while the magnitude of the slow vortical flow velocity may be dependent on the complexity of the LAA geometry.

5.6 Prediction of Stroke Using the $CHADS_2$/$CHADS_2$VASC Scores

The $CHADS_2$ and $CHADS_2$ VASC scores are derived from the prevalence of the stroke risk associated with specified clinical morbidities or risk factors [9, 10]. $CHADS_2$ VASC is composed of scores assigned to congestive heart failure (left ventricular failure), hypertension, age, diabetes, stroke, gender and vascular disease. While $CHADS_2$ is more specific it does not include some high risk cohorts, whereas $CHADS_2$ VASC is highly sensitive but not as specific.

$CHADS_2$ and $CHADS_2$ VASC scores can be considered as aggregates of systemic factors that either interact with pre-existing abnormalities of LAA emptying to promote thrombus formation in the LAA, or as factors that directly modulate the LAA emptying function and LAA remodeling process. These morbidities described in the $CHADS_2$ VASC score can contribute to depressed LAA emptying and possibly the remodeling of the LAA structure, and associate with severe LAA SEC or LAA thrombus [81].

5.6.1 Cerebral thromboembolism

Having prior stroke or cerebral thromboembolism from cardioembolic source is clear evidence of embolic risk and is given an appropriate weighting with a risk score of II in the atrial fibrillation clinical scoring system. In the setting of atrial fibrillation, previous stroke implies previous LAA thrombus formation with embolization, and carries an overall annual risk of recurrent cerebral thromboembolism of up to 17% if left untreated. In the setting of acute stroke with sinus rhythm, depressed LAA function is potentially predictive for the presence of paroxysmal atrial fibrillation [53].

5.6.2 Age

Age is considered a high independent risk for all subtype of the stroke and weighting a score of 1-2 (depending on the age). Even in sinus rhythm there is a reduction of LAA peak emptying velocity with aging (4cm/sec per decade) [82-84]. This implies that there is a reduction of the baseline LAA emptying function with age. In contrast the LAA outlet dimension remains fairly constant after age 20 in normal sinus rhythm. Neither left ventricular size, systolic dysfunction, nor LA or LAA size seem to affect the change in LAA function with aging.

Diastolic dysfunction which is observed with ageing does seem to affect LAA function directly and indirectly. One study measuring LAA wall velocity suggested there is an impairment of the LAA relaxation rather than LAA contraction [66] with ageing. In addition, it was proposed that LV diastolic dysfunction [82] and resultant increased filling pressures may mediate the ageing-related depression of LAA function and higher incidence or severity of LAA SEC/thrombus [81, 85]. In LV diastolic dysfunction, there is an increase in both left atrial active emptying volumes (as the result of the increase left ventricular stiffness) and left atrial active function. The LAA adapts to this resulting in LAA dilatation and increased in active LAA emptying in the setting of LA pressure and volume overload. However, once the limited capacity of the LAA reservoir is exceeded, there is a reduction of LAA function [86] of the enlarged LAA. This reduced baseline LAA peak emptying velocity is worsened by further reduction of LAA emptying as result of atrial fibrillation [54], leading to more severe LAA SEC, thrombus formation and clinical systemic thromboembolism.

5.6.3 Hypertension

Hypertension leads to left ventricular hypertrophy and is an important cause of left ventricular diastolic dysfunction. Hypertension has been associated reduced LAA function in patients in sinus rhythm [87], independent of left ventricular systolic dysfunction. It likely share similar mechanism to that of the ageing process. Whereas ageing is an un-modifiable risk factor, control of hypertension is achievable and can improve LAA emptying function [88]. Similar to the ageing process, when hypertension leads to left ventricular diastolic dysfunction it also increases afterload for the left atrium. The subsequent increased left atrial reservoir function leads to an increase in both LA volume and the LA contractile function. These in turn increase the afterload for the LAA and once exceeding the LAA adaptive capacity lead to reduction of LAA function.

5.6.4 Diabetes Mellitus

Diabetes mellitus carries annual rate risk of thromboembolism of roughly 2%, similar to the thromboembolism risk of being in age group of 65~74 year-olds [10]. There are few if any studies directly investigating how diabetes mellitus affects LAA function. Diabetes can lead to diabetic cardiomyopathy, an entity characterized by the presence of left ventricular diastolic dysfunction [89]. This can therefore be expected to share similar pathophysiology to both hypertension and aging in its effects on the left ventricle and subsequent impairment of LAA function. In contrast to hypertension, there is no reversible component to the left ventricular diastolic dysfunction seen with ageing or diabetic cardiomyopathy. In addition, given the systemic effects of diabetes on microvascular function and protein modification by glycation and glycoxidation the possibility of direct pathological effects of diabetes on LAA function should be considered.

5.6.5 Congestive Cardiac Failure/Left Ventricular Failure

Sinus rhythm is rarely associated with LAA thrombus unless there is presence of structure heart disease, such as left ventricular dysfunction with cardiac failure [90]. In dilated cardiomyopathy, there is a high prevalence of LAA thrombus, despite the preservation of sinus rhythm [91]. Multiple studies to date have shown that dilated cardiomyopathy is associated with depressed LAA function and therefore leads to LAA echocardiographic abnormalities [92-95]. Although the mechanism of LAA dysfunction is not clear, dilatation of the LAA may follow the dysfunction and dilation of the left ventricle [96]. Associated LV diastolic dysfunction may also contribute as indicated earlier.

5.6.6 Gender

Female gender is consistently associated with an increased risk of systemic thromboembolism and echocardiographic findings of higher incidence of LAA SEC in female gender also support a mechanistic association [97, 98]. The mechanism for this observation had been thought to be multifactorial and complex [97]. However, it may be explained by women having a lower baseline LAA emptying function than men even in sinus rhythm [84].

5.6.7 Vascular Disease

Vascular disease includes atherosclerosis of the carotid arteries, aortic arch, peripheral vascular vessel and coronary artery disease. Atheroma of the carotid and aortic arch can lead to embolic cerebral thromboembolism which is non-cardiac in origin. Coronary artery disease such as myocardial infarction can be associated with arrhythmias, including atrial fibrillation, while symptomatic coronary artery disease has been associated with a substantial increase in the risk of intra-cardiac thrombus and cerebral thromboembolism [99]. Ischemia and infarction can both increase LV end diastolic filling pressures, either related to systolic or diastolic dysfunction, and it is possible that LAA and LA booster function are perturbed secondary to this. Depressed LAA function after post-myocardial infarction has been observed as increasing the risk of LAA thrombus and SEC, even in the setting of sinus rhythm [69, 100].

5.6.8 Summary

Previous cerebral thromboembolism carries the highest risk for recurrent stroke in atrial fibrillation cohort. Age, hypertension and diabetes are all associated with higher annual risk of stroke in patients with atrial fibrillation and may share similar mechanisms as result of LV diastolic dysfunction. Left ventricular systolic dysfunction may share part of the mechanism of LV diastolic dysfunction with contributions from either volume or pressure overload. The correlation of coronary artery disease with systemic thromboembolism from the left atrial appendage is not particularly robust, with a relatively low annual risk except in the group with high ischaemic burden and post myocardial infarction. Lastly, women have reduced biological LAA emptying function, predisposing them for thromboembolism in comparing to male gender.

Overall, the $CHADS_2$ VASC score describes the disease process that dynamically and actively affecting the LAA morphology and LAA function through similar mechanisms. Echocardiographic LAA abnormalities, despite being the gold standard in predicting the risk of thromboembolism by detecting slow flow and spontaneous echo contrast, only provides a snapshot analysis and short term stroke risk assessment unless repeated transeosphageal echocardiography can be performed (which would be highly unusual). A table of all predictors for thromboembolism in atrial fibrillation had been summarized as below.

Table 5.1 Prediction of thromboembolism in patients with atrial fibrillation

Type of predictor for cerebral thromboembolism			Annual event rate (%) (RR/OR/HR)	10 year annual event rate (%)(RR/OR/HR)	Remark
Baseline stroke risk for zero on scoring.	$CHADS_2$		1.67 (HR 1.0)	1.24(HR 1.0)	
	$CHADS_2$ VASC		0.78 (HR 1.0)	0.66 (HR 1.0)	
Clinical Score (Clinical Predictors)					
Previous thromboembolism	$CHADS_2$		15.46 (HR 9.31)	7.74 (HR 6.05)	
	$CHADS_2$ VASC		16.07 (HR 20.44)	6.98 (HR 10.44)	
Age	$CHADS_2$ (Age ≥75)		5.97 (HR 3.52)	4.64 (HR 3.59)	
	$CHADS_2$ VASC	Age 65~74	2.88 (HR 3.68)	2.09 (HR 3.12)	
		Age ≥75	4.75 (HR 5.96)	4.27 (HR 6.21)	
Diabetes mellitus	$CHADS_2$		3.0 (HR 1.79)	2.42 (HR 1.93)	
	$CHADS_2$ VASC		3.47 (HR 4.46)	2.02 (HR 3.03)	
Congestive cardiac failure	$CHADS_2$		2.8 (HR 1.67)	2.31 (HR 1.84)	
	$CHADS_2$ VASC		1.9 (HR 1.92)	1.78 (HR 2.69)	
Hypertension	$CHADS_2$		2.42 (HR 1.45)	1.94 (HR 1.56)	
	$CHADS_2$ VASC		2.14 (HR 2.76)	1.49 (HR 2.26)	
Gender	$CHADS_2$		NA	NA	
	$CHADS_2$ VASC		1.24 (HR 1.6)	0.82 (HR 1.24)	
Vascular disease	$CHADS_2$		NA	NA	
	$CHADS_2$ VASC		0.75 (HR 0.97)	1.47 (HR 2.22)	

Echocardiographic LAA abnormalities		Any LAA abnormalities[101]	7.8%		
Qualitative	LAA thrombus[37]		12.9%-17.9%(RR 2.5-2.7)		
	Dense LAA SEC[37, 47, 48]		14.4%-22 %(RR 2.7-3.7)	OR 2.4	
Quantitative	LAA emptying function	LAA emptying velocity <20cm/s [37, 57, 102, 103]	2.6-9.9%(RR 1.7-1.8, OR 4.1)		
		LAA wall contracting velocity	HR 3.46 if LAA wall contracting velocity<8.7cm/s		
		LAA ejection fraction (Higher LAAEF, lower risk) [60, 61]	OR 0.57-0.63 for LAA thrombus if LAA EF >21%		Risk for LAA thrombus
	Shear rate[45]		Lower value is associated with higher risk of LAA SEC		
LAA geometry (LAA morphological predictors)					
LAA neck dimension	Larger LAA neck/outlet axial dimension[13, 18]		OR 3.56 for LAA axial dimension product (long axis X short axis). OR 0.33 with smaller LAA diameters		
LAA volumes	Larger LAA volume [16-20]		OR 7.11 if LAA >34cm^3.		
LAA morphology	Chickenwing[11]		0.7% (OR 1.0)		
	Non Chickenwing [11]	Cactus	4.6% (OR 4)		
		Windsock	4.6% (OR 4.8)		
		Cauliflower (Extensive trabeculation)[11, 13, 14]	4.6% (OR 3.36~8.02, OR 3.1 for trabeculation)		

5.7 Conclusion

To conclude, using current available literature, both clinical, morphological and echocardiographic stroke risk predictors can be explained using rheological/fluid dynamic properties. Although from fluid dynamic theory different LAA morphologies may plausibly give rise to different stroke risk the mechanism by which this might occur has not been established. In addition, the discrepancy in current literature on the association between both small and or large LAA volumes with risk of thromboembolism remains unexplained

5.8 Reference

1. Sandercock, P., et al., *Atrial fibrillation and stroke: prevalence in different types of stroke and influence on early and long term prognosis (Oxfordshire community stroke project).* BMJ, 1992. **305**(6867): p. 1460-5.
2. Conway, D. and G.Y. Lip, *Atrial fibrillation and stroke: more concepts and controversies.* Stroke, 2001. **32**(8): p. 1931-8.
3. Levy, S., *Atrial fibrillation, the arrhythmia of the elderly, causes and associated conditions.* Anadolu Kardiyol Derg, 2002. **2**(1): p. 55-60.
4. Marini, C., et al., *Contribution of atrial fibrillation to incidence and outcome of ischemic stroke: results from a population-based study.* Stroke, 2005. **36**(6): p. 1115-9.
5. Hohnloser, S.H., et al., *Incidence of stroke in paroxysmal versus sustained atrial fibrillation in patients taking oral anticoagulation or combined antiplatelet therapy: an ACTIVE W Substudy.* J Am Coll Cardiol, 2007. **50**(22): p. 2156-61.
6. Odell, J.A., et al., *Thoracoscopic obliteration of the left atrial appendage: potential for stroke reduction?* Ann Thorac Surg, 1996. **61**(2): p. 565-9.
7. Johnson, W.D., et al., *The left atrial appendage: our most lethal human attachment! Surgical implications.* Eur J Cardiothorac Surg, 2000. **17**(6): p. 718-22.
8. Stollberger, C., G. Ernst, and J. Finsterer, *Is the left atrial appendage our most lethal attachment?* Eur J Cardiothorac Surg, 2000. **18**(5): p. 625-6; author reply 627.
9. Gage, B.F., et al., *Validation of clinical classification schemes for predicting stroke: results from the National Registry of Atrial Fibrillation.* JAMA, 2001. **285**(22): p. 2864-70.
10. Olesen, J.B., et al., *Validation of risk stratification schemes for predicting stroke and thromboembolism in patients with atrial fibrillation: nationwide cohort study.* BMJ, 2011. **342**: p. d124.

11. Di Biase, L., et al., *Does the left atrial appendage morphology correlate with the risk of stroke in patients with atrial fibrillation? Results from a multicenter study.* J Am Coll Cardiol, 2012. **60**(6): p. 531-8.
12. Anselmino, M., et al., *Left atrial appendage morphology and silent cerebral ischemia in atrial fibrillation patients.* Heart Rhythm, 2013.
13. Khurram, I.M., et al., *Relationship between left atrial appendage morphology and stroke in patients with atrial fibrillation.* Heart Rhythm, 2013. **10**(12): p. 1843-9.
14. Kimura, T., et al., *Anatomical characteristics of the left atrial appendage in cardiogenic stroke with low CHADS2 scores.* Heart Rhythm, 2013. **10**(6): p. 921-5.
15. Kumar, D.R., et al., *Virchow's contribution to the understanding of thrombosis and cellular biology.* Clin Med Res, 2010. **8**(3-4): p. 168-72.
16. Taina, M., et al., *Left Atrial Appendage Volume Increased in More Than Half of Patients with Cryptogenic Stroke.* PLoS ONE, 2013. **8**(11): p. e79519.
17. Burrell, L.D., et al., *Usefulness of left atrial appendage volume as a predictor of embolic stroke in patients with atrial fibrillation.* Am J Cardiol, 2013. **112**(8): p. 1148-52.
18. Beinart, R., et al., *Left atrial appendage dimensions predict the risk of stroke/TIA in patients with atrial fibrillation.* J Cardiovasc Electrophysiol, 2011. **22**(1): p. 10-5.
19. Ernst, G., et al., *Morphology of the left atrial appendage.* Anat Rec, 1995. **242**(4): p. 553-61.
20. Somerville, W. and R.J. Chambers, *Systemic Embolism in Mitral Stenosis: Relation to the Size of the Left Atrial Appendix.* Br Med J, 1964. **2**(5418): p. 1167-9.
21. Khan, I.A., *Atrial stunning: determinants and cellular mechanisms.* Am Heart J, 2003. **145**(5): p. 787-94.
22. Chang, S.H., et al., *Morphological changes of the left atrial appendage after catheter ablation of atrial fibrillation.* J Cardiovasc Electrophysiol, 2007. **18**(1): p. 47-52.

23. Masawa, N., et al., *Diagnosis of cardiac thrombosis in patients with atrial fibrillation in the absence of macroscopically visible thrombi.* Virchows Arch A Pathol Anat Histopathol, 1993. **422**(1): p. 67-71.
24. Begent, N. and G.V. Born, *Growth rate in vivo of platelet thrombi, produced by iontophoresis of ADP, as a function of mean blood flow velocity.* Nature, 1970. **227**(5261): p. 926-30.
25. Richardson, P.D., *Letter: Effect of blood flow velocity on growth rate of platelet thrombi.* Nature, 1973. **245**(5420): p. 103-4.
26. Shen, F., et al., *Threshold response of initiation of blood coagulation by tissue factor in patterned microfluidic capillaries is controlled by shear rate.* Arterioscler Thromb Vasc Biol, 2008. **28**(11): p. 2035-41.
27. Black, I.W., et al., *Hematologic correlates of left atrial spontaneous echo contrast and thromboembolism in nonvalvular atrial fibrillation.* J Am Coll Cardiol, 1993. **21**(2): p. 451-7.
28. Lip, G.Y., et al., *Fibrin D-dimer and beta-thromboglobulin as markers of thrombogenesis and platelet activation in atrial fibrillation. Effects of introducing ultra-low-dose warfarin and aspirin.* Circulation, 1996. **94**(3): p. 425-31.
29. Sakurai, K., et al., *Left atrial appendage function and abnormal hypercoagulability in patients with atrial flutter.* Chest, 2003. **124**(5): p. 1670-4.
30. Leithauser, B., F. Jung, and J.W. Park, *Rheological and hemostasiological aspects of thrombus formation in the left atrial appendage in atrial fibrillation? A new strategy for prevention of cardioembolic stroke.* Clin Hemorheol Microcirc, 2010. **45**(2-4): p. 311-23.
31. Choudhury, A. and G.Y. Lip, *Atrial fibrillation and the hypercoagulable state: from basic science to clinical practice.* Pathophysiol Haemost Thromb, 2003. **33**(5-6): p. 282-9.
32. Watson, T., E. Shantsila, and G.Y. Lip, *Mechanisms of thrombogenesis in atrial fibrillation: Virchow's triad revisited.* Lancet, 2009. **373**(9658): p. 155-66.

33. Lip, G.Y., et al., *Additive role of plasma von Willebrand factor levels to clinical factors for risk stratification of patients with atrial fibrillation.* Stroke, 2006. **37**(9): p. 2294-300.
34. Habara, S., et al., *Prediction of left atrial appendage thrombi in non-valvular atrial fibrillation.* Eur Heart J, 2007. **28**(18): p. 2217-22.
35. Cohen, A., et al., *D-dimers in atrial fibrillation: a further step in risk stratification of thrombo-embolism?* Eur Heart J, 2007. **28**(18): p. 2179-80.
36. Silva, R.P. and C.R. Rodrigues, *Thrombotic events in two siblings with thrombophilia.* Arq Bras Cardiol, 2006. **87**(6): p. e234-5.
37. Zabalgoitia, M., et al., *Transesophageal echocardiographic correlates of clinical risk of thromboembolism in nonvalvular atrial fibrillation. Stroke Prevention in Atrial Fibrillation III Investigators.* J Am Coll Cardiol, 1998. **31**(7): p. 1622-6.
38. Tamura, H., et al., *Prognostic Value of Low Left Atrial Appendage Wall Velocity in Patients with Ischemic Stroke and Atrial Fibrillation.* Journal of the American Society of Echocardiography, 2012. **25**(5): p. 576-583.
39. Rastegar, R., et al., *Spontaneous echo contrast videodensity is flow-related and is dependent on the relative concentrations of fibrinogen and red blood cells.* J Am Coll Cardiol, 2003. **41**(4): p. 603-10.
40. Chien, S. and K. Jan, *Ultrastructural basis of the mechanism of rouleaux formation.* Microvasc Res, 1973. **5**(2): p. 155-66.
41. Sadanandan, S. and M.V. Sherrid, *Clinical and echocardiographic characteristics of left atrial spontaneous echo contrast in sinus rhythm.* J Am Coll Cardiol, 2000. **35**(7): p. 1932-8.
42. Merino, A., et al., *Echocardiographic "smoke" is produced by an interaction of erythrocytes and plasma proteins modulated by shear forces.* Journal of the American College of Cardiology, 1992. **20**(7): p. 1661-1668.
43. Zotz, R.J., et al., *Left atrial thrombi despite anticoagulant and antiplatelet therapy.* Clin Cardiol, 1994. **17**(7): p. 375-82.
44. Fatkin, D., et al., *Inhibition of red cell aggregation prevents spontaneous echocardiographic contrast formation in human blood.* Circulation, 1997. **96**(3): p. 889-96.

45. Donal, E., et al., *Contrast-enhanced tissue Doppler imaging of the left atrial appendage is a new quantitative measure of spontaneous echocardiographic contrast in atrial fibrillation.* Eur J Echocardiogr, 2008. **9**(1): p. 5-11.
46. Fatkin, D., R.P. Kelly, and M.P. Feneley, *Relations between left atrial appendage blood flow velocity, spontaneous echocardiographic contrast and thromboembolic risk in vivo.* J Am Coll Cardiol, 1994. **23**(4): p. 961-9.
47. Bernhardt, P., et al., *Patients with atrial fibrillation and dense spontaneous echo contrast at high risk a prospective and serial follow-up over 12 months with transesophageal echocardiography and cerebral magnetic resonance imaging.* J Am Coll Cardiol, 2005. **45**(11): p. 1807-12.
48. Asinger, R.W., et al., *Pathophysiologic correlates of thromboembolism in nonvalvular atrial fibrillation: II. Dense spontaneous echocardiographic contrast (The Stroke Prevention in Atrial Fibrillation [SPAF-III] study).* J Am Soc Echocardiogr, 1999. **12**(12): p. 1088-96.
49. Ito, T., et al., *Quantification of left atrial appendage spontaneous echo contrast in patients with chronic nonalvular atrial fibrillation.* J Cardiol, 2001. **37**(6): p. 325-33.
50. Kato, H., et al., *Hemodynamic abnormalities in the left atrial appendage in patients with paroxysmal atrial fibrillation, with special reference to albumin-contrast echocardiographic aspects.* Cardiology, 1999. **92**(2): p. 135-43.
51. Mugge, A., et al., *Assessment of left atrial appendage function by biplane transesophageal echocardiography in patients with nonrheumatic atrial fibrillation: identification of a subgroup of patients at increased embolic risk.* J Am Coll Cardiol, 1994. **23**(3): p. 599-607.
52. Pollick, C. and D. Taylor, *Assessment of left atrial appendage function by transesophageal echocardiography. Implications for the development of thrombus.* Circulation, 1991. **84**(1): p. 223-31.
53. Shimizu, T., et al., *Association between Paroxysmal Atrial Fibrillation and the Left Atrial Appendage Ejection Fraction during Sinus Rhythm in the Acute Stage of Stroke: A Transesophageal Echocardiographic Study.* Journal of Stroke and Cerebrovascular Diseases, 2013. **22**(8): p. 1370-1376.

54. Ozer, N., et al., *Left atrial appendage function in patients with cardioembolic stroke in sinus rhythm and atrial fibrillation.* J Am Soc Echocardiogr, 2000. **13**(7): p. 661-5.
55. Omran, H., et al., *Left atrial chamber and appendage function after internal atrial defibrillation: a prospective and serial transesophageal echocardiographic study.* J Am Coll Cardiol, 1997. **29**(1): p. 131-8.
56. Black, I.W., et al., *Left atrial spontaneous echo contrast: a clinical and echocardiographic analysis.* J Am Coll Cardiol, 1991. **18**(2): p. 398-404.
57. Handke, M., et al., *Left atrial appendage flow velocity as a quantitative surrogate parameter for thromboembolic risk: determinants and relationship to spontaneous echocontrast and thrombus formation--a transesophageal echocardiographic study in 500 patients with cerebral ischemia.* J Am Soc Echocardiogr, 2005. **18**(12): p. 1366-72.
58. Panagiotopoulos, K., et al., *Left Atrial and Left Atrial Appendage Functional Abnormalities in Patients with Cardioembolic Stroke in Sinus Rhythm and Idiopathic Atrial Fibrillation.* Journal of the American Society of Echocardiography, 1998. **11**(7): p. 711-719.
59. Pozzoli, M., et al., *Left atrial appendage dysfunction: a cause of thrombosis? Evidence by transesophageal echocardiography-Doppler studies.* J Am Soc Echocardiogr, 1991. **4**(5): p. 435-41.
60. Iwama, M., et al., *Left atrial appendage emptying fraction assessed by a feature-tracking echocardiographic method is a determinant of thrombus in patients with nonvalvular atrial fibrillation.* J Cardiol, 2012. **59**(3): p. 329-36.
61. Ono, K., et al., *Motion of left atrial appendage as a determinant of thrombus formation in patients with a low CHADS2 score receiving warfarin for persistent nonvalvular atrial fibrillation.* Cardiovasc Ultrasound, 2012. **10**: p. 50.
62. Chen, O.D., et al., *Assessment of the morphology and mechanical function of the left atrial appendage by real-time three-dimensional transesophageal echocardiography.* Chin Med J (Engl), 2012. **125**(19): p. 3416-20.

63. Valocik, G., et al., *Assessment of the left atrial appendage mechanical function by three-dimensional echocardiography.* Eur J Echocardiogr, 2002. **3**(3): p. 207-13.
64. Parvathaneni, L., et al., *Comparison of tissue Doppler dynamics to Doppler flow in evaluating left atrial appendage function by transesophageal echocardiography.* Am J Cardiol, 2005. **95**(8): p. 1011-4.
65. Trambaiolo, P., et al., *Assessment of left atrial appendage wall velocities by transesophageal tissue Doppler echocardiography: a clinical study in patients with sinus rhythm.* J Am Soc Echocardiogr, 2002. **15**(5): p. 425-32.
66. Yoshida, N., et al., *Transthoracic tissue Doppler assessment of left atrial appendage contraction and relaxation: their changes with aging.* Echocardiography, 2010. **27**(7): p. 839-46.
67. Yoshida, N., et al., *Role of transthoracic left atrial appendage wall motion velocity in patients with persistent atrial fibrillation and a low CHADS2 score.* Journal of Cardiology, 2012. **60**(4): p. 310-315.
68. Uretsky, S., et al., *Assessment of left atrial appendage function with transthoracic tissue Doppler echocardiography.* Eur J Echocardiogr, 2009. **10**(3): p. 363-71.
69. Topsakal, R., et al., *Evaluation of left atrial appendage functions in patients with thrombus and spontaneous echo contrast in left atrial appendage by using color Doppler tissue imaging.* Ann Noninvasive Electrocardiol, 2004. **9**(4): p. 345-51.
70. Schött, U. and P.I. Johansson, *Bringing flow into haemostasis diagnostics.* British Journal of Anaesthesia, 2013.
71. Grimm, R.A., et al., *Left atrial appendage "stunning" after electrical cardioversion of atrial flutter: an attenuated response compared with atrial fibrillation as the mechanism for lower susceptibility to thromboembolic events.* J Am Coll Cardiol, 1997. **29**(3): p. 582-9.
72. Veinot, J.P., et al., *Anatomy of the normal left atrial appendage: a quantitative study of age-related changes in 500 autopsy hearts: implications for echocardiographic examination.* Circulation, 1997. **96**(9): p. 3112-5.

73. Al-Saady, N.M., O.A. Obel, and A.J. Camm, *Left atrial appendage: structure, function, and role in thromboembolism.* Heart, 1999. **82**(5): p. 547-54.
74. Erol, B., et al., *Analysis of left atrial appendix by dual-source CT coronary angiography: morphologic classification and imaging by volume rendered CT images.* Eur J Radiol, 2011. **80**(3): p. e346-50.
75. Stein, P.D. and H.N. Sabbah, *Measured turbulence and its effect on thrombus formation.* Circ Res, 1974. **35**(4): p. 608-14.
76. White R John, U.-L., *Laminr vs. Turbulent Flow in a Pipe.* Lecture notes for applied problem solving with Matlab. , 2003.
77. Ma, X., X. Zhang, and W. Guo, *Factors to predict recurrence of atrial fibrillation in patients with hypertension.* Clin Cardiol, 2009. **32**(5): p. 264-8.
78. Mohiaddin, R.H., G.Z. Yang, and P.J. Kilner, *Visualization of flow by vector analysis of multidirectional cine MR velocity mapping.* J Comput Assist Tomogr, 1994. **18**(3): p. 383-92.
79. Kim, W.Y., et al., *Left ventricular blood flow patterns in normal subjects: a quantitative analysis by three-dimensional magnetic resonance velocity mapping.* J Am Coll Cardiol, 1995. **26**(1): p. 224-38.
80. Hong, G.R., et al., *Characterization and quantification of vortex flow in the human left ventricle by contrast echocardiography using vector particle image velocimetry.* JACC Cardiovasc Imaging, 2008. **1**(6): p. 705-17.
81. Willens, H.J., et al., *Correlation of CHADS2 and CHA2DS2-VASc scores with transesophageal echocardiography risk factors for thromboembolism in a multiethnic United States population with nonvalvular atrial fibrillation.* J Am Soc Echocardiogr, 2013. **26**(2): p. 175-84.
82. Ilercil, A., et al., *Influence of age on left atrial appendage function in patients with nonvalvular atrial fibrillation.* Clin Cardiol, 2001. **24**(1): p. 39-44.
83. Illien, S., et al., *Atrial fibrillation: relation between clinical risk factors and transoesophageal echocardiographic risk factors for thromboembolism.* Heart, 2003. **89**(2): p. 165-168.
84. Agmon, Y., et al., *Left atrial appendage flow velocities in subjects with normal left ventricular function.* Am J Cardiol, 2000. **86**(7): p. 769-73.

85. Muhammed Bora Demirçelik, M.Ç., Hülya Çiçekcioğlu, Özgül Uçar, Mustafa Duran, *Effect of left ventricular diastolic dysfunction on left atrial appendage function and thrombotic potential in nonvalvular atrial fibrillation.* Anadolu Kardiyol Derg 2013, 2014. **13**.
86. Tabata, T., et al., *Influence of left atrial pressure on left atrial appendage flow velocity patterns in patients in sinus rhythm.* J Am Soc Echocardiogr, 1996. **9**(6): p. 857-64.
87. Bilge, M., et al., *Transesophageal echocardiography assessment of left atrial appendage function in untreated systemic hypertensive patients in sinus rhythm.* J Am Soc Echocardiogr, 2000. **13**(4): p. 271-6.
88. Bilge, M., et al., *Effect of blood pressure reduction on abnormal left atrial appendage function in untreated systemic hypertensive patients with sinus rhythm.* Angiology, 2001. **52**(9): p. 621-6.
89. Bayeva, M., K.T. Sawicki, and H. Ardehali, *Taking diabetes to heart--deregulation of myocardial lipid metabolism in diabetic cardiomyopathy.* J Am Heart Assoc, 2013. **2**(6): p. e000433.
90. Agmon, Y., et al., *Clinical and echocardiographic characteristics of patients with left atrial thrombus and sinus rhythm: experience in 20 643 consecutive transesophageal echocardiographic examinations.* Circulation, 2002. **105**(1): p. 27-31.
91. Bakalli, A., et al., *Prevalence of left chamber cardiac thrombi in patients with dilated left ventricle at sinus rhythm: the role of transesophageal echocardiography.* J Clin Ultrasound, 2013. **41**(1): p. 38-45.
92. Siostrzonek, P., et al., *Hemodynamic and hemorheologic determinants of left atrial spontaneous echo contrast and thrombus formation in patients with idiopathic dilated cardiomyopathy.* Am Heart J, 1993. **125**(2 Pt 1): p. 430-4.
93. Cemri, M., et al., *Effects of left ventricular systolic dysfunction on left atrial appendage and left atrial functions in patients with chronic nonvalvular atrial fibrillation.* Acta Cardiol, 2002. **57**(2): p. 101-5.
94. Mahilmaran, A., et al., *Relationship of left atrial appendage function to left ventricular function.* Indian Heart J, 2004. **56**(4): p. 293-8.

95. Handke, M., et al., *Predictors of left atrial spontaneous echocardiographic contrast or thrombus formation in stroke patients with sinus rhythm and reduced left ventricular function.* Am J Cardiol, 2005. **96**(9): p. 1342-4.
96. Bakalli, A., et al., *The influence of left ventricular diameter on left atrial appendage size and thrombus formation in patients with dilated cardiomyopathy.* Turk Kardiyol Dern Ars, 2010. **38**(2): p. 90-4.
97. Cove, C.L., et al., *Female sex as an independent risk factor for stroke in atrial fibrillation: Possible mechanisms.* Thromb Haemost, 2013. **111**(3).
98. Wanezaki, M., et al., *Female patients with non-valvular atrial fibrillation are susceptible to cardioembolic stroke because of their left atrial enlargement.* European Heart Journal, 2013. **34**(suppl 1).
99. Sen, S., et al., *Risk factors for intracardiac thrombus in patients with recent ischaemic cerebrovascular events.* J Neurol Neurosurg Psychiatry, 2004. **75**(10): p. 1421-5.
100. Bilge, M., et al., *Frequency of left atrial thrombus and spontaneous echocardiographic contrast in acute myocardial infarction.* The American Journal of Cardiology, 1999. **84**(7): p. 847-849.
101. Echocardiography, T.S.P.i.A.F.I.C.o., *Transesophageal echocardiographic correlates of thromboembolism in high-risk patients with nonvalvular atrial fibrillation. The Stroke Prevention in Atrial Fibrillation Investigators Committee on Echocardiography.* Ann Intern Med, 1998. **128**(8): p. 639-47.
102. Goldman, M.E., et al., *Pathophysiologic correlates of thromboembolism in nonvalvular atrial fibrillation: I. Reduced flow velocity in the left atrial appendage (The Stroke Prevention in Atrial Fibrillation [SPAF-III] study).* J Am Soc Echocardiogr, 1999. **12**(12): p. 1080-7.
103. Kamp, O., et al., *Importance of left atrial appendage flow as a predictor of thromboembolic events in patients with atrial fibrillation.* Eur Heart J, 1999. **20**(13): p. 979-85.

Chapter 6: Impact of Different Left Atrial Appendage Morphology on Slow Vortical Flow Estimated by Flow Dynamics

6.1 Introduction

Early studies in LAA studies had been mainly undertaken using anatomical casts [1-3] whereas more recent studies have used cardiac computed tomography to provide detailed morphology of the LAA *in vivo*. As described in Chapter 5, many studies have shown that LAA morphology can affect the risk of cerebral thromboembolism, independent of clinical stroke risk predictors such as the CHADS2 VASC score[4-7].

LAA morphology was firstly categorised into Chickenwing, Cactus, Windsock and Cauliflower subtypes, with the Cauliflower subtype having the highest risk for cerebral thromboembolism. The initial LAA morphological paper [4]described the Chickenwing LAA morphology as having only a 0.7% annual risk of stroke, whereas the non-Chickenwing LAA morphologies (Cactus, Windsock and Cauliflower subtypes) had only a 4.7% annual risk of stroke (independent of clinical risk score). This was later confirmed on another small cohort; that revealed cauliflower LAA morphology has higher risk of systemic thromboembolism [7]. Lastly, a recent study had shown complex LAA morphology is associated with LAA thrombus formation, independent of clinical risk factors [8]. In all of these studies, the increase risk of stroke has been attributed to slow flow arising from the more complex LAA morphologies. To the best of our knowledge there has been no direct demonstration *in vitro* that flow is altered in different LAA morphologies.

6.1.1: LAA Morphology Classification

The classification system initially described by the first paper in 2012 as the Chickenwing, Cactus, Windsock and Cauliflower subtypes was adapted while acknowledging these are arbitrary classification systems.

1. Chickenwing LAA morphology: The Chicken Wing LAA morphology presents an obvious bend in the proximal or middle part of the dominant lobe, or folding back of the LAA anatomy on itself at some distance from the perceived LAA ostium. This type of LAA may have secondary lobes or twigs.

2. Cactus LAA morphology: The Cactus LAA morphology presents a dominant central lobe with secondary lobes extending from the central lobe in both superior and inferior directions.

3. Windsock LAA morphology: The Windsock LAA morphology presents one dominant lobe of sufficient length as the primary structure. Variations of this LAA type arise with the location and number of secondary or even tertiary lobes arising from the dominant lobe.

4. Cauliflower LAA morphology: The Cauliflower LAA morphology presents limited overall length with more complex internal characteristics. Variations of this LAA type have a more irregular shape of the LAA ostium (oval vs. round) and a variable number of lobes with lack of a dominant lobe.

6.1.2: Computed Fluid with Rheological Property Resemble Severe SEC

Previous echocardiographic studies investigated the rheological property of SEC in left atrial appendage. Echocardiographically, a swirling pattern of blood flow is an intrinsic nature of SEC [9, 10]. In addition, a recent study compared the rheological property differences of severe and mild SEC grading. It was found the average maximal velocity in the presence of severe SEC is only ≤3.6cm/s with a low shear rate of ≤ $45s^{-1}$, while average maximal velocity in the presence of mild SEC was ~7.5cm/s with a shear rate $83s^{-1}$[11]. Therefore, it is reasonably to define the stagnated

computed fluid in a LAA morphology with rheological properties resemble what had been seen in the presence of severe SEC as the region of fluid involved in the vortex (to represent swirling), with low spontaneous velocity of ≤3.6cm/s and low shear rate of ≤ $45s^{-1}$.

This study will seek to investigate whether blood stagnation could be affected by LAA morphology. This will be achieved by quantifying the amount of slow vortical flow, which was thought to be analogous to quantifying the region of relative blood stagnation or spontaneous echo contrast. To achieve the aim, computational fluid dynamics (CFD) with numerical simulation in LAA digital models with varying morphological subtypes were used. The results will then be compared (qualitatively and quantitatively) across different LAA morphologies and related to LAA emptying function. To date there has only been one CFD simulation of an artificial left atrial appendage [12] and the studies included in this chapter are wholly original.

6.2 Method

6.2.1 LAA Morphology

Total of 12 LAA CT data sets were studied, including three examples of each type of LAA morphology. The classification of LAA morphology was verified by two independent operators. None of the LAA examples selected had a filling defect identified on the CT. CT images were acquired using multi-detector computed tomography (MDCT) (Toshiba Aquilion One) during the atrial systolic phase and were all in normal sinus rhythm. The LAA is acquired in the atrial systolic phase as it will match the time for maximum velocity and pressure prescribed in the inlet and outlet boundary condition in LAA models. During image acquisition, the patient was pre-

medicated with metoprolol to achieve a heart rate less than 60/min. In addition 600mcg of sublingual glycerin trinitrate was also administered 2-minutes pre-scanning as standard protocol.

6.2.2 Numerical Simulation

6.2.2.1 IGES (Initial Graphics Exchange Specification) and Mesh File

A 3D digital model of patient-specific CT-derived geometry were extracted from the 12 CT DICOM datasets. It is refined and then converted into IGES format prior to export into ANSYS CFD software for preparation for numerical simulation. During refinement of these digital models, the orifice of the LAA was artificially separated into inlet and outlet in order to allow CFD simulation as shown in **Figure 1A**. In addition, the orifice was elongated by 5mm (**Figure 1B**) to compensate for the length lost from digital modelling, while the inlet was further elongate by 2cm to allow for fully development of laminar/turbulent flow as shown **Figure1C** [13]. These IGES digital files were then transformed to mesh files for numerical simulation, with the minimal tetrahedron volume meshing dimension of 0.2mm and maximum dimension of 0.4mm.

Figure 1

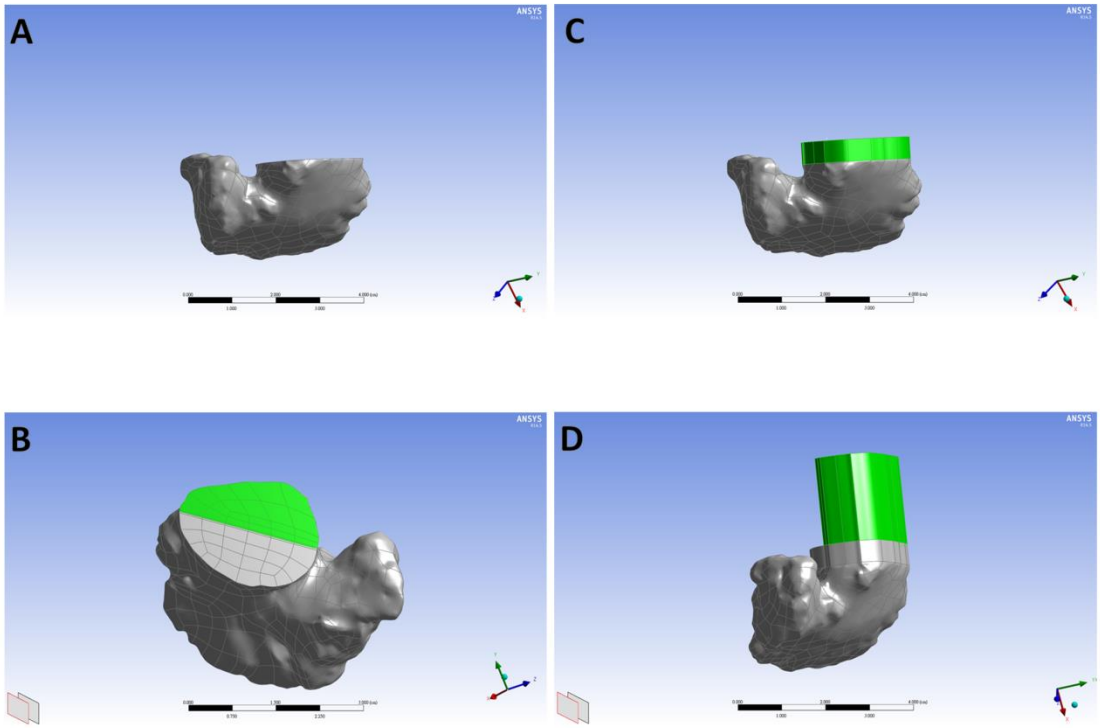

Figure 1: Chickenwing Digital Model

A: *Default IGES Chickenwing Model.* ***B:*** *Artificial Separation of Left Atrial Appendage Orifice into Inlet (Green Colour) and Outlet (grey colour).* ***C:*** *Elongation of Orifice by 5mm to Compensate for the Neck Length Lost from Digital Modelling.* ***D:*** *Elongation of Inlet by 2cm to Allow Full Development of Laminar/Turbulent Flow.*

6.2.2.2 CFD Simulation

Steady flow CFD simulation with no fluid-solid interaction was performed within a turbulence flow model (K-Omega) to allow the calculation of the vortical flow zone. The LAA wall was fixed and non-slip based on the assumption that LAA CFD simulation was at the peak of the atrial systolic phase. The inlet boundary condition was set as 20mmHg as measured in a prior publication using a pressure wire [14]. The outlet boundary is prescribed with a range of lower LAA emptying

velocities (therefore different LAA emptying function) which will relate to the degree of spontaneous echo contrast, ranging from10cm/s, 20cm/s, 30cm/s to 40cm/s[9, 11]. It is observed that SEC generally starts to form with LAA emptying velocities around 40cm/sec. The average maximum velocity within regions of severe SEC is ≤3.6cm/s and shear rate of ≤45s^{-1} while regions of mild SEC have a maximum velocity of ≤7.5cm/s [11]. These published velocities and shear rates corresponding to areas of severe SEC were used to identify areas of slow vortical flow below.

Newtonian flow was assumed with blood density of 6.045Kg/m^3 and temperature of 37 degree Celsius while the haematocrit was fixed at 40% by fixing the viscosity at 0.0035 Pascal/s. Previous *in vitro* studies had shown slow velocity within the vortex increases thrombogenic risk when the velocity is <1mm/s, red blood cells start to aggregate (rouleax) and contribute to thrombus growth while low shear rate initiate thrombus formation[15-17]. After completion of each LAA CFD simulation the total volume (ml) within the slow vortical flow zone with a velocity ≤3.6cm/s and shear rate of ≤ 46s^{-1}) was calculated and was also expressed as percentage of the total LAA volume. These slow vortical flow volumes are considered to be analogous to LAA SEC observed on echocardiography. The values then were analyzed and compared across different LAA morphology classification subtypes as well as across different LAA emptying velocities. Qualitatively, the location of the slow vortical flow region was also evaluated.

6.2.6.3 Statistical Analysis

T-test analyses were used to determine the difference of the mean slow vortical flow volume and percentage (slow vortical volume/LAA volume) that resemble severe SEC across different LAA morphology subgroups and also in various combined groups. Statistical analyses were performed using GraphPad Prism 5.0 (GraphPad Software Inc. La Jolla, California).

6.3 Result

6.3.1 Quantitative Assessment

6.3.1.1 Chickenwing Versus Cactus Versus Windsock Versus Cauliflower

Overall, 48 LAA morphology CFD numerical simulations were performed with 4 different LAA emptying velocities prescribed for each individual LAA morphology. **Figure 2 A-D** shows individual models of different LAA morphological subtypes.

Figure 2

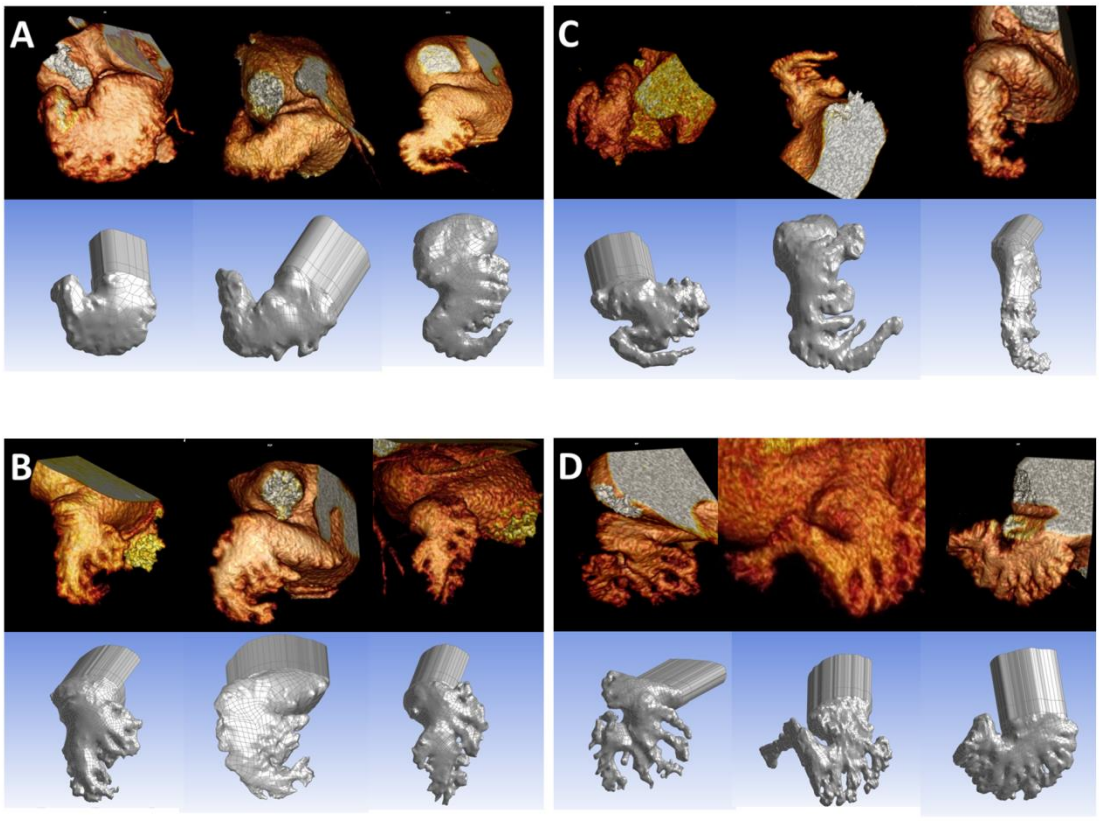

Figure 2: Individual Left Atrial Appendage Studies for CFD Analysis, Classified by Morphological Subtypes. A: *Chickenwing;* ***B:*** *Cactus;* ***C:*** *Windsock;* ***D:*** *Cauliflower Subtypes.*

The individual values of each presumed LAA blood stagnation region (analogous to severe LAA SEC) or the absolute LAA slow vortical flow volume and its percentage to LAA body volume were calculated and listed in **Table 1.** Comparing the LAA slow vortical flow volumes between different LAA morphology, the most obvious observation is the statistically significant higher volume of slow vortical flow in the Cauliflower LAA subtype in comparison to the other LAA morphological subtypes across different LAA emptying velocities under conditions where the LAA emptying velocity is>20cm/s as shown in **Figure 3A**. Once the LAA emptying function is depressed to a critical level below 20cm/s, the slow vortical flow volumes are fairly similar across different LAA morphological subtypes. There is a statistically

significant graded increase in slow vortical flow volume (and % LAA volume) across different LAA morphologies. The smallest, slow vortical flow volume was found in the Chickenwing, progressively increasing in Cactus, Windsock and Cauliflower subtypes.

Table 1:	Different Left Atrial Appendage (LAA) Morphology (Vol=Volume of Slow Vortical Flow (cm3), %=Volume/LAA Volume)																					
	Chickenwing						Cactus						Windsock						Cauliflower			
	1		2		3		1		2		3		1		2		3		1		2		3	
LAA Volume (cm3)	14.53		12.46		11.24		13.53		20.19		8.73		11.6		7.56		5.83		7.80		10.7		10.82	
LAA Emptying Velocity	Vol	%	Vol	%	Vol	%	Vol	%	Vol	%	Vol	%	Vol	%	Vol	%	Vol	%	Vol	%	Vol	%	Vol	%
40 cm/s	0.12	1	0.12	1	0.33	4	0.2	2	0.7	5	0.21	3	0.26	3	0.49	8	0.38	9	1.4	24	1.45	19	1.08	13
30 cm/s	0.17	1	0.27	3	0.54	7	0.22	2	0.7	5	0.6	9	0.96	12	0.72	13	0.3	15	2.23	38	1.76	23	1.24	15
20 cm/s	1.50	13	1.81	20	1.52	19	1.9	21	2.72	18	1.21	18	2.1	27	1.74	30	1.18	28	2.23	38	2.38	31	2.94	37
10 cm/s	2.18	19	2.61	29	2.17	27	2.7	29	3.62	25	2.02	31	2.56	37	2.38	41	1.5	36	2.8	48	2.72	35	3.06	38

Table 1: The Individual Values of the Absolute Left Atrial Appendage Slow Vortical Flow Volume and its Percentage to the Left Atrial Appendage Body Volume of Different Morphological Models.

Figure 3A **Figure 3B**

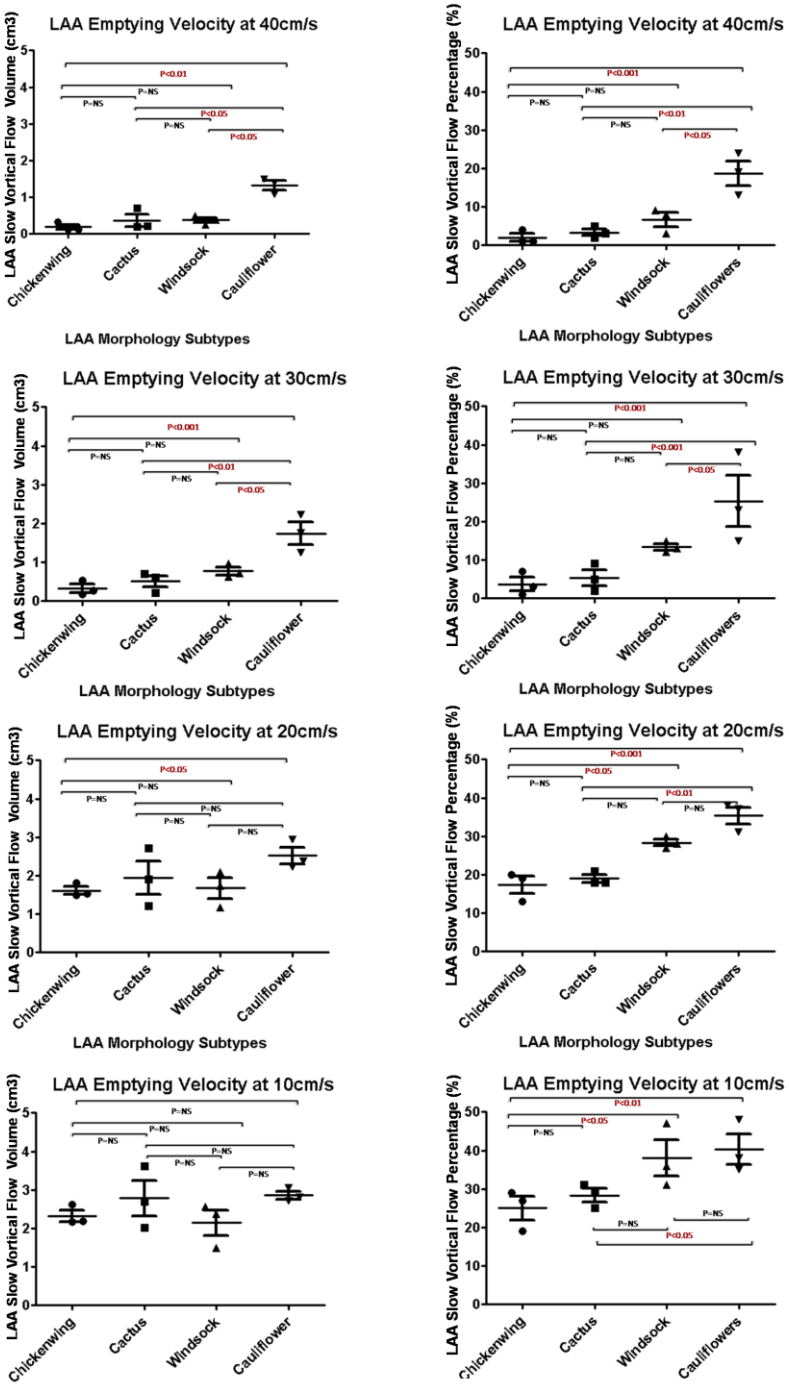

Figure 3: Comparison of Value of Slow Vortical Flow Volume Across Different Morphological Subtypes. A: *Cauliflower Morphology has Statistically Significantly Higher Volume of Slow Vortical Flow. Windsock Morphology Also Has Higher Volume in comparison to Cactus and Chickenwing Morphology. These differences Disappeared When the Left Atrial Appendage Contractile function was Depressed to ≤*

10cm/s. ***B:*** *Similar Trends in Comparing the Percentage of Slow Vortical Flow Volume to Left Atrial Appendage Volume, with Cauliflower Morphology demonstrating the greatest volume assessed as percentage.*

6.3.1.2 Chickenwing, Cactus and Windsock Versus Cauliflower

The initial analysis already shown Cauliflower has the greatest absolute volume of slow flow- stagnating blood flow-of the four LAA subtypes. Further group analysis dividing the four groups into Cauliflower and non-Cauliflower subtypes further strengthens the conclusion that the Cauliflower morphology has statistically significantly greater volumes of slow flow(**Figure 4A**) and greater percentage of LAA volume showing slow vortical flow, except when the LAA emptying velocity reached 10cm/s (**Figure 4B**).

Figure 4A

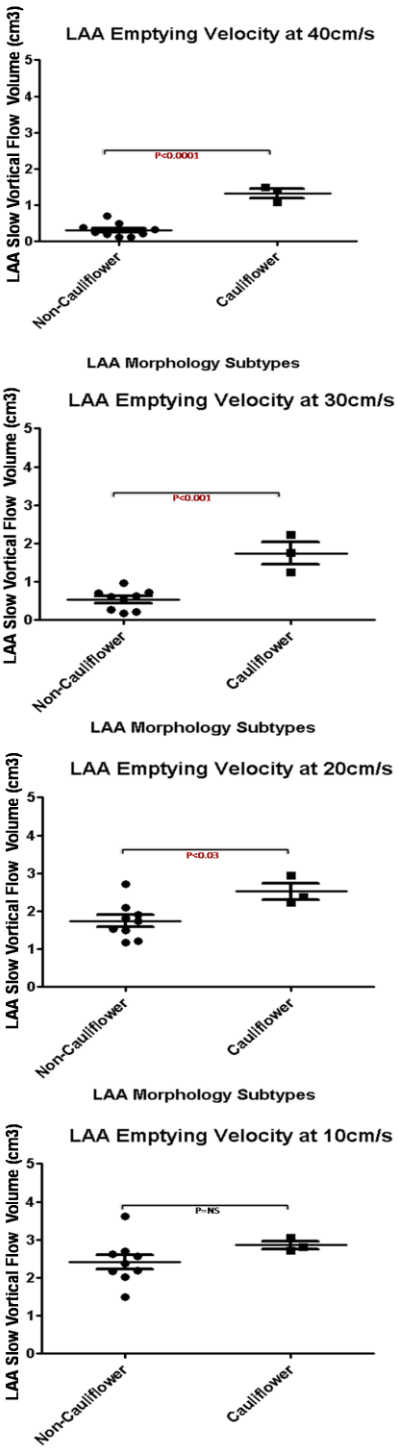

Figure 4B

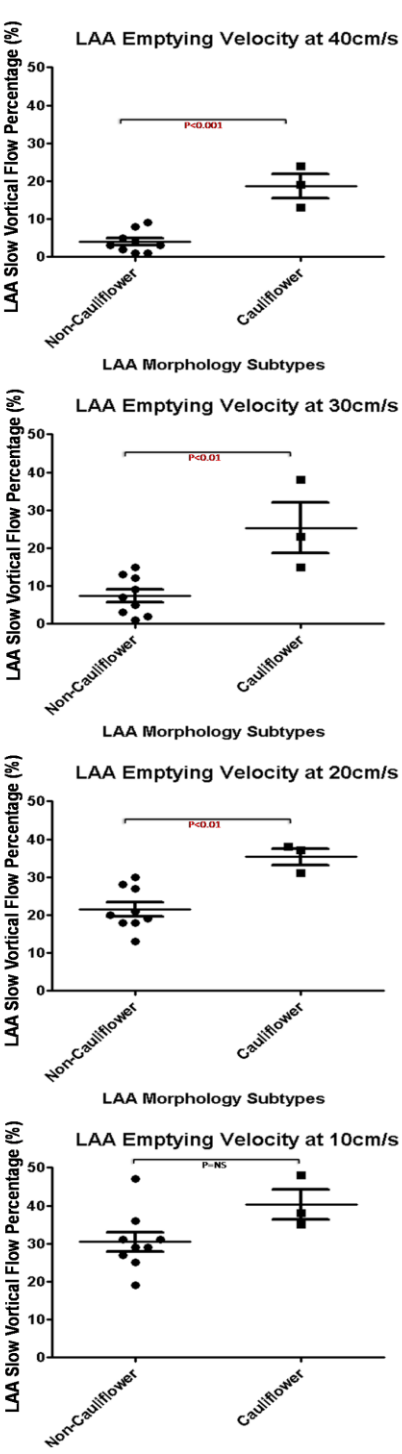

Figure 4: Group Comparison of Value of Slow Vortical Flow Volume of Non-Cauliflower Versus Cauliflower subtypes. A: *Cauliflower Morphology has Statistically Significantly Higher Volume of Slow Vortical Flow.* ***B:*** *Cauliflower Morphology Has the Higher Percentage of Slow Vortical Flow to Left Atrial Appendage Volume.*

6.3.1.3 Chickenwing and Cactus Versus Windsock and Cauliflower

Because the Chickenwing, Cactus groups have been considered the least stroke-prone, the data after combining Chickenwing and Cactus, and combining Windsock with Cauliflower subtypes was also analyzed. The results showed that the Windsock and Cauliflower subtypes had overall statistically significant higher percentage of slow vortical flow in proportion to the LAA volumes, across different LAA emptying function (**Figure 5A**). The absolute volume of slow vortical flow region also is higher in the Windsock/Cauliflower groups, but only when the LAA emptying velocity is equal or greater than 30cm/s (**Figure 5B**).

Figure 5A

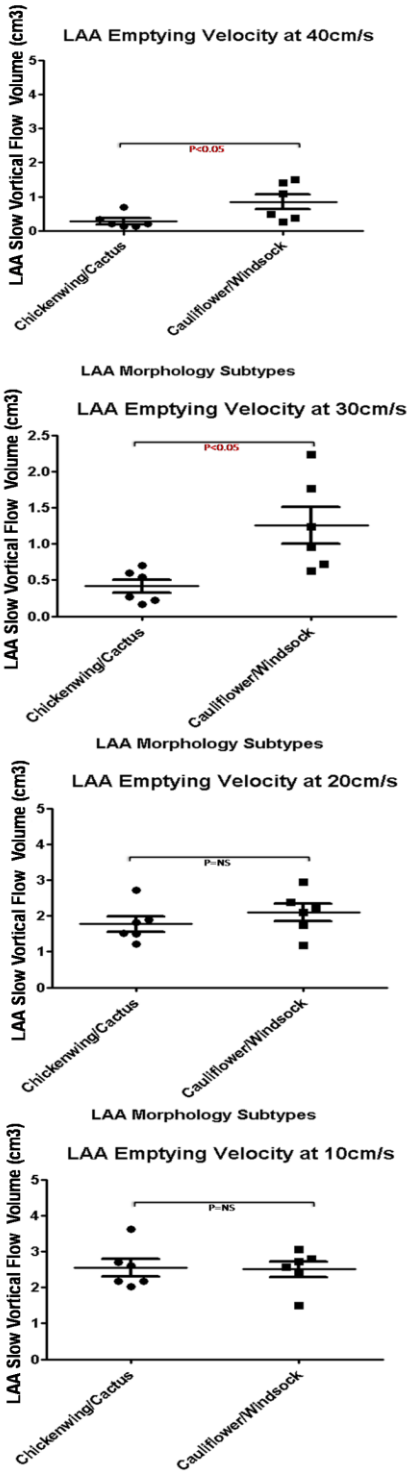

Figure 5B

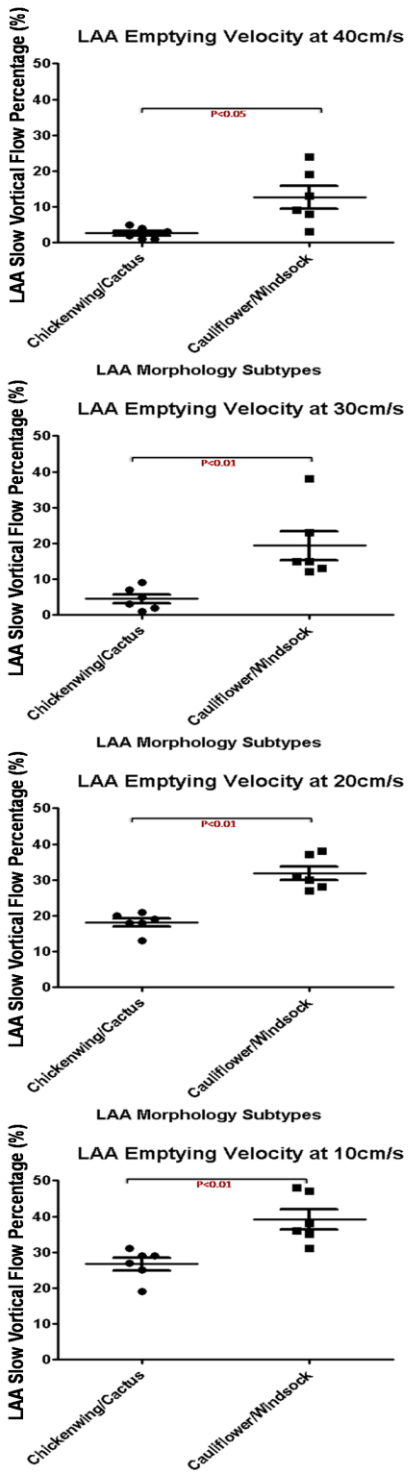

Figure 5: Grouped Comparison of Slow Vortical Flow Volumes of Chickenwing/Cactus Combined Versus Windsock/Cauliflower Combined. A: *LAA volumes (ml) with slow vortical flow* ***B:*** *% of LAA volume with slow vertical flow. Each panel refers to results with varying outflow velocity.*

6.3.1.4 Chickenwing Versus Cactus, Windsock and Cauliflower

One early study described the Chickenwing subtype as having a lower stroke risk compared to other subtypes, whereas three later studies did not show this trend [5-7]. Comparison of Chickenwing to the combined Non-Chickenwing groups did not show any statistically significant difference in absolute volume of slow vortical flow and its percentage to the LAA volumes between the groups (**Figure 6A and 6B**) although the non-Chickenwing group did trend towards greater volumes.

Figure 6A

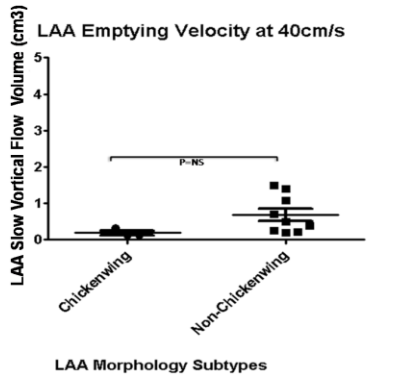

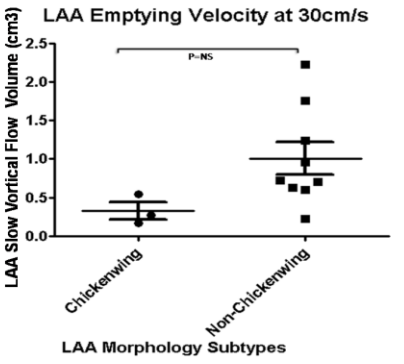

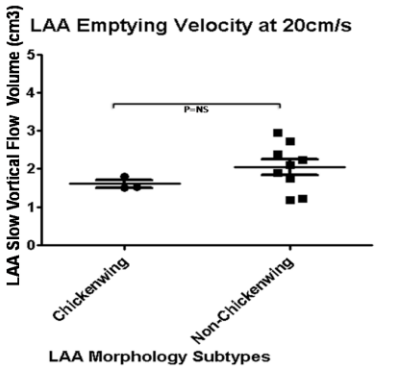

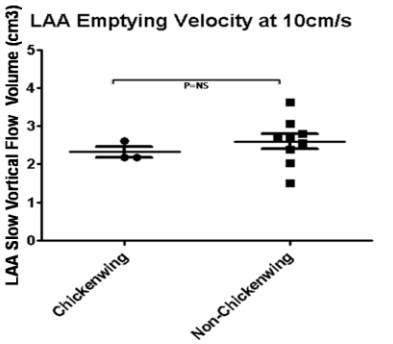

Figure 6B

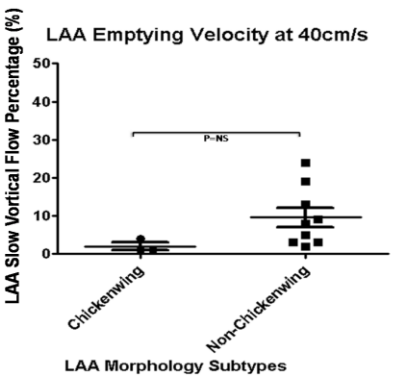

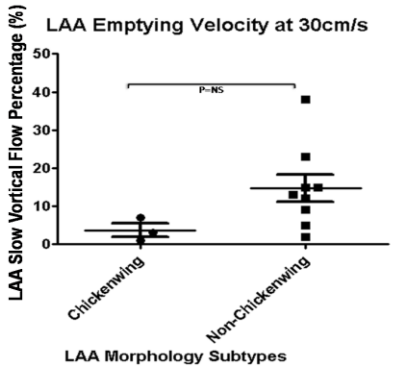

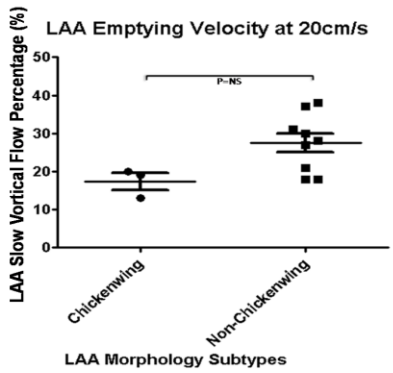

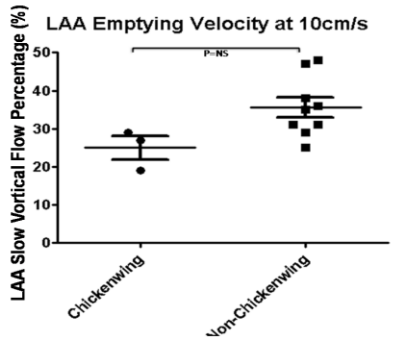

Figure 6: Group Comparison of Value of Slow Vortical Flow Volume of Chickenwing Versus Non-Chickenwing Subtypes. A & B: *Chickenwing Morphology Has* ***no*** *Statistically Significantly Lower Volume of Slow Vortical Flow or Percentage of Slow Vortical Flow to Left Atrial Appendage Volume.*

6.3.2 Qualitative Assessment

One of each LAA morphological subtype simulation results are shown in **Figure 7A** to profile the vortical flow pattern of each morphology subtypes across different magnitude of shear rates with LAA emptying velocity of 40cm/s. **Figure 7B** provides a closer look in both Chickenwing and Cauliflower LAA vortical flow pattern.

The legend of **Figure 7A & B** is that any LAA vortical flow velocity above 7.5cm/s is coded in **RED** colour, while any other colour represents regions of lower velocity and possible SEC formation. From the graph, it is evident that there is a larger volume of slow vortical flow in the LAA neck of Cauliflower subtype when compared to other LAA morphological subtypes at the maximum shear rate for the given LAA morphology and LAA emptying function. At lower magnitudes of shear rate, complicated LAA morphologies with an irregular surface contour tend to have larger visually identifiable slow vortical flow regions in particular evident in the Cauliflower and Windsock subtypes.

Figure 7A

Chicken LAA Morphology Cactus LAA Morphology Windsock LAA Morphology Cauliflower LAA Morphology

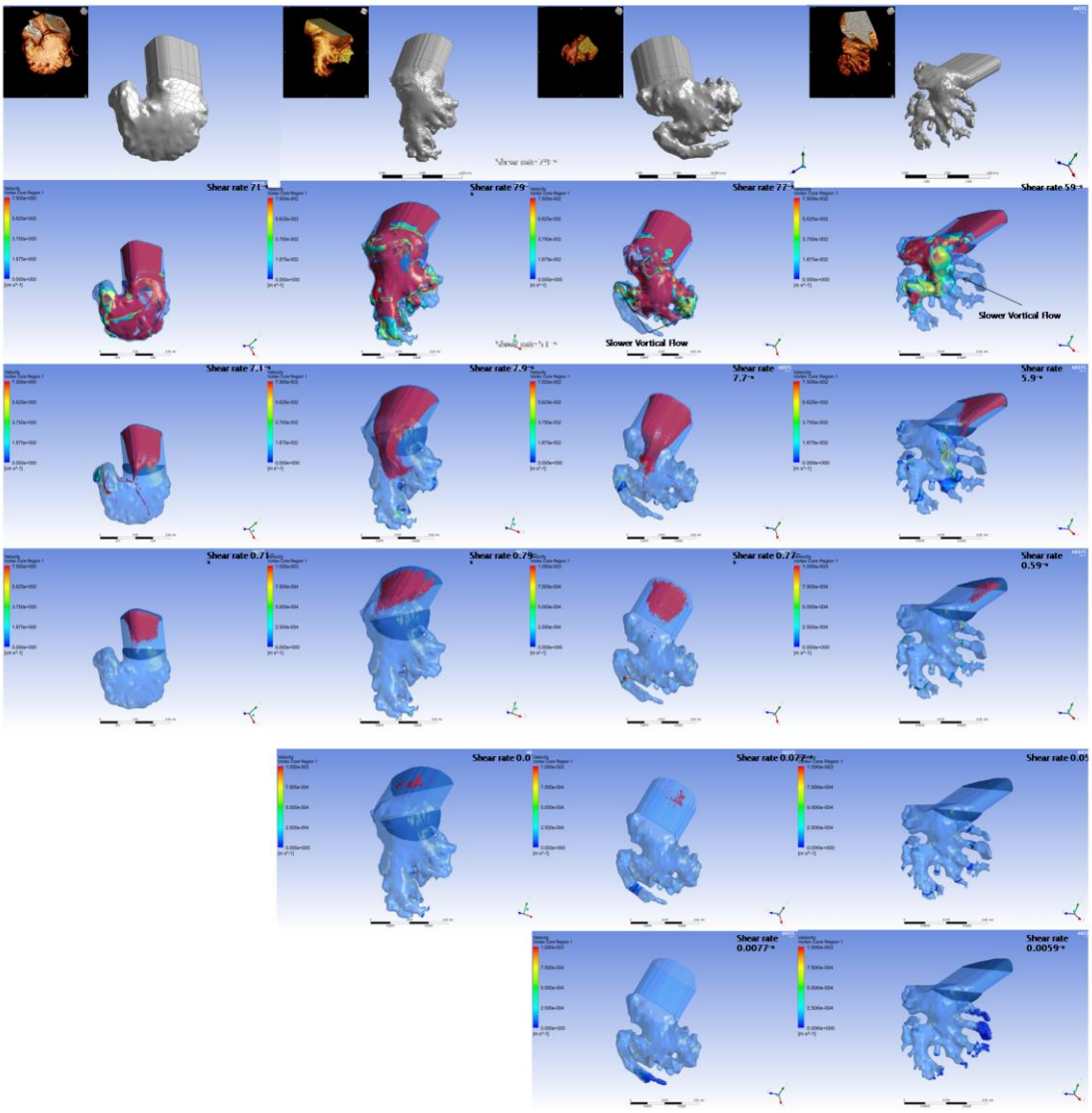

Figure 7B

Chicken LAA Morphology

Cauliflower LAA Morphology

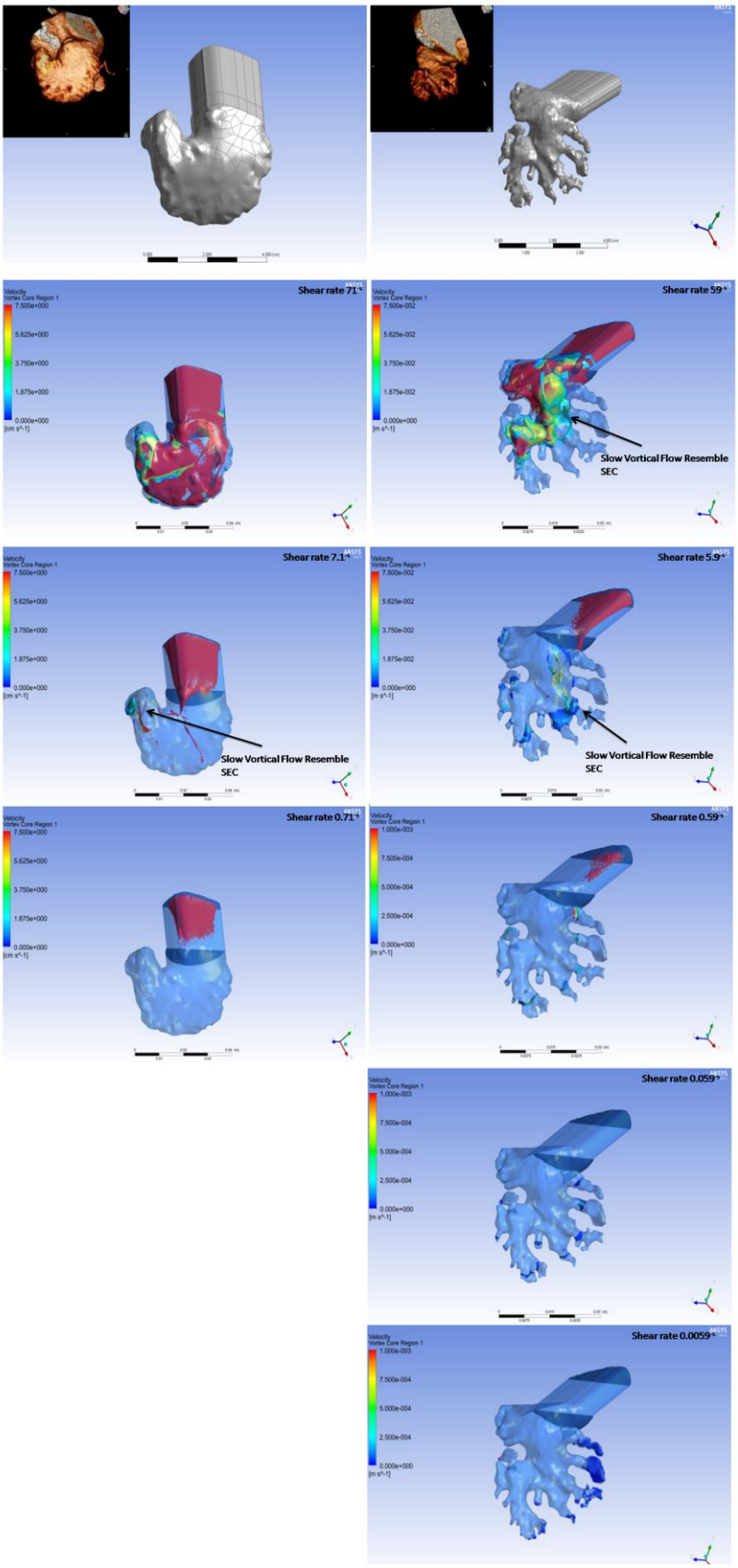

Figure 7A: *One of Each LAA Morphological Subtype Simulation Results are Shown with View to Profile the Vortical Flow Pattern of each Morphology Subtypes Across Different Magnitude of Shear Rates with LAA Emptying Velocity of 40cm/s.* ***Figure 7B:*** *Provides a Closer Look in both Chickenwing and Cauliflower LAA Vortical Flow Pattern. The legend of Figure 7A&B is that any LAA vortical flow velocity above 7.5cm/s is coded in* ***RED*** *colour, while any other colour represents regions of lower velocity and possible SEC formation.*

6.4 Discussion

These CFD numerical simulations have shown that the Cauliflower LAA morphology has the highest volume of stagnant flow, and this is significantly greater than that seen in non-Cauliflower subtypes. This is consistent with the findings across four major LAA morphology studies, in which the Cauliflower LAA subtype confers the highest risk of cerebral thromboembolism, independent of clinical risk score[5-7]. These results lend support for the hypothesis that the mechanism by which LAA morphology modifies risk of stroke is via increasing the volume of stagnant or slow blood flow.

There is inherent difficulty in classifying LAA morphology into 4 categories and this carries high inter-observer and intra-observer variability [6]. Other structural characteristics such as the numbers of lobes of LAA may also be important [8]. Overall, it seems likely that LAA complexity and trabeculation will promote stagnant blood flow and that this explains why Cauliflower and Windsock subtypes have increase slow flow and increased risk of embolism.

From Chapter 5, it is known that LAA shear rate is dependent on LAA morphology in term of neck radius, LAA volume and LAA emptying function, but not to the complexity of LAA geometry. On the other hand, as these simulation results have

shown, slow vortical flow velocity is likely related to the interaction of complex LAA geometry and LAA function. Since both LAA emptying function and blood haemostatic factors were fixed for the purposes of the CFD modelling, the difference in volume of slow vortical flow can only explained by the different complexity of LAA geometry. To the best of our knowledge, this is the first time a geometry-dependent stagnation-flow relationship has been demonstrated in LAA.

The utility of LAA morphology in predicting risk is unclear. This study gives insight as to why this may be the case, while also providing a mechanism for pathobiology. Stasis of blood circulation, assessed in this study by the volume of slow vortical flow, is shown to depend on LAA morphology, but also depends on LAA function and emptying velocity. In addition, other variables, such LAA size, appear to vary in their prevalence across the LAA morphologies- with small LAA being more common in the more complex cauliflower structure. There is a clear interaction between emptying velocity and LAA morphology in determining slow flow volume- **Figure 6**. Where LAA function is very depressed and emptying is very slow, morphology is no longer an important variable and under these conditions, knowledge of LAA morphology is unlikely to improve clinical prediction of embolic risk. Under conditions when velocity is more moderately reduced, then it is likely that morphology will be an important variable.

6.5 Limitation

There are several limitations to this study. Firstly, the classification of LAA morphology is variable and error in classification remains possible. Secondly, only one phase of steady state CFD simulation was assumed with no fluid-solid interaction to simulate LAA wall deformation. LAA wall deformation can be incorporated to allow better simulation of LAA emptying function, and along with unsteady flow can may allow even more accurate depiction of the slow vortical flow

mapping and value estimate. Thirdly, the orifice of the LAA was separated to allow CFD simulation, and in this respect may not resemble true LAA haemodynamics.

Despite these limitations, this study had overcome a major difficulty in classifying the different subtypes of LAA morphology and provided quantitative comparison of these morphologies. Once validated with echocardiographic rheological haemodynamics, CFD assessment of slow flow volumes in the LAA may serve as a better predictor for risk for thromboembolism.

6.6 Conclusion

Using CFD numerical simulation on different LAA morphologies, the results have shown that the complexity of LAA geometry governs the quantity and location of stagnant flow at a given LAA emptying function and provides mechanistic insight into the clinical association of LAA thrombus or cerebral thromboembolism with complex LAA geometry.

6.7 Reference

1. Ernst, G., et al., *Morphology of the left atrial appendage.* Anat Rec, 1995. **242**(4): p. 553-61.
2. Veinot, J.P., et al., *Anatomy of the normal left atrial appendage: a quantitative study of age-related changes in 500 autopsy hearts: implications for echocardiographic examination.* Circulation, 1997. **96**(9): p. 3112-5.
3. Al-Saady, N.M., O.A. Obel, and A.J. Camm, *Left atrial appendage: structure, function, and role in thromboembolism.* Heart, 1999. **82**(5): p. 547-54.
4. Di Biase, L., et al., *Does the left atrial appendage morphology correlate with the risk of stroke in patients with atrial fibrillation? Results from a multicenter study.* J Am Coll Cardiol, 2012. **60**(6): p. 531-8.
5. Anselmino, M., et al., *Left atrial appendage morphology and silent cerebral ischemia in atrial fibrillation patients.* Heart Rhythm, 2013.
6. Khurram, I.M., et al., *Relationship between left atrial appendage morphology and stroke in patients with atrial fibrillation.* Heart Rhythm, 2013. **10**(12): p. 1843-9.
7. Kimura, T., et al., *Anatomical characteristics of the left atrial appendage in cardiogenic stroke with low CHADS2 scores.* Heart Rhythm, 2013. **10**(6): p. 921-5.
8. Yamamoto, M., et al., *Complex Left Atrial Appendage Morphology and Left Atrial Appendage Thrombus Formation in Patients With Atrial Fibrillation.* Circ Cardiovasc Imaging, 2014.
9. Fatkin, D., R.P. Kelly, and M.P. Feneley, *Relations between left atrial appendage blood flow velocity, spontaneous echocardiographic contrast and thromboembolic risk in vivo.* J Am Coll Cardiol, 1994. **23**(4): p. 961-9.
10. Black, I.W., et al., *Left atrial spontaneous echo contrast: a clinical and echocardiographic analysis.* J Am Coll Cardiol, 1991. **18**(2): p. 398-404.
11. Donal, E., et al., *Contrast-enhanced tissue Doppler imaging of the left atrial appendage is a new quantitative measure of spontaneous echocardiographic contrast in atrial fibrillation.* Eur J Echocardiogr, 2008. **9**(1): p. 5-11.

12. Zhang, L.T. and M. Gay, *Characterizing left atrial appendage functions in sinus rhythm and atrial fibrillation using computational models.* J Biomech, 2008. **41**(11): p. 2515-23.
13. Moyle, K.R., L. Antiga, and D.A. Steinman, *Inlet conditions for image-based CFD models of the carotid bifurcation: is it reasonable to assume fully developed flow?* J Biomech Eng, 2006. **128**(3): p. 371-9.
14. Miller, D.E., D.H. Tucker, and W.J. Jacoby, Jr., *THE GIANT "A" WAVE OF THE LEFT ATRIAL APPENDAGE.* Circulation, 1963. **28**: p. 1110-5.
15. Begent, N. and G.V. Born, *Growth rate in vivo of platelet thrombi, produced by iontophoresis of ADP, as a function of mean blood flow velocity.* Nature, 1970. **227**(5261): p. 926-30.
16. Richardson, P.D., *Letter: Effect of blood flow velocity on growth rate of platelet thrombi.* Nature, 1973. **245**(5420): p. 103-4.
17. Furie, B. and B.C. Furie, *Mechanisms of thrombus formation.* N Engl J Med, 2008. **359**(9): p. 938-49.

Chapter 7: Conclusion

7.1 Conclusion

Through numerical simulation on different biological structural geometries, these projects have examined how biomechanical and rheological mechanisms may be linked to two clinical scenarios in cardiovascular medicine.

7.2 Left Main Coronary Artery Disease

Firstly, from the review of LMCA literature, it is discovered that isolated LMCA disease has the propensity to develop atherosclerotic plaque in the very proximal LMCA, as opposed to the distal LMCA segment location seen in disease of the LMCA associated with multi-vessel disease. In addition, the incidence of plaque rupture is higher in isolated LMCA disease. This suggests that in relation to localized LMCA disease, local biomechanical forces such as WSS may play an important role. In relation to the proximal LMCA, one clinical variant is the LMCA with a highly vertical displaced anomalous ostium (sharp vertical take-off angulation from aorta). This had been be considered malignant, but systematic investigation of the rheological effects of this variant had not been undertaken.

The study therefore investigated the impact of the varying vertical take-off angulation of LMCA from aorta on biomechanical forces in the proximal segment of LMCA. Firstly, a systematic survey of the LMCA using CT coronary angiography to clarify realistic ranges of angulation was undertaken. Using this information, CFD simulation was applied to the LMCA with varying vertical LMCA take-off anglulation from the aorta. It is found the more acute the LMCA take-off angle from the aorta the larger the low WSS zone in LMCA ostium/proximal segment and higher peak WSS proximally; especially in the presence of significant coronary stenosis. This potentially provides a mechanism for very proximalatherosclerotic plaque in the

LMCA segment with angulated LMCA and higher incidence of plaque rupture in isolated LMCA disease. In addition, from these LMCA sub-studies, it is found that movement of LMCA does not have to be considered in numerical simulation as there is minimal movement and only minor variation in LMCA morphology between systolic and diastolic phase. This drastically reduces the numerical simulation time and makes application of CFD very feasible. On the other hand, the preliminary evaluation also showed that the accurate understanding of WSS quantity and mapping demands incorporation of the aorta in all modelling of the LMCA.

7.3 Left Atrial Appendage Morphology

In the second project, review of LAA morphology literature revealed that different LAA morphological subtypes are associated with different risks of thromboembolism. Both LAA geometry and the LAA contractile function played important roles in determining the degree of shear and the amount of the spontaneous echo contrast (SEC) in the LAA. Echocardiographic studies had shown poor LAA contractile function leads to low shear rate and dense spontaneous echo contrast-SEC, a marker of sluggish blood flow- in the LAA.

The application of a novel CFD simulation across the four different LAA morphology subsets has demonstrated that the Cauliflower LAA subtype contained the greatest volume of slow vortical flow at low shear rate across different LAA emptying velocities (LAA function). This rheological mechanistic observation correlates well with the clinical observation with highest rate of clinical thromboembolism associates with the Cauliflower subtype in the setting of low CHADS VASC score atrial fibrillation. In addition, this simulation model can serve as a potential clinical tool in quantifying the absolute quantity of slow vortical flow at low shear rate for a given complex LAA geometry at a given LAA function. We anticipate that in future studies this CFD approach will lead to the resolution of discrepancies in the LAA morphological classification of complex geometries for individual patients and provide quantitative prediction ofrisk of thromboembolism for any given geometry.

7.4 Summary

In summary, numerical simulation has provided mechanistic insight into two areas of cardiovascular medicine. It is anticipated that this approach will provide a potential clinical tool for more accurate clinical risk assessment.